NATIONAL ADVISORY COMMITTEE FOR AERONAUTICS

TECHNICAL NOTE

No. 1328

CALCULATION OF COMPRESSIBLE FLOWS PAST AERODYNAMIC SHAPES BY USE OF THE STREAMLINE CURVATURE

By W. Perl

Flight Propulsion Research Laboratory
Cleveland, Ohio

Washington
June 1947

NATIONAL ADVISORY COMMITTEE FOR AERONAUTICS

TECHNICAL NOTE NO. 1328

CALCULATION OF COMPRESSIBLE FLOWS PAST AERODYNAMIC SHAPES BY USE OF THE STREAMLINE CURVATURE

By W. Perl

SUMMARY

A simple approximate method is given for the calculation of isentropic irrotational flows past symmetrical airfoils, including mixed subsonic-supersonic flows. The method is based on the choice of suitable values for the streamline curvature in the flow field and subsequent integration of the equations of motion. The method yields limiting solutions for potential flow. The effect of circulation is considered.

A comparison of derived velocity distributions with existing results that are based on calculation to the third order in the thickness ratio indicates satisfactory agreement. The results are also presented in the form of a set of compressibility correction rules that lie between the Prandtl-Glauert rule and the von Kármán-Tsien rule (approximately). The different rules correspond to different values of a local shape parameter $\sqrt{YC_a}$, in which Y is the ordinate and C_a is the curvature at a point on an airfoil. Bodies of revolution, completely supersonic flows, and the significance of the limiting solutions for potential flow are also briefly discussed.

INTRODUCTION

The problem of calculating compressible potential flows past aerodynamic shapes will be considered in this paper by the following method: An assumption is made as to the variation of the curvature of the streamlines in the flow field and the equations of motion, expressed in terms of the streamline curvature, are thereupon integrated.

This basic method of calculating fluid flows is not new. It has been described in reference 1 for use in calculating pressure distributions on closely spaced airfoils in cascade. More recently

the method was applied to the compressible flow past an isolated airfoil and to the incompressible flow past a symmetrical airfoil in a closed channel. The results of reference 2 are compared with those of the present paper.

The method is applied to isolated airfoils and the results are compared with those of references 3 and 4. The limiting solution for potential flow by this method is identified with the "limiting line" phenomenon (reference 5) and discussed in relation to the flow through a converging-diverging channel. Application of the method to bodies of revolution is indicated.

THEORY FOR SYMMETRICAL AIRFOILS

The flows calculated in this paper are of the steady, continuous, isentropic, irrotational type. (See fig. 1.) The equations of motion are considered in the following form:

Equation of irrotationality (reference 6, p. 43):

$$\frac{\partial v}{\partial n} + Cv = 0 \tag{1}$$

Equation of continuity of mass flow:

$$\int_0^{n_o} \rho_o v_o dn = \int_0^{n} \rho v dn \tag{2}$$

Bernoulli's equation and equation of state for isentropic flow:

$$\frac{\rho}{\rho_o} = \left(\frac{p}{p_o}\right)^{\frac{1}{\gamma}} = \left[1 - \frac{\gamma-1}{2} M_o^2 \left(\frac{v^2}{v_o^2} - 1\right)\right]^{\frac{1}{\gamma-1}} \tag{3}$$

where

v velocity at a point P of flow field

n distance measured along potential line from airfoil (streamline) to point P on streamline in flow field

n_o perpendicular distance between same two streamlines in free stream

C curvature of streamline at point P, positive when streamline is convex in positive n direction. (C is the reciprocal of the radius of curvature.)

ρ density

p pressure

γ ratio of specific heats

M Mach number

The subscript o denotes free-stream conditions.

Consider the symmetrical flow past a symmetrical airfoil section (fig. 1). The potential lines of the flow pattern are assumed straight and perpendicular to the free-stream direction, or x-direction, thereby relaxing the condition of orthogonality between stream and potential lines. This assumption is exactly satisfied at the mid-chord station of the section if the section has fore-and-aft symmetry with respect to the mid-chord station. The assumption, in effect, renders the analysis for one chordwise station independent of that for another.

The element of length dn in equations (1) and (2) is therefore replaced by the element of length dy in the y-direction and equations (1) and (2) are written, respectively:

$$dy = -\frac{dv}{Cv} \tag{4}$$

$$\int_0^{y_o} dy = \int_Y^y \frac{\rho}{\rho_o}\frac{v}{v_o}\,dy \tag{5}$$

The differentials in equations (4) and (5) are understood to be taken in the y-direction at constant x. The lower limits of integration in equation (2) are on the streamline that coincides with the airfoil contour. The corresponding lower limits in equation (5) are therefore 0 and Y, respectively, where Y is the airfoil ordinate,

a function of the chordwise location x. The upper limits of integration in equation (5) are on a streamline that becomes parallel to the x-axis at infinity; that is:

$$\lim_{y\to\infty} y = y_o$$

Hence, the continuity condition (5), which for finite y, y_o may be written

$$\int_0^Y dy = \int_Y^y \frac{\rho}{\rho_o}\frac{v}{v_o}\,dy - \int_Y^{y_o} dy$$

becomes in the limit as $y\to\infty$

$$Y = \int_Y^{\infty} \left(\frac{\rho v}{\rho_o v_o} - 1\right) dy \tag{6}$$

Without loss of generality, the free-stream density ρ_o and velocity v_o are hereinafter considered as unity (or what is the same, ρ and v are written in place of ρ/ρ_o and v/v_o, respectively). Combination of the approximate irrotational condition (4) and the approximate continuity condition (6) yields

$$Y = \int_1^V \frac{(\rho v - 1)}{Cv}\,dv \tag{7}$$

in which the lower limit of integration, unity, is the free-stream velocity at $y = \infty$, and the upper limit V, corresponding to the airfoil ordinate Y, is the unknown desired velocity at the airfoil.

A streamline curvature function is now to be chosen. It must satisfy the boundary conditions of known airfoil curvature C_a at the surface of the airfoil and zero curvature at infinity. For convenience, in the integration of equation (7), the curvature C is chosen as a function not of the coordinates x, y of the flow field directly but of the velocity $v(x, y)$. The function chosen is

$$C = C_a \left(\frac{v-1}{V-1}\right)^{\eta} \tag{8}$$

in which the airfoil curvature C_a, the unknown airfoil velocity V, and the parameter η (which will be discussed later) are functions only of chordwise location x, hence are constant as far as the integration in equation (7) is concerned.

The velocity v in the flow field is obtained by substitution of equation (8) into equation (4) and integration (at constant x),

$$\frac{y}{Y} - 1 = -\frac{(V-1)^{\eta}}{YC_a} \int_V^v \frac{dv}{v(v-1)^{\eta}} \tag{9}$$

The streamline curvature function $C(y)$ determined by equations (8) and (9) varies monotonically, as y increases at constant x, from the value C_a at the airfoil where $y = Y$ to the asymptotic value zero at $y = \infty$. The manner of this variation depends on the known airfoil shape parameter YC_a, the airfoil velocity V, and the parameter η.

The airfoil velocity V is given in terms of the airfoil shape parameter YC_a, the free-stream Mach number M_o, and the parameter η by equations (7), (3), and (8), which yield:

$$YC_a = (V-1)^{\eta} \int_1^V \frac{v\left[1 - \frac{\gamma-1}{2} M_o^2 (v^2-1)\right]^{\frac{1}{\gamma-1}} - 1}{v(v-1)^{\eta}} dv \tag{10}$$

The parameter η is limited in its possible range of values by the conditions that must be satisfied infinitely far from the airfoil, that is, as $v \to 1$. These conditions are:

(a) The curvature $C \to 0$.

(b) The distance $y \to \infty$.

(c) The continuity integral (equation (10)) is finite. Condition (a) requires, by equation (8), that $0 < \eta < \infty$. Condition (b) requires that the integral in equation (9) diverge as the upper limit $v \to 1$, which it does for $1 \leq \eta < \infty$. Condition (c) requires that the integral in equation (10) converge at the lower limit, which it does for $-\infty < \eta < 2$. All three conditions therefore limit the permissible range of η to

$$1 \leq \eta < 2 \tag{11}$$

Equation (10) and condition (11) represent the basic result of the present method. The velocity V at a point on the surface of a symmetrical airfoil at a given subsonic free-stream Mach number M_o is obtained by assuming that the known data are the shape parameter YC_a and the incompressible, or low-speed, velocity V_i at that point on the airfoil. The parameter η is first obtained from

equation (10) with $M_o = 0$ and $V = V_i$. It will appear from later applications that the value of η thus determined falls within the range given by expression (11) over the region of the airfoil of greatest interest. With this value of η, equation (10) then gives the velocity V at the point under consideration for the desired Mach number M_o.

The main uncertainty of the present method is represented by the chosen curvature function given in equation (8). The approximation involved in the use of this function has been minimized by the method just described of fixing the parameters V and η. By this method the streamline-curvature function satisfies an approximate form of the equations of motion (equation (10)) and yields the known exact value of the airfoil velocity in the incompressible case. Furthermore, the curvature function exactly satisfies the boundary conditions of end values C_a and 0 and varies between these end values in the correct general manner (for stations near the maximum velocity station), namely, monotonically.

As a further condition on the chosen curvature function, the final solution given by equation (10) should reduce to the Prandtl-Glauert rule for small disturbance of the free stream. Thus, neglecting powers of $v-1$ and $V-1$ equal to or higher than the second, equation (10) reduces to

$$YC_a = (V-1)^\eta \int_1^V \frac{v\left[1 - \frac{1}{2}M_o^2\,(v+1)(v-1) - \ldots\right] - 1}{v(v-1)^\eta}\,dv$$

$$= (V-1)^\eta \int_1^V \frac{(v-1)(1-M_o^2)}{(v-1)^\eta}\,dv$$

$$= (1-M_o^2)(V-1)^\eta \int_1^V (v-1)^{1-\eta}\,dv$$

or, integrating and solving for $V-1$,

$$V-1 = \sqrt{\frac{2-\eta}{1-M_o^2}}\sqrt{YC_a} \qquad (12)$$

Equation (12) shows that, if η is adjusted to give the correct value of $V-1$ for $M_o = 0$, or

$$V_i-1 = \sqrt{2-\eta}\sqrt{YC_a} \qquad (13)$$

then the compressible value for any subsonic M_o is given by

$$V\text{-}1 = \frac{V_i\text{-}1}{\sqrt{1-M_o^2}} \tag{14}$$

which is the Prandtl-Glauert rule.

The foregoing considerations indicate that the results should not be critical with respect to choice of form of curvature function. A somewhat different form of curvature function satisfying all the foregoing conditions is

$$C = C_a \left(\frac{\log_e v}{\log_e V}\right)^{\eta} \tag{15}$$

Comparative results based on this function will be discussed later.

The basic relation (10) connecting the velocity V (expressed as airfoil velocity increment V-1) at a point on a symmetrical airfoil, the airfoil curvature parameter $\sqrt{YC_a}$ at the same point, and various free-stream Mach number M_o is shown graphically in figures 2, 3, and 4 for $\gamma = 1.4$. The numerical data from which these curves were plotted are given in tables I and II. Included in tables I and II are some corresponding computations based on the curvature function (15). The integral in equation (10) was evaluated by Simpson's rule and checked by the closed-form result obtainable in the case $\eta = 1$. The velocity increment above free-stream velocity V-1 was plotted against $\sqrt{YC_a}$, hereinafter called the curvature parameter, rather than against YC_a because $\sqrt{YC_a}$ is proportional to the thickness ratio of the airfoil (see, for example, equation (19)) and V-1 is therefore approximately linear with respect to this quantity for small values (equation (12)).

Figures 3(a) to 3(h) correspond to positive velocity increments above free-stream velocity, that is, evaluation of equation (10) for $V > 1$. Figures 4(a) to 4(h) correspond to negative velocity increments ($V < 1$) such as produced on surfaces of negative curvature and ordinate (hence the negative sign attached to $\sqrt{YC_a}$). In this case the curvature function, instead of the one given by equation (8), is properly taken as

$$C = C_a \left(\frac{1-v}{1-V}\right)^{\eta}$$

which allows equation (10) to be evaluated without ambiguity as regards the terms to the power η. The curves of negative velocity

increment (figs. 4(a) to 4(h)) may be regarded as continuations of the corresponding curves of positive velocity increment (figs. 3(a) to 3(h)).

It is of interest to note that a parameter equivalent to the parameter $\sqrt{YC_a}$ was derived by the authors of reference 8 from a dimensional consideration of equation (4) and used to correlate critical Mach number data for various symmetrical airfoil sections.

APPLICATION AND RESULTS

Kaplan Section

Kaplan (reference 3) has calculated the compressible-flow zero-lift velocity distribution for a particular family of symmetrical airfoils. The method used was an extension of the Ackeret method wherein the potential function is expressed as a power series in the thickness ratio of the section. The corresponding series for the velocity distribution was evaluated to the term in the third power of the thickness ratio. A limiting value of free-stream Mach number was found, for a given thickness ratio, above which the terms of the power series that were calculated (the first three) indicated a probable failure of the series to converge. This free-stream Mach number was presumed to constitute an upper limit for the existence of a continuous potential flow.

The method of the present analysis was tested by determining the velocity distributions for the Kaplan section from figures 2, 3, and 4 (drawn to a scale commensurate with the precision of the data of tables I and II). As an example of the procedure used, the velocity increment $V-1$ for the mid-chord location $x = 0$ of the Kaplan section of thickness ratio 0.10 was obtained as follows. The section ordinates and corresponding curvature parameter $\sqrt{YC_a}$ are given in figure 5. The incompressible velocity distribution V_1-1, obtained by conformal mapping, is shown in figure 6 ($M_o = 0$). At $x = 0$ the values $\sqrt{YC_a} = 0.1925$ and $V_1-1 = 0.1667$ from figures 5 and 6, respectively, correspond in figure 3(a) to an interpolated value of $\eta = 1.297$. For these values of η and $\sqrt{YC_a}$, the velocity increments $V-1$ for values of M_o of 0.5, 0.7, 0.8, 0.85, and 0.9 were interpolated from figures 3(c), 3(e), 3(f), 3(g), and 3(h), respectively. Velocity increments were obtained in this manner in the chordwise range $0 \leq x < 0.616$. In the chordwise range $0.616 < x < 1.0$, the values of $\sqrt{YC_a}$ are indicated in figure 5 as imaginary, resulting from a positive ordinate and a negative curvature. The theory presented, based on the curvature function of equation (8), cannot handle such values of the curvature parameter. Approximate

compressible velocity increments were obtained in this chordwise range by first noting that the parameter η increased toward the value 2.0 with increase in chordwise distance from the center (fig. 5). Now the limiting value $\eta = 2.0$ corresponds to the Prandtl-Glauert rule, as will be shown under COMPRESSIBILITY CORRECTION RULES. In the range $0.616 < x < 1.0$; therefore, the compressible velocity increments were calculated from the incompressible values by equation (14).

The velocity distributions thus obtained for the Kaplan section of thickness ratio 0.10 are shown in figure 6. The distributions for $M_o = 0.85$ and $M_o = 0.9$ do not extend all the way to the mid-chord location but come to an end (with infinite slope) at the chordwise locations $x = 0.145$ and 0.390, respectively. The immediate reason for this behavior is evident from figure 2. For example, at the limiting location $x = 0.145$ for $M_o = 0.85$, the value of η was 1.312 (fig. 5). On the set of basic curves for $\eta = 1.312$ and similar in appearance to figure 2, a vertical line drawn at $\sqrt{YC_a} = 0.181$ corresponding to $x = 0.145$ would be tangent to the $M_o = 0.85$ curve, at which point the velocity increment V-1 would be 0.550. No solution exists at this value of $\sqrt{YC_a}$ for M_o higher than 0.85; or, for fixed $M_o = 0.85$, no solution exists for higher values of $\sqrt{YC_a}$ such as correspond to chordwose locations closer to mid-chord than $x = 0.145$. The points of infinite slope on the basic curves of figure 2 correspond to a limiting solution for potential flow by the present method. This phenomenon, hereinafter called the "potential limit phenomenon," is discussed in appendix A.

The potential limit points for the Kaplan 10-percent section at $M_o = 0.85$ and 0.9 were actually obtained from accurately determined plots of the infinite slope loci of figure 3. These plots are given in figure 7. The vacuum-line boundary curve in figure 5 corresponds to $p/p_o = 0$ in equation (3). The intersection of the curve of η against $\sqrt{YC_a}$ for the Kaplan 10-percent section (fig. 5), with, for example, the $M_o = 0.85$ contour in figure 7(a) determined the potential limit values of η and $\sqrt{YC_a}$; hence by figure 5 determined the chordwise location at which a potential limit point existed for $M_o = 0.85$. The potential limit value of η then determined the potential limit V-1 by figure 7(b). The free-stream Mach number at which the mid-chord location $x = 0$ is a potential limit point, that is, the lowest M_o at which a potential limit occurs, is indicated by point A in figure 7(a). By interpolation this limit value of M_o is estimated as 0.843 and the corresponding V-1 (fig. 7(b)) as 0.573. For comparison, the lower critical Mach number (the lowest free-stream Mach number at which sonic velocity occurs on the airfoil) was determined as 0.748.

The velocity distribution at the lowest potential limit Mach number, obtained by interpolation from the other velocity distributions, is shown in figure 6. The velocity gradient at mid-chord appears to be finite and different from zero. The reason for this behavior can be seen from the expression for the velocity gradient

$$\frac{dV}{dx} = \frac{\partial V}{\partial \sqrt{YC_a}} \frac{d\sqrt{YC_a}}{dx} + \frac{\partial V}{\partial \eta} \frac{d\eta}{dx} \tag{16}$$

in which the first partial derivative is taken at constant η and the second at constant $\sqrt{YC_a}$. (The acceleration of the fluid along the surface s of the airfoil is $V \frac{dV}{ds}$. Hence, the following discussion applies also to the fluid acceleration.) At a potential limit point both $\partial V/\partial\sqrt{YC_a}$ and $\partial V/\partial\eta$ are infinite (fig. 2). If $d\sqrt{YC_a}/dx$ and $d\eta/dx$ are not zero at the chordwise station corresponding to a potential limit point, the velocity gradient dV/dx is infinite there, as is the case with the velocity distributions for $M_o = 0.85$ and 0.9 in figure 6. If $d\sqrt{YC_a}/dx$ and $d\eta/dx$ are zero, which is the case at the mid-chord station of the Kaplan 10-percent section, the occurrence of a potential limit at this point leads to an indeterminate expression for the velocity gradient in equation (16). Closer analytical and graphical examination indicates the finite gradient shown in figure 6 (hence, a finitely discontinuous change in fluid acceleration across the mid-chord station).

The lowest potential limit values of M_o, the corresponding values at mid-chord of V-1, and the local Mach number M for symmetrical sections of three thickness ratios ($t = 0.05$, 0.10, and 0.20) were computed. The value of M was obtained by combining Bernoulli's equation in the form of equation (3) and in the form

$$\left(\frac{p}{p_o}\right)^{\frac{\gamma-1}{\gamma}} = \frac{1 + \frac{\gamma-1}{2} M_o^2}{1 + \frac{\gamma-1}{2} M^2} \tag{17}$$

resulting in

$$M = \frac{M_o V}{\sqrt{1 - \frac{\gamma-1}{2} M_o^2 (V^2-1)}} \tag{18}$$

The values are listed in the following table and compared with values obtained by Kaplan in reference 3:

t	Curvature method			Kaplan method		
	M_o	V-1	M	M_o	V-1	M
0.05	0.898	0.324	1.269	0.890	0.249	1.164
.10	.843	.573	1.491	.833	.456	1.320
.20	.763	1.200	2.257	.743	.864	1.625

The limiting values of M_o by the two methods agree fairly closely; the values of V-1, hence also M, less so. The less satisfactory agreement of V-1 is to be expected from the rapidity with which V-1 varies with M_o in the neighborhood of the potential limit solution (fig. 6).

The comparison of the velocity distributions for the 10-percent thickness section by the two methods is given in figure 8. The velocity distributions for $M_o = 0.75$ (fig. 8(b)) and 0.83 (fig. 8(c)) were obtained by interpolation from cross plots of the velocity distributions of figure 6, guided by the potential limit points previously determined. In the region of greatest interest on the contour, namely the supersonic region given approximately at $M_o = 0.83$ by $0 < x < 0.4$, the velocity by the Kaplan method increases with M_o at a greater rate than the velocity by the curvature method. A convenient criterion of the accuracy of velocity distributions in local supersonic regions has been pointed out by Tsien and Fejer, namely, if a velocity distribution indicates a local supersonic region, a velocity distribution can be derived in this region that must be greater than the original velocity distribution; the difference between the two distributions decreasing as the extent of the local supersonic region increases. This greater velocity distribution for the supersonic region is the well-known Prandtl-Meyer solution for the flow over a curved surface (reference 8(a)). The Prandtl-Meyer velocity distribution extends, in the case considered here, from the chordwise location for a local Mach number $M = 1$ to the mid-chord location. The Prandtl-Meyer solution is obtained from the change in slope of the airfoil surface $\Delta\theta$ from the $M = 1$ location to the point under consideration. This change in slope expressed in degrees is equivalent to the pressure number P, which is a function of the local (supersonic) Mach number M. From a plot of slope θ of airfoil surface against x, included in figure 5, and a table of P against Mach angle, it is therefore a simple matter to obtain the Prandtl-Meyer local Mach number distribution in the supersonic region. The local Mach number M and the free-stream Mach number M_o then determine the local velocity V by equation (18). If the pressure number P is defined in terms of the

flow deflection angle $\Delta\theta$ as $P = 1000 - \Delta\theta$, the pressure number may be computed by the methods of reference 8(a). The variation of pressure number and flow deflection angle with Mach angle is shown in the following table:

PRESSURE NUMBER AND MACH ANGLE IN PRANDTL-MEYER SOLUTION FOR SUPERSONIC FLOW

[$\gamma = 1.4$]

Pressure number, P	Flow deflection angle, $\Delta\theta = 1000 - P$ (deg)	Mach angle $\mu = \sin^{-1}\frac{1}{M}$
1000	0	90° 00'
999	1	67° 43'
998	2	62° 00'
997	3	58° 10'
996	4	44° 12'
995	5	52° 43'
994	6	50° 36'
993	7	48° 43'
992	8	47° 03'
991	9	45° 32'
990	10	44° 09'
989	11	42° 51'
988	12	41° 39.5'
987	13	40° 32.5'

The Prandtl-Meyer solutions obtained in this manner for the velocity distributions by the Kaplan method and by the curvature method are shown in figure 8(c). The velocity distribution obtained by the curvature method is evidently closer to the true distribution than that of the Kaplan method in the local supersonic region for $M_o = 0.83$, because the curvature velocity distribution is less and the Kaplan velocity distribution is greater than the corresponding Prandtl-Meyer distribution. Application of the Prandtl-Meyer solution to the potential limit velocity distribution by the curvature method for $M_o = 0.843$ (fig. 8(d)) indicates a rapid decrease in validity of the results by the curvature method for free-stream Mach numbers close to the lowest potential limit Mach number.

From these and similar calculations for thickness ratio of 5 and 20 percent, it is concluded that the curvature method gives results of at least the same order of accuracy as the Kaplan method over approximately the middle half of the Kaplan section. Over the rest of the section the Kaplan method may well be more accurate.

Biconvex Section

The method of curvature may be expected to increase in validity with decrease in the variation of the curvature parameter $\sqrt{YC_a}$ along the airfoil. The symmetrical biconvex section (one formed of two circular arcs) was considered as an example which is more favorable in this respect than the Kaplan section. The biconvex section of 0.20 thickness ratio was analyzed for its incompressible velocity distribution by conformal mapping. The curvature parameter $\sqrt{YC_a}$ was calculated from the relation

$$\sqrt{YC_a} = \sqrt{\frac{Y}{Y_{max}}} \frac{\sqrt{2}\, t}{\sqrt{1 + t^2}} \tag{13}$$

in which Y_{max} is the section ordinate at the mid-chord location and t is the thickness ratio. The section ordinates Y, the slope θ, the curvature parameter $\sqrt{YC_a}$, and the parameter η, determined as for the Kaplan 0.10 thickness ratio section, are given in figure 9. The velocity distributions for $M_o = 0$, 0.5, 0.7, and 0.8 are given in figure 10. The curvature method cannot handle velocities less than the free-stream value (unity), which correspond to positive values of the curvature parameter; these velocities were obtained by the Prandtl-Glauert rule.

The lowest free-stream Mach number M_o for which a potential limit occurs at mid-chord is 0.790. The corresponding values of local velocity increment and local Mach number are 1.819 and 1.704, respectively. The Prandtl-Meyer solution (fig. 10) indicates inadequacy of the curvature method in this case at a free-stream Mach number somewhat less than 0.8. The local velocity increments of the biconvex section of thickness ratio 0.20 are higher than those of the Kaplan section of thickness ratio 0.10. The ratio of the increments of the biconvex section to those of the Kaplan section of thickness ratio 0.10 are, in general, less than the ratio of the thicknesses of the two sections.

CONDITIONS IN FIELD OF AIRFOIL

The variation of streamline curvature and of local velocity with distance from the airfoil is given by equations (8) and (9).

For the purpose of illustration, it will be sufficient first to make the simpler calculations corresponding to the curvature function (15) in place of (8). Equations (4) and (15) yield

$$dy = - \frac{(\log_e V)^{\eta}}{C_a} \frac{d(\log_e v)}{(\log_e v)^{\eta}}$$

which, after integration and adjustment of the constant of integration to satisfy the boundary conditions, becomes

$$\frac{y}{Y} = 1 + \frac{\log_e V}{YC_a (\eta-1)} \left[\left(\frac{\log_e V}{\log_e v} \right)^{\eta-1} - 1 \right] \qquad (20)$$

The curvature variation is given by equations (15) and (20). For $\eta = 1$ these equations are indeterminate. In this case, equations (4) and (15) (or the well-known limiting form of equation (20)) yield

$$\frac{y}{Y} = 1 + \frac{\log_e V}{YC_a} \log_e \left(\frac{\log_e V}{\log_e v} \right) \qquad \eta = 1 \qquad (21)$$

The curvature and velocity variations given by equations (15), (20), and (21) are shown in figure 11 and 12, respectively, for various values of η and M_o. The value of YC_a of 0.03704 chosen for the calculation was that corresponding to the mid-chord location of the 10-percent thick Kaplan section. The corresponding values of V for the various M_o were those previously computed for the Kaplan 10-percent thick section. Although these values of V correspond to only a single value of η based on the curvature function (8), the use of these same values for various η and with the curvature function (15) give the trend of curvature and velocity variations sufficiently well for the purpose of illustration. The curvature and velocity variations of figures 11 and 12 show the expected trend with free-stream Mach number M_o, namely, a slower decrease to free-stream conditions as M_o is increased. The limitation of a single curvature function such as equation (8) or (15) is apparent from figure 13, for it yields basically the same kind of curvature variation in the supersonic region as in the subsonic region. A more rigorous analysis should take into explicit account the different type of curvature variation found in supersonic flows.

The extent of the local supersonic regions in the field of the 10-percent thick Kaplan section was next calculated by the more appropriate equation (9), using the data derived in connection with

the velocity distributions. The results are shown in figure 14, in which the local Mach number $M = 1$ boundary is plotted for $M_o = 0.75$, 0.8, 0.83, and 0.843 in terms of airfoil semichord as unit distance.

The rapid increase in lateral extent of the supersonic region with increase of free-stream Mach number, particularly near the potential limit, is apparent in figure 14. At the potential limit $M_o = 0.843$, the local supersonic region extends laterally into the flow field a distance of about 1 chord.

The finite nonzero slope at $x = 0$ of the sonic boundary at the potential limit should also be noted. This finite slope is associated with the finite velocity gradient at the surface of the Kaplan section previously discussed. It appears from equation (9) that the slope of a constant velocity (hence, for given M_o, constant M) boundary will be associated with the surface velocity gradient at the same value of x in being finite or infinite. Hence, if the lowest potential limit solution occurs at a point on a symmetrical airfoil at which $d\sqrt{YC_a}/dx$, $d\eta/dx$ are not zero, then the consequent infinite velocity gradient at that point on the surface will cause a cusp in the $M = 1$ boundary in the field. This cusp (the possibility of which was suggested by L. Richard Turner of the NACA Cleveland staff) amounts to an envelope of the Mach lines in the (supersonic) neighborhood. This behavior is in agreement with a known property of potential limit solutions, namely, that a potential limit point in a flow field lies on an envelope of Mach lines (reference 5).

CIRCULATORY FLOW PAST CIRCULAR ARC MEAN CAMBER LINE

The curvature method was next applied to the calculation of the type of velocity distribution that produces "design" lift, that is, lift without a velocity peak near the nose of the airfoil. The circular arc camber line at zero angle of attack was chosen for this calculation in order that a comparison analogous to that for the Kaplan section could be made (reference 4). The camber ratio assumed was 4 percent, corresponding to an incompressible design lift coefficient of 0.520.

A difficulty of principle arises in obtaining the curvature parameter $\sqrt{YC_a}$ for the circular arc section. The ordinate Y as developed in the curvature method is actually the component in the y-direction of the distance between a point on the airfoil contour and a point on the airfoil streamline infinitely far from the airfoil (the airfoil streamline is the streamline that includes the airfoil contour). In the case of the symmetrical airfoil, this projected distance is the airfoil ordinate as measured from the chord line. When lift is produced, however, a point on the airfoil streamline

infinitely far from the airfoil in the x-direction is also infinitely far from the airfoil in the y-direction. Nevertheless, inasmuch as the slope dy/dx of the airfoil streamline for the circular arc rapidly approaches zero with increasing distance from the circular arc, it might be expected that the velocity distribution on the circular arc would not be critical with respect to the finitely distant point on the airfoil streamline from which the ordinate Y is measured.

This situation was studied by obtaining in the usual manner the compressible velocity increment at the mid-chord location, for curvature parameters $\sqrt{YC_a}$ corresponding to various values of Y as determined by points on the incompressible ($M_o = 0$) airfoil streamline at various distances from the circular arc. The resulting velocity increments $(V-1)_{max}$ are plotted for various free-stream Mach numbers M_o in figure 15 against a quantity f characterizing the distance along the airfoil streamline. The quantity f is the ratio in incompressible flow of the velocity decrement at a point on the airfoil streamline to the maximum velocity increment on the circular arc. As the variable point on the airfoil streamline approaches the circular arc, the value of η decreases from 1.28 at $f = 0.0032$ to the lower limiting value 1 at $f = 0.0102$ corresponding to a distance of 0.67 chord from the extremity of the circular arc. At points on the streamline closer to the circular arc there is no value of η that yields the known incompressible maximum velocity increment for the corresponding value of $\sqrt{YC_a}$. Compressible maximum velocity increments for these points were thereupon arbitrarily obtained from figure 2 using $\eta = 1$.

Included in figure 15 are the maximum-velocity increments calculated from the formulas and constants given in reference 4. The maximum-velocity increment by the curvature method is seen to be always less than Kaplan's value and not to vary greatly with f.

Guided by the results for the Kaplan 10-percent thick symmetrical section, which had about the same incompressible maximum velocity increment as the 4-percent camber circular arc mean line, and also by the comparison with Kaplan's results in figure 15, the curvature parameter $\sqrt{YC_a}$ for obtaining complete velocity distributions was determined with respect to a reference point on the airfoil streamline at which the incompressible velocity decrement was 1 percent of the maximum velocity increment ($f = 0.01$, 0.68 chord from leading edge). The basic data are given in figure 16 and the resulting velocity distributions are compared with the corresponding results by the Kaplan method in figure 17. The velocity distributions at $M_o = 0.8$ by both methods are less than the Prandtl-Meyer solution by about

the same amount and no definite conclusion as to the comparative accuracy of the two methods is indicated. The uncertainty introduced into the results by the ambiguity of determination of the curvature parameter $\sqrt{YC_a}$ could presumably be further resolved by additional comparisons with results by other methods or by calculation of higher approximations by use of the streamline curvature.

COMPRESSIBILITY-CORRECTION RULES

A compressibility-correction rule may be defined as a rule by which the velocity or pressure at a point of a compressible flow field is expressed as a function only of the low-speed, or incompressible, velocity or pressure at that point and the free-stream Mach number. Thus, the curves of figure 2 when cross-plotted against M_o constitute a set of compressibility-correction rules for the velocity V. In general, each value of η yields a compressibility-correction rule. The rules for $\eta = 1.0$ and $\eta = 1.8$ are shown in figure 18 in terms of the pressure coefficient C_p, defined as

$$C_p = \frac{p-p_o}{\frac{1}{2}\rho_o v_o^2} = \frac{\frac{p}{p_o} - 1}{\frac{\gamma}{2} M_o^2} \tag{22}$$

in which p/p_o is given in terms of the velocity V by equation (3). Also shown in figure 18 are the potential limit curves, obtained from figure 7(d), the sonic line ($M = 1$ in equation (17)), and the absolute limit or vacuum line ($p/p_o = 0$ in equation (22)). The difference between the rules for different values of η illustrate the allowance for differences in airfoil shape ($\sqrt{YC_a}$), which correspond to the same low-speed pressure coefficient.

Each compressibility-correction rule has its own potential limit curve. The limit curve for $\eta = 1.8$ intersects the vacuum line and would extend to local velocities higher than that corresponding to zero pressure, which of course is impossible. Hence, where a potential limit curve intersects the vacuum line, the vacuum line becomes the limit curve.

In figure 19 comparison of the compressibility correction rules by the curvature method is made with the rules of

(a) Prandtl-Glauert, equation (14)

(b) Kaplan (reference 3) results for mid-chord location

(c) The rule for $\eta = 1.0$ based on function (15), $C = C_a \left(\frac{\log_e v}{\log_e V}\right)^{\eta}$

(d) Greene (reference 2)

(e) Garrick-Kaplan, "arithmetic-mean" rule of reference 10

(f) von Kármán-Tsien, equation (62) of reference 9

Portions of the potential limit curve corresponding to each rule are indicated.

The compressibility-correction curve corresponding to the curvature function (15) rises somewhat more steeply than that corresponding to equation (8) for the same value of η. It should be noted that the two compressibility correction rules for $\eta = 1$ do not indicate the difference in calculated pressure coefficient at a given point on an airfoil (given $\sqrt{YC_a}$) as a result of choice of curvature function. In figure 19 the curve for curvature function (15) corresponds to $\sqrt{YC_a} = 0.305$ and that for curvature function (8) to $\sqrt{YC_a} = 0.317$. For a given value of $\sqrt{YC_a}$ and low-speed pressure coefficient, the results by both curvature functions differ negligibly.

The Prandtl-Glauert rule has been drawn in figure 19 to the vacuum line ($M = \infty$) because this rule can be regarded as the limit of the rules derivable by the present method as η approaches the value 2.0. This fact becomes evident from equation (10), in which, as η approaches 2.0, the velocity V must approach unity in order for the integral to converge. The approximation leading to the Prandtl-Glauert rule (equation (14)) can therefore be made. As η approaches 2.0 the vacuum line becomes a greater and greater portion of the complete potential limit curve (fig. 18) until in the limit the vacuum line becomes the entire potential limit curve. (See figs. 7(b) and 7(d).)

The Greene rule, on the other hand, can be regarded as the limiting rule obtained by allowing η to approach zero. For $\eta = 0$, equation (10) becomes

$$YC_a = \int_1^V \left[1 - \frac{\gamma-1}{2} M_o^2 \left(v^2-1\right)\right]^{\frac{1}{\gamma-1}} dv - \log_e V \qquad (23)$$

$$= (V_i - 1) - \log_e V_i$$

This last equality, namely V as a function of V_i and M_o, is Greene's rule. As has been shown, the significance of $\eta = 0$ is that the curvature C becomes zero at a finite distance from the airfoil and remains zero for greater distances. Although this circumstance might imply a severe limitation on the validity of

Greene's rule, this particular derivation is actually more restrictive than necessary for it leads not only to Greene's rule but to the additional equation involving YC_a. A more general discussion of Greene's rule is given in appendix B.

In general, the compressibility-correction curves derived in this paper lie between the Prandtl-Glauert curves on the one hand and (approximately) the von Kármán-Tsien curves on the other. It may be emphasized here that the presentation of the present results in the form of a set of compressibility correction rules does not imply an equivalence of these results to a simple speed distortion of the flow field in going from incompressible to compressible flows. Evidently any derived set of compressible-flow patterns for various free-stream Mach numbers can be compared with the corresponding incompressible-flow pattern by means of a set of compressibility correction rules. A simple speed distortion implies the existence of only a single compressibility correction rule from which compressible-flow boundary velocities are obtained from given incompressible-flow boundary velocities regardless of the shape of boundary that produces the incompressible-flow velocities. The present results, however, yield different compressible-flow velocities for the same incompressible velocities depending on the shape of airfoil ($\sqrt{YC_a}$) that produces the incompressible velocities.

SUPERSONIC FLOW

In completely supersonic isentropic potential flow the same equations of motion hold as in the subsonic case, namely, in the form assumed in this paper, equations (1), (2), and (3). The application of these equations, however, to the calculation of the supersonic velocity distribution on airfoils is in certain respects different from the subsonic calculation. The differences as well as similarities will be illustrated by derivation of the linearized (small perturbation) equation for the velocity distribution on an arbitrary thin airfoil in supersonic potential flow.

For small perturbation of the free stream the approximation for the density ratio that led to equation (12) is

$$\rho v - 1 = (1-M_o^2)(v-1) \tag{24}$$

Equation (7) therefore becomes

$$Y = -(M_o^2-1)\int_1^V \frac{(v-1)}{C}\,dv \tag{25}$$

The curvature C is by definition $d\beta/ds$ where s is the distance along a streamline and β is the (positive clockwise) angle between the streamline and a fixed (say the free-stream) direction. Equation (25) may therefore be written

$$Y = -(M_0^2-1)\int_0^{s_a} (v-1)\,\frac{dv}{d\beta}\,ds \qquad (26)$$

in which the path of integration is determined as follows: The assumption is made that at a point in the flow field any field quantity, such as v, $dv/d\beta$, or ds, is constant along a straight line connecting the point with a point on the airfoil and making an angle μ with the free-stream direction. (See sketch.)

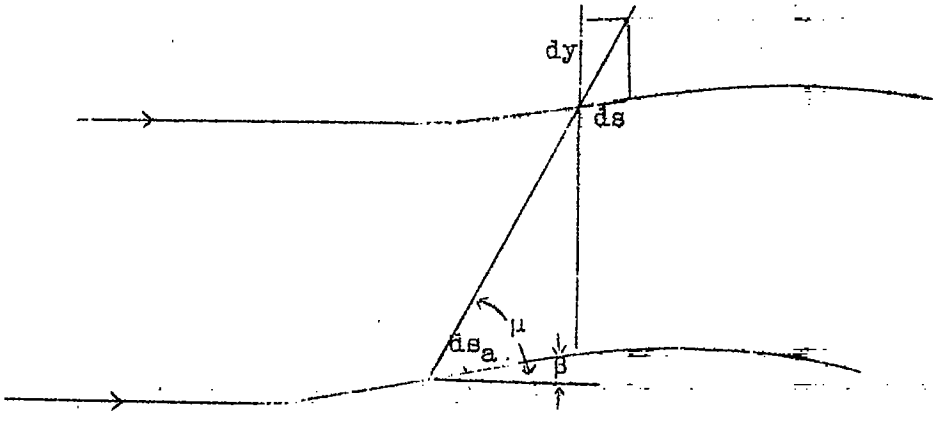

Completely supersonic potential flow

By this assumption a correspondence is set up between points in the field and points on the airfoil for which the integrand in equation (26) has the same value. Hence the original path of integration from infinity to a point on the airfoil in a direction normal to the airfoil can be replaced by a path along the airfoil itself, from the leading edge to the same point, at a distance s_a from the leading edge (the contribution to the integral from points upstream of the leading edge is zero because for such points the straight line at angle μ on which the field quantities are constant does not intersect the airfoil and extends infinitely far ahead of the airfoil, where free-stream conditions exist).

Differentiating both sides of equation (26) with respect to the distance s_a along the airfoil contour yields

$$\frac{dY}{ds_a} = -(M_o^2-1)(v-1)\frac{dv}{d\beta} \tag{27}$$

But $\frac{dY}{ds_a} = -\beta$. Hence

$$\frac{v-1}{\beta}\frac{dv}{d\beta} = \frac{1}{M_o^2-1} \tag{28}$$

Inasmuch as all variables have been assumed to differ from their free-stream values by small amounts, the quotient $\frac{v-1}{\beta}$ can be set equal to the derivative $dv/d\beta$. Equation (28) therefore becomes

$$\frac{dv}{d\beta} = \pm\frac{1}{\sqrt{M_o^2-1}} \tag{29}$$

Finally the significance of the angle μ is obtained from equations (4) and (29), and the sketch of completely supersonic potential flow,

$$\tan\mu = \frac{dy}{ds} = -\frac{dv}{Cvds} = -\frac{dv}{d\beta}$$

$$= \pm\frac{1}{\sqrt{M_o^2-1}} \tag{30}$$

or

$$\sin\mu = \frac{1}{M_o} \tag{31}$$

Hence μ is the Mach angle and equation (29) can be written

$$\frac{dv}{d\beta} = \pm\tan\mu \tag{32}$$

which (recalling that the free-stream velocity is unity) is the basic solution for linearized two-dimensional supersonic flow (reference 8(b)). All the properties of linearized two-dimensional supersonic flow can be deduced from the preceding derivation (these properties were, of course, a guide in setting up the derivation).

The fact that the linearized theory for completely supersonic flows relates streamline curvatures at points connected by Mach lines (characteristics) would indicate that in obtaining higher approximations to the flow pattern in large local or completely supersonic regions the curvature function should properly be specified along Mach lines rather than along normals to the free-stream direction. This circumstance indicates a possible refinement of the present treatment for mixed subsonic-supersonic flows. Consider a mixed subsonic-supersonic flow pattern calculated by the curvature method. The curvature in the local supersonic region can be assumed constant (and equal to the corresponding airfoil curvature) along the characteristics emanating from the airfoil at the appropriate local Mach angle. The curvature function thus determined is continuously joined to the curvature function previously calculated at the boundary of the supersonic region. As a guide in this process the curvature of the streamlines determined by the original calculation could be used (this information would also be of use in determining higher approximations throughout the entire flow field). The equations of motion (1), (2), and (3) are thereupon integrated, graphically or otherwise. If the local supersonic region is small, this procedure may not yield more accurate results than the original calculation. It may, however, yield a closer evaluation of the accuracy of the original calculation than the Prandtl-Meyer solution applied to the local supersonic region.

The preceding remarks also make evident the possible occurrence of a curvature maximum away from the airfoil (in a direction normal to the free stream). Such a maximum will probably occur in a large local supersonic region when the point under consideration on the airfoil is preceded along the airfoil by points of greater airfoil curvature.

BODIES OF REVOLUTION

The method given for the two-dimensional flow can be applied similarly to the case of axially symmetric flow over a body of revolution. Thus, if the symmetrical section (fig. 1) is considered as a meridian section of a body of revolution the continuity condition (equation (6)) becomes (free-stream velocity and density are unity),

$$\frac{Y^2}{2} = \int_Y^\infty (\rho v - 1)\, y\, dy \tag{33}$$

The irrotationality condition (equation (1)) and the Bernoulli-state equation (3) remain unchanged. If the curvature function (8) is assumed, substitution of equations (3), (4), and (9) into equation (33) yields an equation analogous to (10). From this equation a set of basic curves analogous to those of figure 2 could be derived by computation. (The computations would be lessened by use of the curvature function (15) instead of (8) because equation (20) is easier to evaluate than equation (9).)

It will be sufficient here to indicate the results in the case of small disturbance of the free stream, or $v \longrightarrow 1$. In this case equations (9) or (20) yield

$$\frac{y}{Y} - 1 = \frac{(V-1)}{YC_a\,(\eta-1)}\left[\left(\frac{V-1}{v-1}\right)^{\eta-1} - 1\right] \tag{34}$$

Substitution of equations (24), (34), (4), and (8) into (33) gives

$$(V-1)^2\left[1 + \frac{V-1}{YC_a\,(3-2\eta)}\right] = \frac{(2-\eta)}{(1-M_o^2)}\,\frac{YC_a}{2} \tag{35}$$

It may be shown as before that the parameter η is now restricted to the range

$$1 \leqq \eta < 1.5 \tag{36}$$

The parameter η can again be taken as the value that in equation (35) yields the exact (known) velocity increment for $M_o = 0$.

Equation (35) differs in form from the corresponding expression for two-dimensional flow given in equation (12) by virtue of the second term in the brackets. The effect of this term is to reduce the velocity increment for a given M_o, that is, to reduce the effect of speed on the local velocities and pressures. For example, the increase with free-stream Mach number M_o of the maximum velocity increment on slender ellipsoids of revolution is by equation (35) about 70 percent of the increase given by the Prandtl-Glauert rule.

If the curvature function is chosen as

$$C = C_a\left(\frac{v-1}{V-1}\right)^{\eta}\left(\frac{y}{Y}\right)^{\xi} \tag{37}$$

then with $\xi = 1$ a basic equation the same as (10) is obtained, with the exception that $\frac{YC_a}{2}$ replaces YC_a on the left-hand side. Hence the same basic computations as already made for the two-dimensional case could be used here (with $1 \leqq \eta < 2$). Although a more gradual rise of velocity increment with Mach number is thus obtained than for the same section in two-dimensional flow, the rise is greater than given by the Prandtl-Glauert rule. The Prandtl-Glauert rule is, in fact, again the limiting rule for small disturbances. It seems, however, that the Prandtl-Glauert rule may overestimate the effect of subsonic compressibility speeds on slender bodies of revolution.

Perhaps the most reliable way of obtaining compressible velocity distributions for bodies of revolution by use of a single curvature function is to use the function (37) with η and ξ adjusted in each case to satisfy both the known incompressible value and the compressible value for infinitesimally small disturbance of the stream, the compressible value being considered as known or obtainable from the general linear-perturbation theory of compressible fluids. The permissible values of η and ξ that satisfy the required conditions at infinity lie in the acute-angled sectors of the ξ against η plane bounded by the lines $\eta = 1$ and $\xi = 2\eta - 3$.

SUMMARY OF RESULTS

The present study of compressible potential flows past aerodynamic shapes indicates the following:

1. The method presented for the calculation of compressible-flow velocity distributions yields results for symmetrical sections in satisfactory agreement with existing results based on calculation to the third order in the thickness ratio.

2. The results can be presented in the form of a set of compressibility-correction rules that lie between the Prandtl-Glauert rule and the von Kármán-Tsien rule (approximately). The different rules correspond to different values of a local shape parameter $\sqrt{YC_a}$, in which Y is the ordinate and C_a is the curvature at a point on an airfoil.

3. The effect of circulation at design lift conditions, that is, without velocity peaks, can be taken into account.

4. Conditions in the field of the airfoil can be calculated simply.

5. The method given for two-dimensional flow can be applied also to bodies of revolution.

6. The general method of using the streamline curvature appears applicable to any subsonic or supersonic flow problem in which a satisfactorily accurate estimate of the curvature of the streamlines can be made in the portion of the flow field of interest.

Flight Propulsion Research Laboratory,
National Advisory Committee for Aeronautics,
Cleveland, Ohio, May 24, 1946.

APPENDIX A

THE POTENTIAL LIMIT PHENOMENON AND THE ANALOGY WITH FLOW THROUGH A CHANNEL

The points of infinite slope on the basic curves (figs. 2 and 3) have been seen to correspond to limiting solutions for potential flow by the present curvature method. These points correspond to points on an airfoil at which the local Mach number M is greater than 1 and at which the fluid acceleration is infinite if $d\sqrt{YC_a}/ds$ and $d\eta/ds$ are not zero. Furthermore the M = 1 boundary in the flow field contains a cusp if the fluid at the laterally corresponding point on the airfoil has infinite acceleration. This cusp constitutes an envelope of the Mach lines in the (supersonic) neighborhood. These properties permit identification of the points in the flow field corresponding to points of infinite slope on the basic curves with points on the limiting line of reference 5.

In the determination of the essential reason for the existence of a limiting potential flow solution, as well as the significance of the possibilities $d\sqrt{YC_a}/ds = d\eta/ds = 0$, the analogy with the flow through a converging diverging channel is illuminating. Consider first the one-dimensional flow through the channel. The equation of continuity can be written

$$\rho VA = 1 \tag{38}$$

in which A is the cross-sectional area of the channel and all quantities are expressed as fractions of their values at a reference station 0 upstream of the minimum section, called the channel free-stream station. Equation (38) yields with equation (3) a family of curves of velocity V against area A with channel free-stream Mach number M_0 as parameter (fig. 20). These curves exhibit points of infinite slope analogous to those of figure 2. If for the moment only subsonic flow in the channel is considered (branch BC in fig. 20), there exists at C a minimum channel area for given M_0 or for given channel area a maximum M_0 for continuous one-dimensional flow. The fluid acceleration along the axis x of the channel is

$$V \frac{dV}{dx} = V \frac{dV}{dA} \frac{dA}{dx} \tag{39}$$

in which, by equation (38), (18), and (3)

$$\frac{dV}{dA} = \frac{V}{A\,(M^2-1)} \tag{40}$$

At a point of infinite slope in figure 20, $dV/dA = \infty$; hence the fluid acceleration is infinite unless possibly $dA/dx = 0$. The limiting solution occurs, by equation (40), at a local Mach number of unity. Thus, by a one-dimensional argument independent of the irrotationality condition a limiting solution analogous to that for the isolated airfoil has been derived. It may be noted that the upper-branch solutions CD (fig. 20), as well as the upper-branch solutions of the basic curves (fig. 2), correspond to the over-lapping supersonic flow patterns that have been obtained by the hodograph method. (See reference 11.)

The analogy between the channel and the isolated airfoil can be made still closer by consideration of the two-dimensional features of the flow in the minimum section of the channel. As the channel free-stream Mach number M_O is increased by increasing the over-all pressure difference across the channel through external means, the maximum local Mach number at the wall increases at a greater rate. For a sufficiently high but subsonic M_O, local supersonic regions appear in the neighborhood of the walls (fig. 21). This flow pattern corresponds to the solution symmetrical with respect to the y-axis studied by Meyer (reference 12), G. I. Taylor (reference 13), and others. It is analogous to the continuous mixed subsonic-supersonic flow pattern for isolated airfoils. The one-dimensional continuity treatment indicated an upper subsonic limit for M_O. The two-dimensional flow pattern for channels indicates a similar upper limit on M_O and, in addition, provides the desired insight into the isolated airfoil case.

The limit on M_O comes about because the flow at station 0 (fig. 21) must pass through the minimum section. The local mass flow intensity ρv is, however, a maximum at a local Mach number of unity and will be less than the flow intensity at the channel free-stream station in portions of the local supersonic regions AB and FG, which increase as M_O is increased. When a further increase in extent of the local supersonic regions would result in a decreased mass flow through the minimum section from the cause just indicated, then the mass flow has reached its maximum possible value and the channel is said to be "choked."

The explanation for the limiting solution in the isolated airfoil case is similarly formulated. Along the potential line AD traversing the local supersonic region (fig. 1) the mass flow

intensity ratio $\frac{\rho v}{\rho_o v_o}$ is a maximum at the sonic point C and less than unity over a section AB in the supersonic region. When the mass flow intensity, integrated over BD, produces an insufficient mass flow to counterbalance the decreased contribution to the mass flow across AB in accordance with the requirements of continuity and isentropy (equation (6)), then the limit solution for point A on the airfoil has been reached. The flow field, though infinite in extent, can under this condition be said to be choked. Evidently a local supersonic region must exist before the limiting velocity is reached.

The essentially one-dimensional continuity argument just given is not entirely sufficient to prove the existence of a limit solution in the two-dimensional case. Equation (6) alone, for example, could always be satisfied by a suitable choice of $v(y)$; or large streamline curvatures resulting in large flow deflections might set in at supercritical speeds, thus destroying the validity of equation (6). These possibilities are eliminated by the irrotationality condition, which controls and limits the lateral variation of velocity in the flow field. Thus, the isolated airfoil limiting solution is actually produced by the combination of irrotationality, continuity, Bernoulli's equation, equation of state, and boundary conditions in equation (10). The condition of completely irrotational flow is not, however, absolutely necessary for a limit solution. Rotational flows characterized, for example, by almost any function of v on the right-hand side of equation (1) would yield limit solutions, at least for small values of the function (rotation). The equations of motion in the form analyzed appear, in fact, to offer a convenient means of including rotational effects and effects of changes in the equation of state.

Finally, some remarks are made concerning the possible relation of the actual shock wave on an airfoil in the mixed subsonic-supersonic (supercritical) flow regime to the potential limit solution. As noted in references 5 and 14, the observed shock on an airfoil in the supercritical flow regime appears to be formed as a result of the ever-present random pressure disturbances, some of which travel upstream at relative sonic speed and pile up to form the downstream boundary, roughly speaking, of the local supersonic region. In other words, shock would not arise in a completely steady flow; and an increase of free-stream Mach number (a nonsteady effect) would presumably permit attainment of the potential-limit solution. Although it seems possible that the potential-limit solution might in some cases limit the local Mach number at which the shock stabilizes, the maximum local Mach numbers corresponding to the potential limits of this paper are for the most part greater on normal airfoils than those at which the shock stabilizes. Hence, the actual shock normally prevents the potential-limit solution from being reached. There appears to be no direct relation between the two phenomena.

The question as to what would happen if the potential limit solution could be attained in some manner on an isolated airfoil can perhaps best be answered by again considering the converging-diverging channel. In the channel the limit solution can not only be reached (point C in fig. 20) but the second solution (branch CD) can also exist. The mechanism that produces this second solution is the over-all pressure difference across the channel, applied through external means. This pressure difference, when sufficiently increased causes the shock, which has formed in the local supersonic regions in a manner similar to that on an isolated airfoil, to move downstream from the minimum section as a more or less normal shock spanning the channel. The region of the channel between the minimum section and the shock contains the second solution. Thus, the upper branch solution CD can exist as a continuation of the lower branch solution BC with no shock in the neighborhood of the limit solution, point C. The fluid acceleration of equation (39) is finite at the limit point which occurs at the minimum section $dA/dx = 0$. In the isolated airfoil case the analogous occurrence of a potential limit solution at a point where $\frac{d\sqrt{YC_a}}{ds} = \frac{d\eta}{ds} = 0$ (equation (25)) leads to the conjecture whether a similar transition through the potential limit solution could not be effected at such a point. In normal isolated airfoil operation the only mechanism available for increasing the local Mach number is to move the airfoil faster. The over-all ambient pressure remains atmospheric. The fact that in the channel the necessarily asymmetrical boundary conditions of over-all pressure difference (the same channel area at beginning and end of the channel is assumed) can produce an asymmetrical flow pattern containing a transition through the limit solution would therefore indicate that on an isolated airfoil subject to the symmetrical boundary condition of constant atmospheric pressure a transition through the potential limit solution could not be effected. Artificial means, however, such as the proper combination of airfoil shape and suction slot in the airfoil might "pull the shock through" in a local region near the airfoil and thus effect a transition through the potential limit solution to operation on an upper branch of the basic curves, (fig. 3).

APPENDIX B

THE COMPRESSIBILITY CORRECTION RULE OF GREENE

The compressibility correction rule of Greene (reference 2) can be derived as follows: For a fixed airfoil ordinate Y, the right-hand side of equation (7) may be written for both compressible and incompressible flows to yield the equation

$$\int_1^V \frac{\rho v - 1}{Cv}\, dv = \int_1^{V_i} \frac{v_i - 1}{C_i v_i}\, dv_i \tag{41}$$

in which, for a given airfoil, both the compressible and incompressible curvature functions C and C_i satisfy the same boundary conditions.

The Greene rule corresponds to the equation, equivalent to equation (18) of reference 2:

$$\int_1^V \frac{\rho V - 1}{v}\, dv = \int_1^{V_i} \frac{v_i - 1}{v_i}\, dv_i \tag{42}$$

or

$$\int_1^V \rho dv - \log_e V = (V_i - 1) - \log_e V_i \tag{43}$$

For $\gamma = 1.4$, the integral in equation (43) can be evaluated in closed form. The result is:

$$\int_1^V \rho dv = \int_1^V \left[1 - 0.2\, M_o^2\, (v^2 - 1)\right]^{2.5} dv$$

$$= \frac{0.1398}{G(M_o)} \left[F(\varphi) - F(\varphi_o)\right] \tag{44}$$

where

$$G(M_o) = \frac{M_o}{(1 + 0.2\, M_o^2)^3} \tag{45}$$

$$F(\varphi) = \frac{\sin 2\varphi}{6}(\cos 4\varphi + 9\cos 2\varphi + 23) + 5\varphi \qquad (46)$$

$$\sin \varphi_o = \frac{\sqrt{0.2\ M_o}}{\sqrt{1 + 0.2\ M_o^2}} \qquad (47)$$

$$\sin \varphi = V \sin \varphi_o$$

The functions $G(M_o)$ and $F(\varphi)$ are plotted in figures 22 and 23, respectively.

Transition from equation (41) to (42) requires a certain correspondence between the compressible curvature function C and the incompressible curvature function C_i. In order to see this correspondence, consider the integrands of equation (41) plotted against v and v_i, respectively (fig. 24(a)). A one-to-one correspondence between v and v_i can evidently always be established such that the elemental areas making up the integrals in equation (41) are equal, as indicated by the cross-hatched elements in figure 24(a); thus,

$$\frac{\rho v^{-1}}{Cv}\,dv = \frac{v_i^{-1}}{C_i v_i}\,dv_i \qquad (49)$$

Aside from cases where a large local supersonic region exists next to the airfoil, in which case it is possible for the curvature to have a maximum away from the airfoil, as indicated by the dotted line in figure 24(b), the compressible curvature function C and the incompressible curvature function C_i both start from the same value C_a at the airfoil and decrease monotonically (for chordwise stations near that of maximum velocity) to zero at $y = \infty$ or $v = v_i = 1$. Hence, a one-to-one correspondence between v and v_i can be established in figure 24(b) such that $C = C_i$ at corresponding v and v_i. If this one-to-one correspondence is the same as that by which equation (49) was obtained from (41), the curvature functions cancel out of equation (49), which can then be integrated to yield equation (42).

In general, the two correspondences just discussed are not the same. In this case the correspondence in v and v_i leading to equation (49) can be regarded as retained and a compressible curvature function assumed that is obtained by this correspondence from the incompressible curvature function (indicated by the dot-dash line in figure 24(b)). This procedure again yields equation (42) from (49) by cancelation of C and C_i and integration. The compressible curvature function thus set up satisfies the boundary conditions and constitutes the essential approximation of Greene's

rule (in addition to the neglect of the curvature of the potential lines involved in equation (7)).

The potential limit curve corresponding to Greene's rule is that for which

$$\frac{dv}{dv_i} = \infty \tag{50}$$

or, by equation (49)

$$\rho v = 1 \tag{51}$$

REFERENCES

1. Stodola, A.: Steam and Gas Turbines. Vol. II. McGraw-Hill Book Co., Inc., 1927, p. 992.

2. Greene, Leonard Michael: The Attenuation Method for Compressible Flow Systems, Jour. Aero. Sci., vol. 12, no. 3, July 1945, pp. 329-338.

3. Kaplan, Carl: The Flow of a Compressible Fluid Past a Curved Surface. NACA ARR No. 3K02, 1943.

4. Kaplan, Carl: The Flow of a Compressible Fluid Past a Circular Arc Profile. NACA ARR No. L4G15, 1944.

5. Tsien, Hsue-Shen: The "Limiting Line" in Mixed Subsonic and Supersonic Flow of Compressible Fluids. NACA TN No. 961, 1944.

6. Glauert, H.: The Elements of Aerofoil and Airscrew Theory. Univ. Press (Cambridge), 1926.

7. Oswatitsch, Kl., and Wieghardt, K.: Zur Abschätzung der kritischen Machschen Zahl. Zentrale für wissenschaftliches Berichtswesen der Luftfahrtforschung des Generalluftzeugmeisters (ZWB), Tech. Berichte, Bd. 10, Nr. 5, May 1943, pp. 157-159.

8. (a) Taylor, G. I., and Maccoll, J. W.: Two-Dimensional Flow past a Curved Surface. Vol. II of Aerodynamic Theory, div. H, ch. IV, sec. 6, W. F. Durand, ed., Julius Springer (Berlin), 1943 (C.I.T. reprint), pp. 243-249.

   (b) Taylor, G. I., and Maccoll, J. W.: The Motion past Thin Airfoils. Op. cit., sec. 1, pp. 234-236.

9. von Kármán, Th.: Compressibility Effects in Aerodynamics. Jour. Aero. Sci., vol. 8, no. 9, July 1941, pp. 337-356.

10. Garrick, I. E., and Kaplan, Carl: On the Flow of a Compressible Fluid by the Hodograph Method. I - Unification and Extension of Present-Day Results. NACA ACR No. L4C24, 1944.

11. Ringleb, Friedrich: Exakte Lösungen der Differentialgleichungen einer adiabatischen Gasströmung. Z.f.a.M.M., Bd 20, Heft 4, Aug. 1940, pp. 185-198.

12. Meyer, Th.: Ueber zweidimensionale Bewegungsvorgänge in einem Gas, das mit Ueberschallgeschwindigkeit strömt. Forschungsarbeiten auf dem Gebiete des Ingenieurwesens, Heft 62, VDI-Verlag G.m.b.H. (Berlin), 1908, pp. 31-67.

13. Taylor, G. I.: The Flow of Air at High Speeds past Curved Surfaces. R.& M. No. 1381, British A.R.C., 1930.

14. Stack, John: Compressible Flows in Aeronautics. Jour. Aero. Sci., vol. 12, no. 2, April 1945, pp. 127-143; discussion, pp. 143-148.

TABLE I

BASIC CALCULATIONS BY CURVATURE METHOD FOR POSITIVE VELOCITY INCREMENTS

$\log_e V$ / $V-1$		0.04 0.0408	0.08 0.0833	0.12 0.1275	0.16 0.1735	0.20 0.2214	0.24 0.2712	0.28 0.3231	0.32 0.3771	0.36 0.4333	0.40 0.4918	0.44 0.5527
M_o	η	$\sqrt{YC_a}$										
Curvature function, $C = C_a\left(\frac{V-1}{V-1}\right)^{\eta}$												
0	1.0	0.0404	0.0816	0.1237	0.1666	0.2104	0.2552	0.3008	0.3474	0.3950	0.4435	0.4931
	1.2	.0452	.0915	.1388	.1871	.2366	.2872	.3390	.3920	.4462	.5017	.5585
	1.4	.0523	.1059	.1609	.2173	.2752	.3345	.3954	.4579	.5220	.5878	.6554
	1.6	.0642	.1302	.1982	.2681	.3401	.4143	.4906	.5692	.6501	.7335	.8194
	1.8	.0910	.1850	.2823	.3829	.4869	.5945	.7057	.8209	.9400	1.0633	1.1908
	1.9	.1287	.2624	.4010	.5447	.6938	.8485	1.0088	1.1753	1.3479	1.5271	1.7130
.4	1.0	.0369	.0744	.1124	.1509	.1899	.2294	.2694	.3099	.3509	.3923	.4341
	1.2	.0414	.0834	.1262	.1697	.2139	.2588	.3045	.3509	.3980	.4458	.4943
	1.4	.0479	.0966	.1465	.1974	.2493	.3023	.3564	.4116	.4678	.5252	.5837
	1.6	.0587	.1189	.1807	.2441	.3091	.3757	.4441	.5142	.5861	.6598	.7354
	1.8	.0833	.1692	.2580	.3496	.4440	.5416	.6423	.7463	.8536	.9644	1.0788
	1.9	.1179	.2402	.3669	.4982	.6343	.7752	.9212	1.0725	1.2294	1.3919	1.5604
.5	1.0	.0348	.0699	.1055	.1413	.1774	.2137	.2503	.2871	.3240	.3610	.3981
	1.2	.0390	.0785	.1186	.1591	.2001	.2416	.2835	.3259	.3686	.4117	.4551
	1.4	.0452	.0911	.1378	.1853	.2337	.2828	.3327	.3834	.4349	.4871	.5401
	1.6	.0554	.1121	.1702	.2295	.2902	.3523	.4159	.4808	.5472	.6151	.6844
	1.8	.0787	.1597	.2433	.3294	.4181	.5096	.6039	.7011	.8012	.9045	1.0109
	1.9	.1114	.2268	.3463	.4701	.5982	.7308	.8681	1.010	1.1576	1.3101	1.4680
.6	1.0	.0321	.0643	.0965	.1287	.1609	.1931	.2251	.2569	.2883	.3195	.3501
	1.2	.0359	.0721	.1085	.1452	.1820	.2189	.2558	.2928	.3298	.3666	.4032
	1.4	.0415	.0837	.1263	.1695	.2131	.2571	.3015	.3463	.3914	.4368	.4825
	1.6	.0511	.1032	.1563	.2104	.2655	.3216	.3788	.4369	.4960	.5562	.6173
	1.8	.0726	.1472	.2240	.3030	.3842	.4676	.5535	.6418	.7326	.8259	.9219
	1.9	.1028	.2093	.3194	.4332	.5510	.6727	.7986	.9289	1.0636	1.2029	1.3471
.7	1.0	.0285	.0568	.0846	.1122	.1392	.1657	.1915	.2165	.2405	.2634	.2850
	1.2	.0319	.0637	.0955	.1269	.1581	.1888	.2192	.2489	.2779	.3061	.3333
	1.4	.0370	.0741	.1114	.1487	.1860	.2232	.2603	.2972	.3337	.3699	.4055
	1.6	.0455	.0915	.1382	.1855	.2332	.2814	.3301	.3792	.4286	.4784	.5284
	1.8	.0647	.1310	.1989	.2685	.3398	.4128	.4876	.5642	.6426	.7229	.8051
	1.9	.0917	.1865	.2843	.3853	.4895	.5970	.7080	.8226	.9409	1.0631	1.1892
.8	1.0	.0237	.0466	.0686	.0896	.1093	.1276	.1442	.1588	.1711	.1807	.1870
	1.2	.0267	.0525	.0888	.1020	.1253	.1473	.1679	.1868	.2038	.2186	.2307
	1.4	.0308	.0612	.0912	.1205	.1490	.1767	.2033	.2287	.2527	.2751	.2955
	1.6	.0380	.0760	.1140	.1517	.1893	.2266	.2634	.2998	.3355	.3705	.4041
	1.8	.0541	.1092	.1657	.2223	.2802	.3390	.3987	.4594	.5209	.5832	.6464
	1.9	.0769	.1561	.2375	.3212	.4072	.4957	.5866	.6801	.7763	.8752	.9769
.85	1.0	.0206	.0400	.0580	.0743	.0888	.1009	.1102	.1162	.1177	.1135	.1008
	1.2	.0231	.0452	.0660	.0854	.1031	.1187	.1320	.1423	.1492	.1518	.1488
	1.4	.0268	.0529	.0779	.1018	.1243	.1452	.1642	.1810	.1952	.2064	.2139
	1.6	.0331	.0659	.0980	.1296	.1603	.1901	.2188	.2461	.2719	.2959	.3179
	1.8	.0474	.0952	.1436	.1923	.2414	.2907	.3404	.3903	.4403	.4904	.5405
	1.9	.0674	.1365	.2073	.2798	.3541	.4300	.5078	.5875	.6691	.7527	.8382
.9	1.0	.0167	.0315	.0441	.0538	.0600	.0615	.0557	.0348	.0475	.0880	.1251
	1.2	.0187	.0358	.0507	.0652	.0725	.0779	.0779	.0698	.0453	.0534	.1016
	1.4	.0219	.0422	.0608	.0773	.0918	.1027	.1097	.1116	.1067	.0911	.0514
	1.6	.0270	.0531	.0779	.1010	.1224	.1416	.1584	.1721	.1821	.1878	.1879
	1.8	.0390	.0777	.1162	.1543	.1919	.2288	.2651	.3004	.3347	.3678	.3995
	1.9	.0556	.1121	.1696	.2279	.2871	.3472	.4082	.4700	.5327	.5962	.6606
Curvature function, $C = C_a\left(\frac{\log_e V}{\log_e V}\right)^{\eta}$												
0	1.0	.0402	.0808	.1218	.1633	.2052	.2475	.2903	.3335	.3772	.4214	.4660
.5	1.0	.0347	.0693	.1039	.1384	.1729	.2072	.2415	.2752	.3088	.3421	.3750
.6	1.0	.0319	.0636	.0950	.1261	.1568	.1870	.2168	.2460	.2744	.3021	.3290
.7	1.0	.0285	.0561	.0833	.1098	.1355	.1603	.1842	.2068	.2282	.2481	.2664
.8	1.0	.0235	.0460	.0675	.0876	.1062	.1231	.1381	.1508	.1609	.1679	.1712

NATIONAL ADVISORY
COMMITTEE FOR AERONAUTICS

TABLE I - CONTINUED

BASIC CALCULATIONS BY CURVATURE METHOD FOR POSITIVE VELOCITY INCREMENTS - CONTINUED

$\log_e V$		0.48	0.52	0.56	0.60	0.64	0.68	0.72	0.76	0.80	0.84	0.88
$V - 1$		0.6161	0.6820	0.7507	0.8221	0.8965	0.9739	1.0544	1.1383	1.2255	1.3164	1.4109
M_o	η	$\sqrt{YC_a}$										
Curvature function, $C = C_a\left(\frac{V-1}{V-1}\right)^{\eta}$												
0	1.0	0.5438	0.5955	0.6484	0.7023	0.7575	0.8138	0.8713	0.9301	0.9902	1.0516	1.1143
	1.2	.6166	.6761	.7370	.7994	.8632	.9286	.9955	1.064	1.1343	1.2062	1.2798
	1.4	.7247	.7958	.8689	.9439	1.0209	1.0100	1.1812	1.2646	1.3502	1.4383	1.5286
	1.6	.9078	.9990	1.0929	1.1896	1.2893	1.3920	1.4978	1.6070	1.7194	1.8354	1.9549
	1.8	1.3227	1.4593	1.6006	1.7469	1.8983	2.0550	2.2172	2.3852	2.5589	2.7390	2.9252
	1.9	1.9058	2.1059	2.3136	2.5291	2.7527	2.9848	3.2256	3.4758	3.7350	4.0045	4.2839
.4	1.0	.4764	.5190	.5620	.6053	.6489	.6927	.7366	.7808	.8249	.8691	.9132
	1.2	.5435	.5933	.6438	.6949	.7467	.7989	.8518	.9052	.9590	1.0132	1.0678
	1.4	.6433	.7041	.7659	.8289	.8931	.9583	1.0247	1.0922	1.1607	1.2305	1.3012
	1.6	.8129	.8924	.9738	1.0573	1.1428	1.2305	1.3202	1.4123	1.5064	1.6030	1.7017
	1.8	1.1968	1.3187	1.4446	1.5745	1.7087	1.8472	1.9900	2.1378	2.2901	2.4476	2.6099
	1.9	1.7350	1.9159	2.1035	2.2979	2.4994	2.7082	2.9247	3.1493	3.3817	3.6230	3.8730
.5	1.0	.4352	.4722	.5092	.5459	.5823	.6185	.6554	.6878	.7222	.7559	.7887
	1.2	.4989	.5428	.5869	.6312	.6755	.7199	.7641	.8083	.8522	.8959	.9391
	1.4	.5938	.6482	.7033	.7590	.8153	.8722	.9297	.9876	1.0460	1.1048	1.1640
	1.6	.7553	.8276	.9015	.9770	1.0540	1.1326	1.2127	1.2945	1.3778	1.4629	1.5495
	1.8	1.1206	1.2337	1.3502	1.4703	1.5941	1.7216	1.8531	1.9887	2.1283	2.2724	2.4207
	1.9	1.6316	1.8010	1.9764	2.1581	2.3463	2.5412	2.7430	2.9523	3.1687	3.3933	3.6257
.6	1.0	.3802	.4097	.4383	.4661	.4928	.5183	.5425	.5652	.5861	.6052	.6221
	1.2	.4396	.4756	.5111	.5461	.5805	.6140	.6466	.6783	.7088	.7380	.7657
	1.4	.5283	.5742	.6203	.6662	.7121	.7579	.8034	.8486	.8934	.9378	.9817
	1.6	.6793	.7423	.8063	.8711	.9369	1.0035	1.0710	1.1395	1.2086	1.2787	1.3496
	1.8	1.0206	1.1220	1.2263	1.3335	1.4437	1.5571	1.6735	1.7934	1.9165	2.0433	2.1735
	1.9	1.4962	1.6504	1.8100	1.9751	2.1459	2.3226	2.5054	2.6948	2.8904	3.0932	3.3030
.7	1.0	.3237	.3404	.3548	.3668	.3759	.3819	.3842	.3822	.3754	.3629	.3435
	1.2	.3594	.3843	.4076	.4293	.4491	.4668	.4821	.4949	.5047	.5113	.5145
	1.4	.4406	.4749	.5084	.5408	.5722	.6023	.6310	.6581	.6836	.7074	.7292
	1.6	.5787	.6291	.6797	.7302	.7808	.8314	.8817	.9321	.9821	1.0321	1.0819
	1.8	.8893	.9754	1.0636	1.1539	1.2462	1.3408	1.4376	1.5369	1.6384	1.7427	1.8495
	1.9	1.3194	1.4538	1.5926	1.7360	1.8841	2.0371	2.1951	2.3586	2.5272	2.7019	2.8824
.8	1.0	.1894	.1868	.1780	.1603	.1285	.0600	.1160	.1874	.2484	.3060	.3619
	1.2	.2398	.2452	.2462	.2419	.2309	.2108	.1771	.1169	.0957	.1936	.2676
	1.4	.3139	.3297	.3427	.3524	.3584	.3602	.3569	.3476	.3313	.3059	.2684
	1.6	.4376	.4695	.5000	.5291	.5565	.5822	.6059	.6276	.6472	.6581	.6797
	1.8	.7105	.7754	.8411	.9077	.9752	1.0436	1.1129	1.1834	1.2549	1.3278	1.4020
	1.9	1.0815	1.1891	1.2998	1.4138	1.5311	1.6519	1.7764	1.9047	2.0371	2.1739	2.3151
.85	1.0	.0725	.0475	.1135	.1645	.2129	.2609	.3095	.3589	.4091	.4601	.5117
	1.2	.1382	.1158	.0675	.0895	.1575	.2154	.2707	.3255	.3804	.4357	.4913
	1.4	.2169	.2145	.2050	.1858	.1513	.0810	.1228	.2063	.2763	.3417	.4050
	1.6	.3376	.3547	.3688	.3795	.3862	.3886	.3858	.3772	.3617	.3377	.3030
	1.8	.5907	.6408	.6908	.7406	.7904	.8401	.8897	.9393	.9889	1.0390	1.0896
	1.9	.9258	1.0156	1.1076	1.2019	1.2987	1.3980	1.5000	1.6050	1.7129	1.8244	1.9393
.9	1.0	.1628	.2040	.2446	.2870	.3312	.3772	.4248	.4738	.5240	.5749	.6264
	1.2	.1445	.1898	.2335	.2790	.3262	.3753	.4261	.4785	.5322	.5869	.6425
	1.4	.0785	.1402	.1917	.2426	.2944	.3476	.4023	.4586	.5163	.5751	.6349
	1.6	.1807	.1605	.1251	.0281	.1397	.2144	.2815	.3463	.4105	.4748	.5392
	1.8	.4297	.4571	.4835	.5078	.5299	.5496	.5668	.5815	.5936	.6034	.6110
	1.9	.7259	.7914	.8585	.9265	.9956	1.0659	1.1375	1.2107	1.2855	1.3625	1.4417
Curvature function, $C = C_a\left(\frac{\log_e V}{\log_e V}\right)^{\eta}$												
0	1.0	.5112	.5568	.6030	.6497	.6969	.7447	.7930	.8420	.8914	.9415	.9922
.5	1.0	.4074	.4393	.4706	.5012	.5311	.5600	.5879	.6147	.6402	.6644	.6870
.6	1.0	.3548	.3796	.4031	.4253	.4459	.4648	.4818	.4967	.5092	.5192	.5263
.7	1.0	.2828	.2972	.3091	.3185	.3247	.3275	.3263	.3204	.3089	.2905	.2631
.8	1.0	.1699	.1629	.1480	.1207	.0642	.0989	.1659	.2223	.2751	.3263	.3766

592

TABLE I - CONCLUDED

BASIC CALCULATIONS BY CURVATURE METHOD FOR POSITIVE VELOCITY INCREMENTS - CONCLUDED

$\log_e V$		0.92	0.96	1.00	1.04	1.08	1.12	1.16	1.20	1.24	1.28	1.32
$V-1$		1.5093	1.6117	1.7183	1.8292	1.9447	2.0649	2.1899	2.3201	2.4556	2.5986	2.7434
M_o	η	$\sqrt{YC_a}$										
Curvature function, $C = C_a\left(\frac{V-1}{V-1}\right)^{\eta}$												
0	1.0	1.1784	1.2439	1.3108								
	1.2	1.3553	1.4326	1.5118								
	1.4	1.6215	1.7168	1.8148								
	1.6	2.0781	2.2051	2.3361								
	1.8	3.1182	3.3180	3.5249								
	1.9	4.5741	4.8752	5.1879								
.4	1.0	.9572	1.0010	1.0444	1.0875	1.1301	1.1721	1.2133	1.2539	1.2935	1.3321	1.3696
	1.2	1.1228	1.1780	1.2334	1.2889	1.3446	1.4002	1.4558	1.5113	1.5665	1.6216	1.6763
	1.4	1.3730	1.4458	1.5197	1.5945	1.6703	1.7471	1.8248	1.9033	1.9828	2.0632	2.1444
	1.6	1.8029	1.9064	2.0123	2.1208	2.2317	2.3452	2.4613	2.5802	2.7018	2.8261	2.9535
	1.8	2.7777	2.9508	3.1298	3.3141	3.5048	3.7016	3.9047	4.1146	4.3313	4.5551	4.7864
	1.9	4.1321	4.4008	4.6794	4.9680	5.2675	5.5779	5.8996	6.2334	6.5794	6.9382	7.3104
.5	1.0	.8205	.8511	.8805	.9086	.9351	.9600	.9831	1.0045	1.0240	1.0416	1.0576
	1.2	.9818	1.0241	1.0656	1.1064	1.1464	1.1854	1.2236	1.2608	1.2970	1.3323	1.3667
	1.4	1.2235	1.2832	1.3431	1.4033	1.4636	1.5241	1.5847	1.6455	1.7065	1.7677	1.8294
	1.6	1.6578	1.7278	1.8194	1.9128	2.0080	2.1051	2.2039	2.3048	2.4078	2.5131	2.6207
	1.8	2.5737	2.7314	2.8940	3.0616	3.2345	3.4128	3.5967	3.7866	3.9826	4.1849	4.3940
	1.9	3.8665	4.1160	4.3746	4.6424	4.9201	5.2079	5.5060	5.8152	6.1358	6.4681	6.8129
.6	1.0	.6368	.6491	.6586	.6653	.6690	.6696	.6671	.6614	.6527	.6414	.6277
	1.2	.7920	.8165	.8394	.8603	.8795	.8968	.9123	.9261	.9386	.9501	.9610
	1.4	1.0249	1.0675	1.1095	1.1508	1.1914	1.2315	1.2712	1.3105	1.3499	1.3895	1.4298
	1.6	1.4213	1.4939	1.5675	1.6420	1.7176	1.7944	1.8725	1.9523	2.0337	2.1172	2.2031
	1.8	2.3076	2.4456	2.5876	2.7339	2.8847	3.0401	3.2004	3.3660	3.5371	3.7139	3.8971
	1.9	3.5202	3.7451	3.9781	4.2192	4.4693	4.7284	4.9968	5.2753	5.5642	5.8638	6.1750
.7	1.0	.3438	.3155	.2759	.2185	.1206	.1521	.2544	.3311			
	1.2	.5137	.5088	.4994	.4851	.4657	.4407	.4098	.3725			
	1.4	.7491	.7670	.7831	.7972	.8098	.8211	.8315	.8415			
	1.6	1.1316	1.1813	1.2310	1.2811	1.3316	1.3829	1.4353	1.4892			
	1.8	1.9592	2.0719	2.1878	2.3071	2.4302	2.5573	2.6886	2.8246			
	1.9	3.0692	3.2626	3.4628	3.6701	3.8851	4.1081	4.3392	4.5794			
.8	1.0	.4170	.4714	.5851	.5778	.6293						
	1.2	.3341	.3970	.4574	.5159	.5725						
	1.4	.2120	.1107	.1609	.2629	.3419						
	1.6	.6929	.7043	.7142	.7229	.7311						
	1.8	1.4781	1.5561	1.6363	1.7190	1.8048						
	1.9	2.4611	2.6123	2.7690	2.9314	3.1002						
.85	1.0	.5635	.6153	.6666								
	1.2	.5472	.6031	.6586								
	1.4	.4672	.5284	.5888								
	1.6	.2530	.1756	.0859								
	1.8	1.1410	1.1936	1.2478								
	1.9	2.0582	2.1814	2.3092								
.9	1.0	.6780	.7293									
	1.2	.6983	.7542									
	1.4	.7560	.8126									
	1.6	.6038	.6684									
	1.8	.6168	.6214									
	1.9	1.5236	1.6085									
Curvature function, $C = C_a\left(\frac{\log_e V}{\log_e V}\right)^{\eta}$												
0	1.0	1.0435	1.0954	1.1460								
.5	1.0	.7078	.7269	.7439	.7586	.7710	.7808	.7879	.7921	.7932	.7913	.7862
.6	1.0	.5303	.5308	.5275	.5201	.5081	.4911	.4686	.4399	.4044	.3607	.3067
.7	1.0	.2230	.1604	.0534	.1694	.2702	.3374	.3970	.4512			
.8	1.0	.4262	.4751	.5229	.5694	.6143						
$\log_e V$		1.36	1.40	1.44	1.48	1.52	1.56	1.60	1.64	1.68	1.72	
$V-1$		2.8962	3.0552	3.2207	3.3929	3.5722	3.7588	3.9530	4.1552	4.3656	4.5845	
M_o	η	$\sqrt{YC_a}$										
Curvature function, $C = C_a\left(\frac{V-1}{V-1}\right)^{\eta}$												
.4	1.0	1.4061	1.4413	1.4753	1.5081	1.5398	1.5705	1.6003	1.6295	1.6585	1.6876	
	1.2	1.7308	1.7848	1.8386	1.8920	1.9453	1.9985	2.0518	2.1055	2.1597	2.2149	
	1.4	2.2265	2.3096	2.3937	2.4788	2.5652	2.6528	2.7420	2.8329	2.9258	3.0210	
	1.6	3.0838	3.2172	3.3539	3.4939	3.6375	3.7849	3.9363	4.0921	4.2524	4.4175	
	1.8	5.0253	5.2721	5.5273	5.7909	6.0636	6.3458	6.6373	6.9397	7.2522	7.5761	
	1.9	7.6965	8.0968	8.5121	8.9429	9.3899	9.8537	10.3354	10.8353	11.3540	11.8923	
.5	1.0	1.0719	1.0846	1.0964	1.1074	1.1181						
	1.2	1.4005	1.4338	1.4668	1.5000	1.5337						
	1.4	1.8916	1.9546	2.0186	2.0838	2.1507						
	1.6	2.7309	2.8433	2.9599	3.0792	3.2022						
	1.8	4.6102	4.8336	5.0648	5.3040	5.5518						
	1.9	7.1707	7.5417	7.9269	8.3265	8.7415						
Curvature function, $C = C_a\left(\frac{\log_e V}{\log_e V}\right)^{\eta}$												
.5	1.0	0.7780	0.7669	0.7531	0.7371	0.7195						

NATIONAL ADVISORY COMMITTEE FOR AERONAUTICS

TABLE II

BASIC CALCULATIONS BY CURVATURE METHOD FOR NEGATIVE VELOCITY INCREMENTS

$\log_e \frac{V}{V-1}$		-0.04 -0.0392	-0.12 -0.1131	-0.20 -0.1813	-0.28 -0.2442	-0.36 -0.3023	-0.44 -0.3560	-0.52 -0.4055	-0.60 -0.4512
M_o	η	$\sqrt{YC_a}$							
Curvature function, $C = C_a\left(\frac{V-1}{V-1}\right)^{\eta}$									
0	1.0	0.0396	0.1165	0.1904	0.2615	0.3299	0.3958	0.4592	0.5203
	1.2	.0443	.1299	.2118	.2902	.3654	.4374	.5065	.5729
	1.4	.0510	.1494	.2429	.3320	.4169	.4979	.5751	.6488
	1.6	.0624	.1820	.2950	.4018	.5029	.5986	.6892	.7751
	1.8	.0880	.2555	.4124	.5592	.6967	.8256	.9465	1.0599
	1.9	.1243	.3597	.5787	.7824	.9721	1.1486	1.3131	1.4663
4.4	1.0	.0366	.1077	.1767	.2437	.3086	.3716	.4325	.4915
	1.2	.0406	.1199	.1963	.2700	.3411	.4097	.4759	.5396
	1.4	.0469	.1377	.2248	.3082	.3883	.4650	.5385	.6090
	1.6	.0573	.1676	.2724	.3720	.4667	.5568	.6425	.7241
	1.8	.0808	.2348	.3796	.5156	.6434	.7635	.8666	.9829
	1.9	.1140	.3302	.5317	.7195	.8947	1.0580	1.2105	1.3528
.5	1.0	.0345	.1022	.1684	.2330	.2958	.3570	.4165	.4743
	1.2	.0385	.1138	.1869	.2578	.3265	.3930	.4574	.5197
	1.4	.0444	.1307	.2138	.2939	.3710	.4451	.5165	.5852
	1.6	.0541	.1588	.2587	.3540	.4448	.5316	.6144	.6934
	1.8	.0764	.2223	.3598	.4892	.6112	.7261	.8344	.9366
	1.9	.1078	.3123	.5033	.6815	.8480	1.0034	1.1487	1.2845
.6	1.0	.0319	.0953	.1577	.2191	.2793	.3382	.3958	.4521
	1.2	.0356	.1059	.1748	.2420	.3076	.3716	.4337	.4942
	1.4	.0411	.1215	.1996	.2753	.3486	.4196	.4882	.5545
	1.6	.0501	.1475	.2409	.3306	.4166	.4990	.5780	.6537
	1.8	.0706	.2060	.3340	.4550	.5693	.6774	.7797	.8764
	1.9	.0996	.2890	.4662	.6319	.7870	.9322	1.0681	1.1954
.7	1.0	.0286	.0862	.1438	.2012	.2581	.3143	.3697	.4240
	1.2	.0319	.0958	.1591	.2217	.2834	.3441	.4035	.4617
	1.4	.0367	.1096	.1812	.2513	.3199	.3868	.4520	.5153
	1.6	.0448	.1327	.2179	.3004	.3801	.4571	.5314	.6031
	1.8	.0631	.1848	.3005	.4106	.5152	.6147	.7092	.7991
	1.9	.0890	.2587	.4180	.5675	.7080	.8400	.9639	1.0804
.8	1.0	.0243	.0746	.1261	.1784	.2312	.2840	.3366	.3887
	1.2	.0270	.0825	.1389	.1957	.2526	.3092	.3653	.4207
	1.4	.0312	.0941	.1574	.2205	.2831	.3450	.4059	.4658
	1.6	.0380	.1135	.1880	.2613	.3331	.4033	.4718	.5384
	1.8	.0532	.1568	.2566	.3525	.4447	.5331	.6179	.6991
	1.9	.0749	.2186	.3544	.4828	.6042	.7190	.8675	.9301
.85	1.0	.0216	.0669	.1147	.1641	.2145	.2654	.3164	.3673
	1.2	.0240	.0740	.1260	.1793	.2334	.2877	.3419	.3958
	1.4	.0275	.0841	.1422	.2010	.2601	.3186	.3771	.4349
	1.6	.0335	.1010	.1689	.2359	.3030	.3691	.4341	.4978
	1.8	.0469	.1389	.2286	.3156	.4000	.4817	.5605	.6366
	1.9	.0659	.1928	.3137	.4287	.5382	.6422	.7412	.8352
.9	1.0	.0182	.0580	.1015	.1475	.1952	.2441	.2935	.3431
	1.2	.0203	.0638	.1109	.1603	.2112	.2630	.3152	.3675
	1.4	.0230	.0722	.1242	.1782	.2334	.2891	.3450	.4007
	1.6	.0279	.0860	.1460	.2072	.2688	.3305	.3918	.4524
	1.8	.0390	.1170	.1946	.2712	.3466	.4205	.4927	.5630
	1.9	.0548	.1612	.2639	.3628	.4580	.5494	.6371	.7212

NATIONAL ADVISORY
COMMITTEE FOR AERONAUTICS

$\log_e \frac{V}{V-1}$		-0.08 -0.0769	-0.16 -0.1479	-0.24 -0.2134	-0.32 -0.2739	-0.40 -0.3297	-0.48 -0.3812	-0.56 -0.4288	-0.64 -0.4727
M_o	η	$\sqrt{YC_a}$							
Curvature function, $C = C_a\left(\frac{\log_e V}{\log_e V}\right)^{\eta}$									
0	1.0	0.0793	0.1569	0.2331	0.3078	0.3812	0.4533	0.5241	0.5936
.5	1.0	.0693	.1382	.2068	.2750	.3425	.4094	.4757	.5412
.6	1.0	.0643	.1291	.1940	.2590	.3237	.3882	.4523	.5160
.7	1.0	.0580	.1172	.1775	.2384	.2998	.3612	.4226	.4839
.8	1.0	.0496	.1020	.1563	.2122	.2692	.3269	.3852	.4437

TABLE II - CONCLUDED

BASIC CALCULATIONS BY CURVATURE METHOD FOR NEGATIVE VELOCITY INCREMENTS - CONCLUDED

$\log_e V$ / $V-1$		-0.68 / -0.4934	-0.76 / -0.5323	-0.84 / -0.5683	-0.92 / -0.6015	-1.00 / -0.6321	-1.08 / -0.6604	-1.16 / -0.6865	-1.24 / -0.7106
M_o	η	$\sqrt{YC_a}$							
		Curvature function, $C = C_a\left(\frac{V-1}{V-1}\right)^{\eta}$							
0	1.0	0.5792	0.6361	0.6909	0.7439	0.7951	0.8445	0.8924	0.9387
	1.2	.6364	.6976	.7564	.8129	.8673	.9197	.9702	1.0189
	1.4	.7192	.7864	.8508	.9123	.9713	1.0277	1.0819	1.1339
	1.6	.8566	.9339	1.0073	1.0770	1.1434	1.2065	1.2666	1.3239
	1.8	1.1664	1.2664	1.3603	1.4487	1.5319	1.6102	1.6840	1.7537
	1.9	1.6090	1.7422	1.8663	1.9823	2.0905	2.1915	2.2860	2.3744
.4	1.0	.5487	.6041	.6577	.7097	.7601	.8089	.8563	.9022
	1.2	.6012	.6605	.7177	.7730	.8264	.8779	.9277	.9758
	1.4	.6767	.7416	.8039	.8638	.9212	.9765	1.0296	1.0807
	1.6	.8017	.8757	.9462	1.0134	1.0775	1.1387	1.1972	1.2530
	1.8	1.0830	1.1774	1.2662	1.3501	1.4292	1.5039	1.5745	1.6412
	1.9	1.4857	1.6099	1.7259	1.8344	1.9358	2.0308	2.1198	2.2031
.5	1.0	.5304	.5850	.6379	.6894	.7393	.7877	.8348	.8805
	1.2	.5800	.6383	.6947	.7492	.8020	.8530	.9024	.9502
	1.4	.6512	.7148	.7759	.8348	.8914	.9459	.9985	1.0491
	1.6	.7688	.8408	.9095	.9753	1.0381	1.0982	1.1557	1.2108
	1.8	1.0329	1.1239	1.2097	1.2909	1.3676	1.4402	1.5089	1.5739
	1.9	1.4114	1.5302	1.6413	1.7454	1.8428	1.9342	2.0198	2.1002
.6	1.0	.5070	.5605	.6126	.6633	.7127	.7607	.8075	.8530
	1.2	.5529	.6099	.6652	.7188	.7708	.8213	.8702	.9176
	1.4	.6185	.6803	.7400	.7976	.8532	.9069	.9587	1.0088
	1.6	.7263	.7958	.8624	.9263	.9875	1.0463	1.1026	1.1567
	1.8	.9680	1.0546	1.1366	1.2144	1.2881	1.3579	1.4242	1.4872
	1.9	1.3147	1.4265	1.5314	1.6298	1.7221	1.8088	1.8903	1.9669
.7	1.0	.4774	.5296	.5807	.6306	.6793	.7269	.7733	.8185
	1.2	.5185	.5739	.6279	.6805	.7316	.7814	.8298	.8768
	1.4	.5769	.6366	.6945	.7506	.8050	.8577	.9087	.9581
	1.6	.6721	.7386	.8026	.8642	.9234	.9806	1.0355	1.0884
	1.8	.8845	.9658	1.0430	1.1165	1.1865	1.2530	1.3165	1.3769
	1.9	1.1899	1.2929	1.3898	1.4810	1.5668	1.6477	1.7240	1.7959
.8	1.0	.4402	.4910	.5409	.5900	.6380	.6851	.7311	.7761
	1.2	.4753	.5288	.5813	.6327	.6830	.7320	.7798	.8265
	1.4	.5243	.5816	.6375	.6919	.7449	.7965	.8466	.8954
	1.6	.6032	.6660	.7269	.7859	.8430	.8982	.9516	1.0033
	1.8	.7770	.8515	.9229	.9913	1.0567	1.1194	1.1794	1.2369
	1.9	1.0271	1.1189	1.2057	1.2878	1.3656	1.4393	1.5091	1.5753
.85	1.0	.4178	.4679	.5172	.5658	.6135	.6603	.7062	.7512
	1.2	.4491	.5017	.5534	.6042	.6539	.7026	.7502	.7967
	1.4	.4918	.5477	.6025	.6561	.7084	.7594	.8091	.8575
	1.6	.5601	.6209	.6800	.7376	.7935	.8477	.9003	.9514
	1.8	.7100	.7807	.8486	.9141	.9769	1.0374	1.0955	1.1514
	1.9	.9246	1.0095	1.0903	1.1671	1.2401	1.3095	1.3755	1.4384
.9	1.0	.3926	.4419	.4906	.5388	.5862	.6328	.6786	.7235
	1.2	.4195	.4711	.5220	.5722	.6215	.6699	.7173	.7637
	1.4	.4559	.5104	.5641	.6168	.6684	.7189	.7682	.8164
	1.6	.5121	.5707	.6281	.6842	.7389	.7922	.8441	.8946
	1.8	.6314	.6977	.7621	.8243	.8845	.9427	.9989	1.0532
	1.9	.8018	.8790	.9529	1.0237	1.0913	1.1561	1.2180	1.2774

NATIONAL ADVISORY
COMMITTEE FOR AERONAUTICS

$\log_e V$ / $V-1$		-0.72 / -0.5133	-0.80 / -0.5507	-0.88 / -0.5852	-0.96 / -0.6171				
M_o	η	$\sqrt{YC_a}$							
		Curvature function, $C = C_a\left(\frac{\log_e V}{\log_e V}\right)^{\eta}$							
0	1.0	0.6620	0.7292	0.7953	0.8604				
.5	1.0	.6060	.6700	.7332	.7957				
.6	1.0	.5791	.6416	.7035	.7647				
.7	1.0	.5450	.6057	.6660	.7258				
.8	1.0	.5023	.5609	.6193	.6774				

592

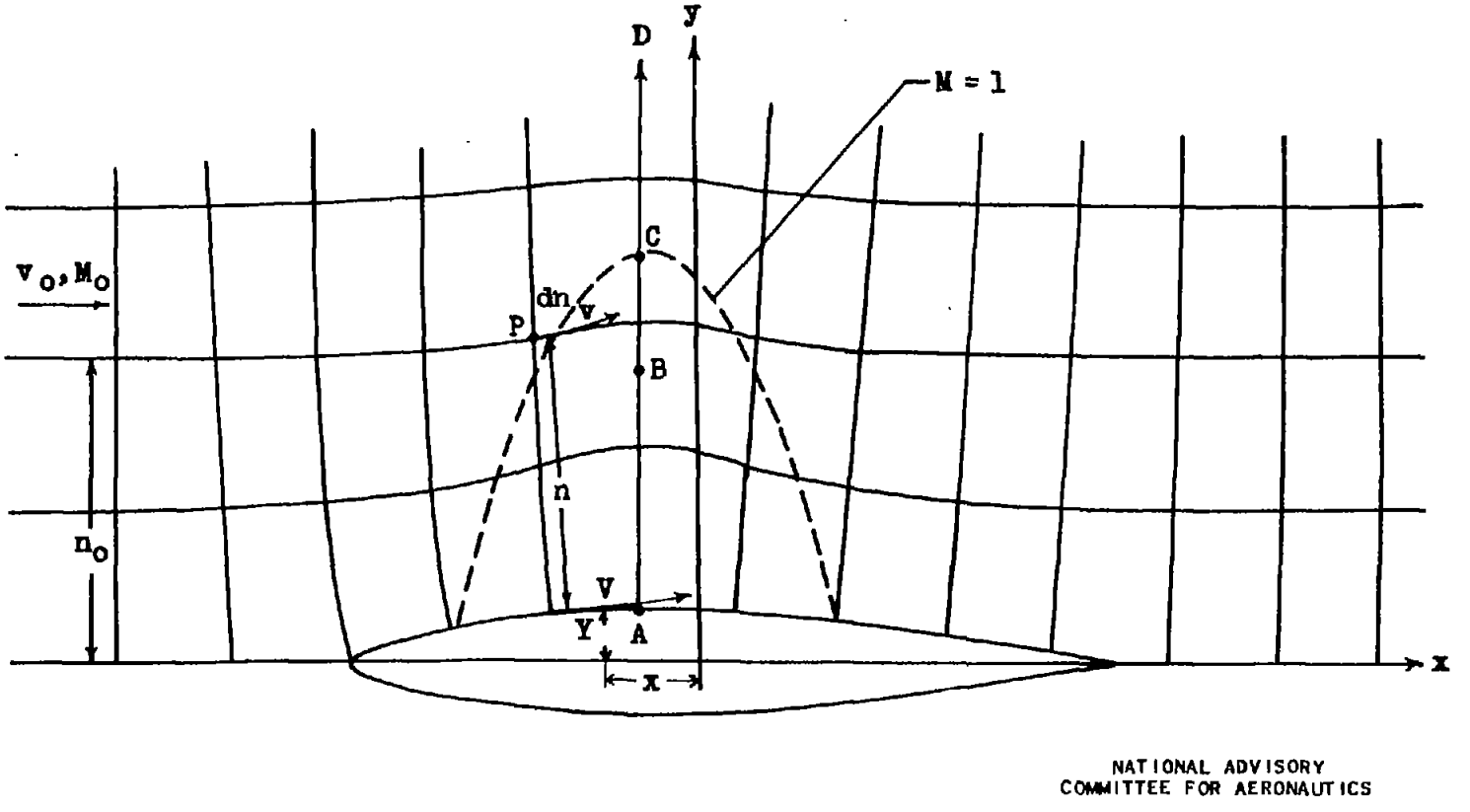

Figure 1.- Compressible potential flow past symmetrical airfoil.

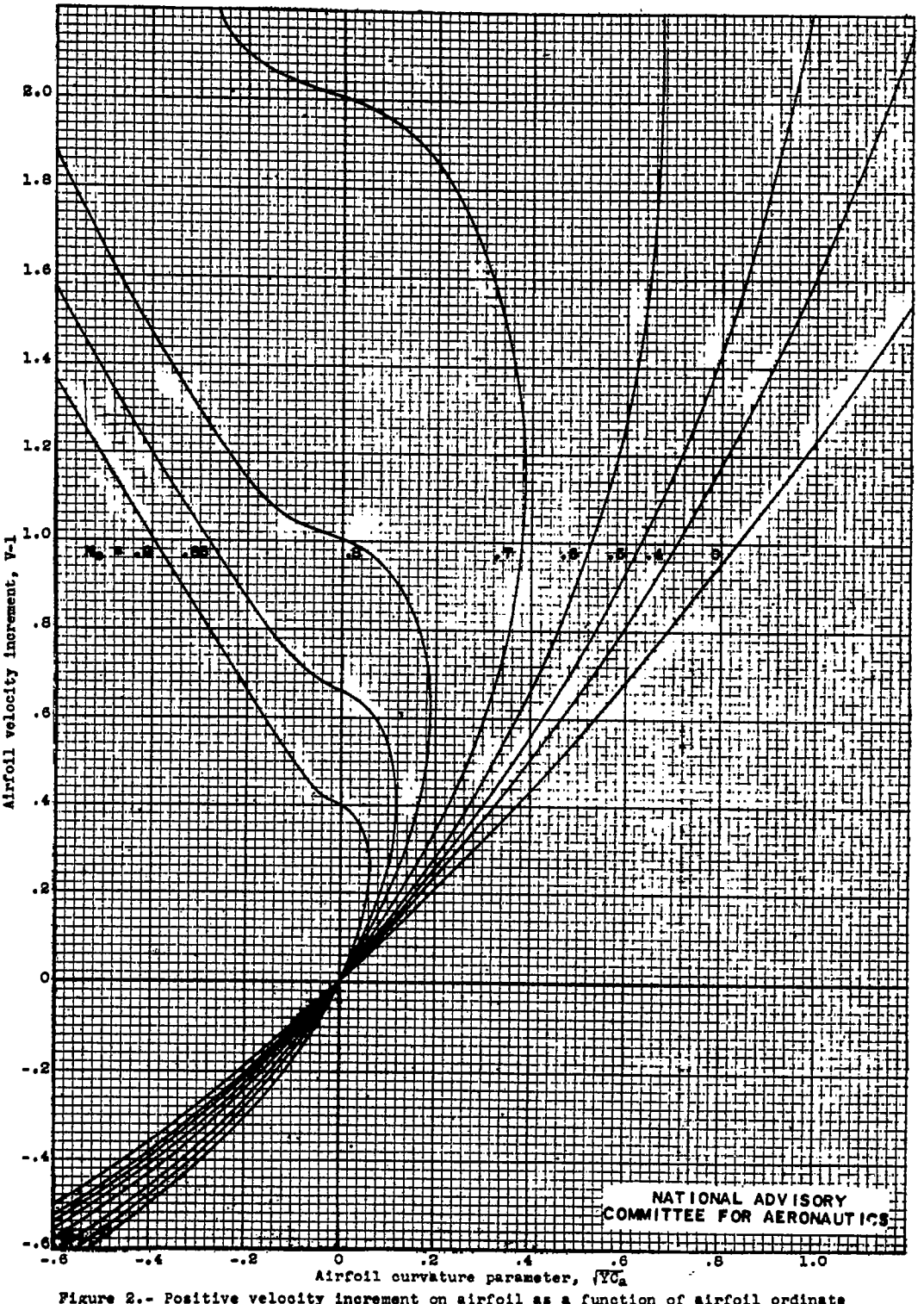

Figure 2.- Positive velocity increment on airfoil as a function of airfoil ordinate Y and airfoil curvature C_a for various values of free-stream Mach number M_o. Values computed from equation (10) and tabulated in table I. $\eta = 1.0$.

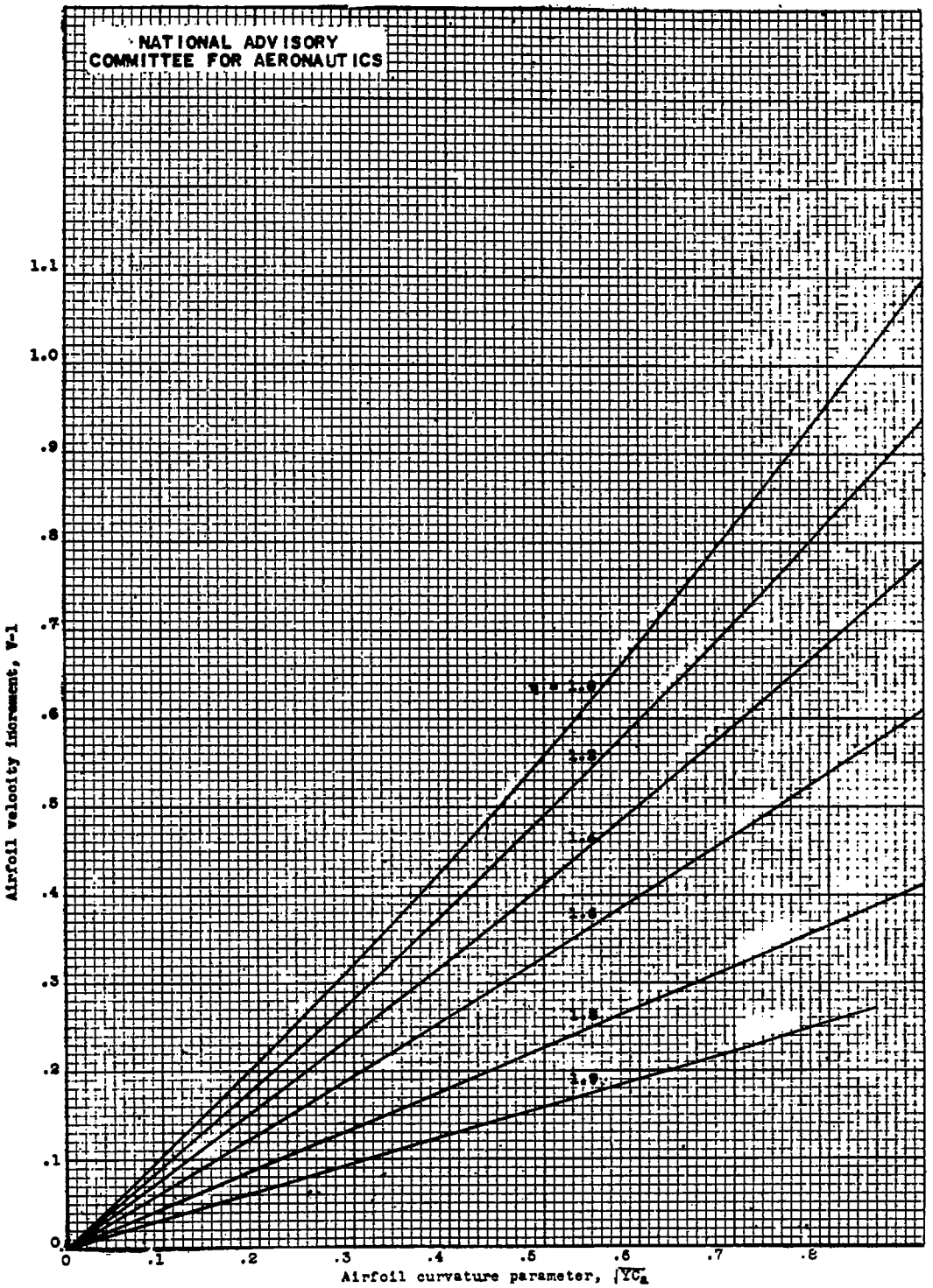

(a) Free-stream Mach number $M_0 = 0$.

Figure 3.- Positive velocity increment on airfoil as a function of airfoil ordinate Y and airfoil curvature C_a for various values of η. Values computed from equation (10) for $V > 1$ and tabulated in table I.

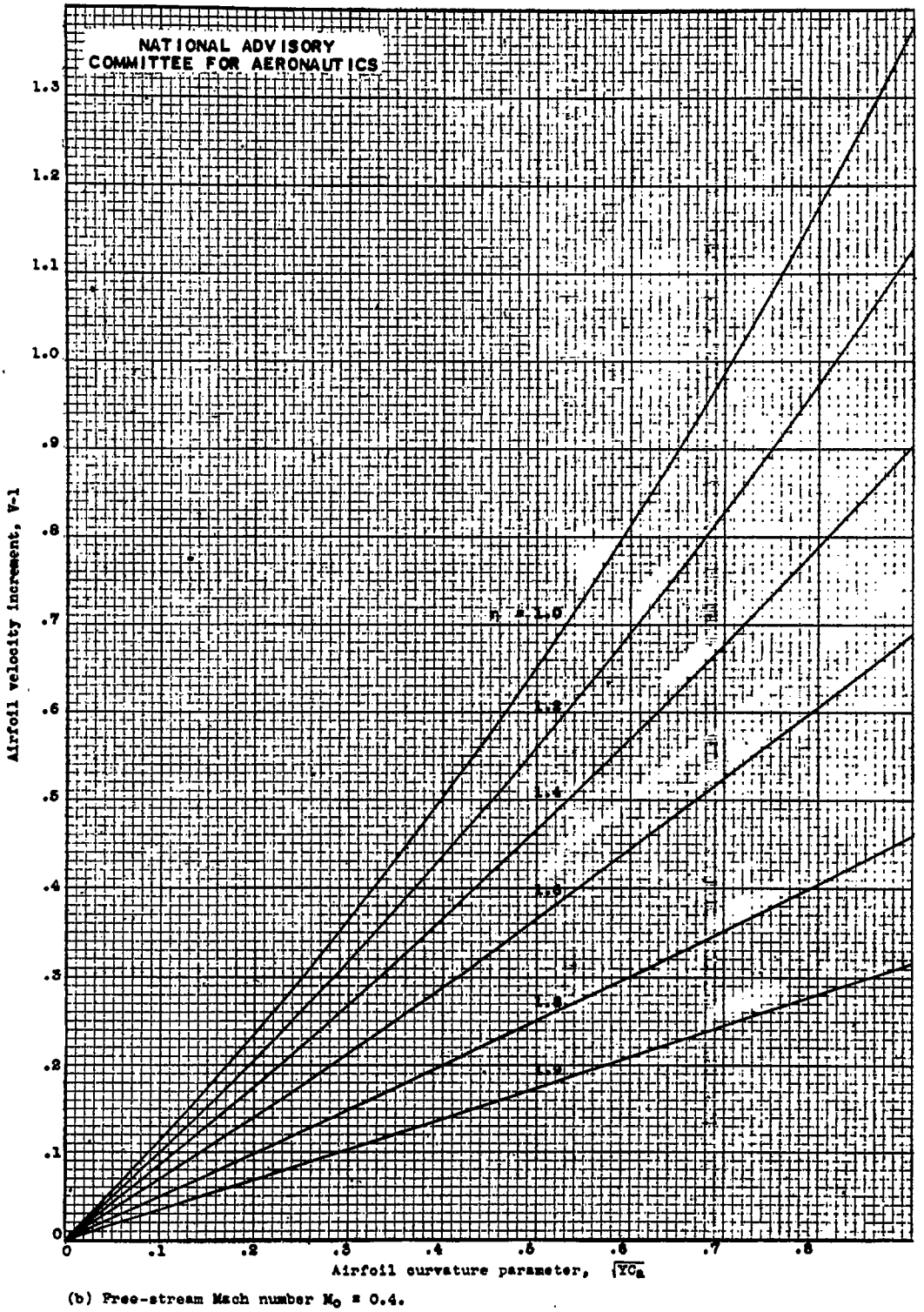

(b) Free-stream Mach number M_0 = 0.4.

Figure 3.- Continued. Positive velocity increment on airfoil as a function of airfoil ordinate Y and airfoil curvature C_a for various values of η. Values computed from equation (10) for V > 1 and tabulated in table I.

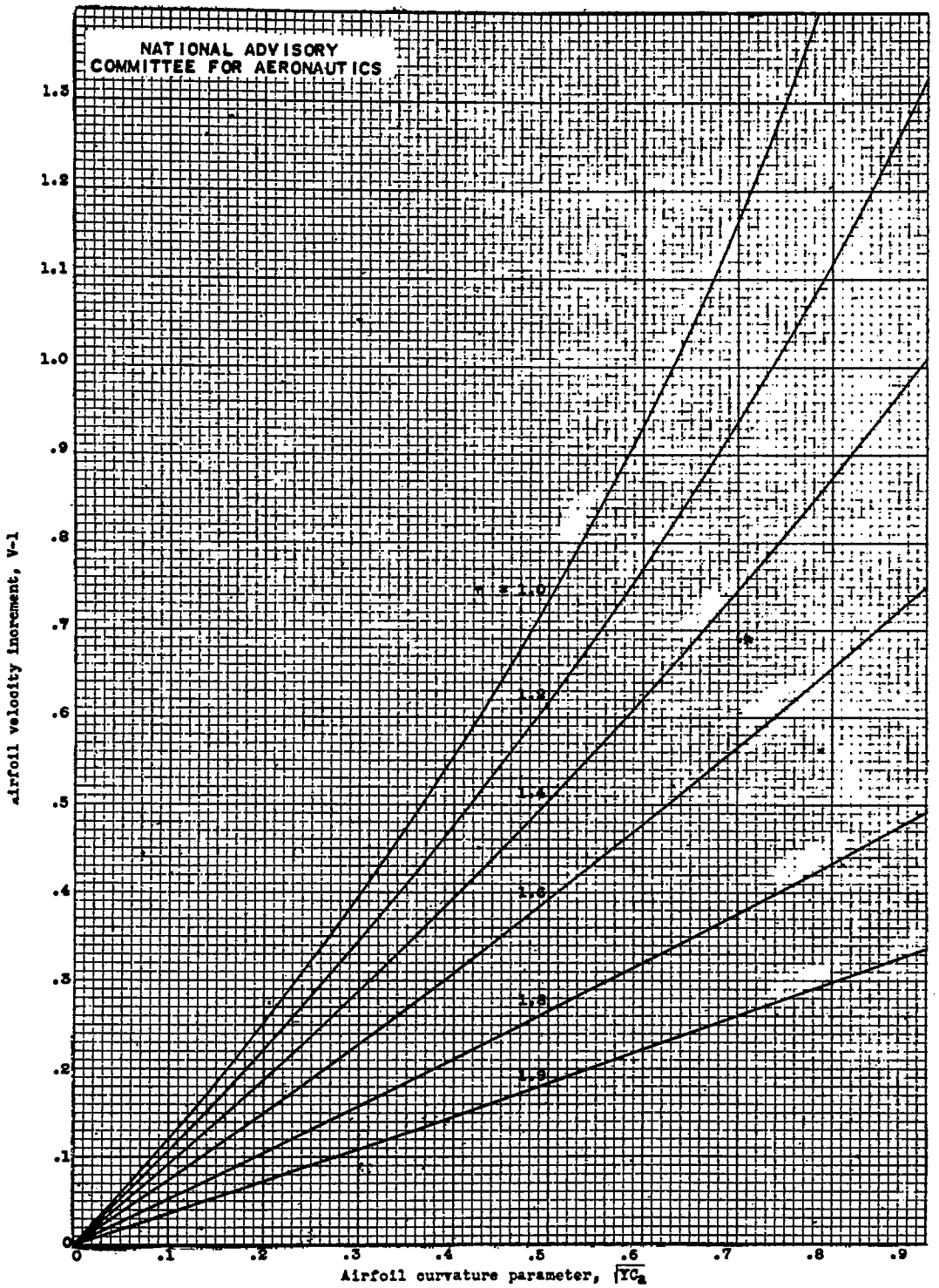

(c) Free-stream Mach number $M_0 = 0.5$.

Figure 3.- Continued. Positive velocity increment on airfoil as a function of airfoil ordinate Y and airfoil curvature C_a for various values of η. Values computed from equation (10) for $V > 1$ and tabulated in table I.

Fig. 3d

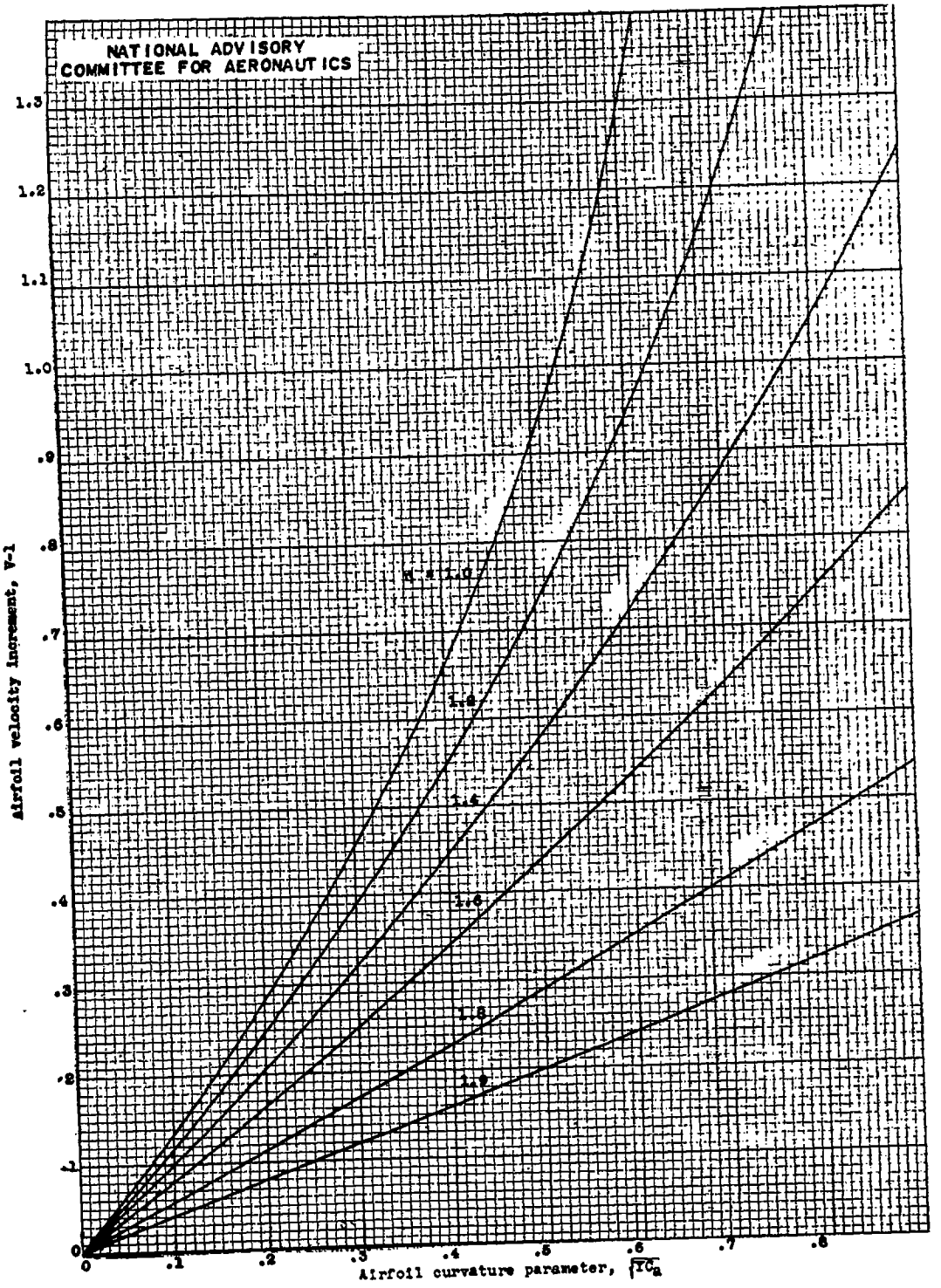

(d) Free-stream Mach number $M_0 = 0.6$.

Figure 3.- Continued. Positive velocity increment on airfoil as a function of airfoil ordinate Y and airfoil curvature C_a for various values of η. Values computed from equation (10) for $V > 1$ and tabulated in table I.

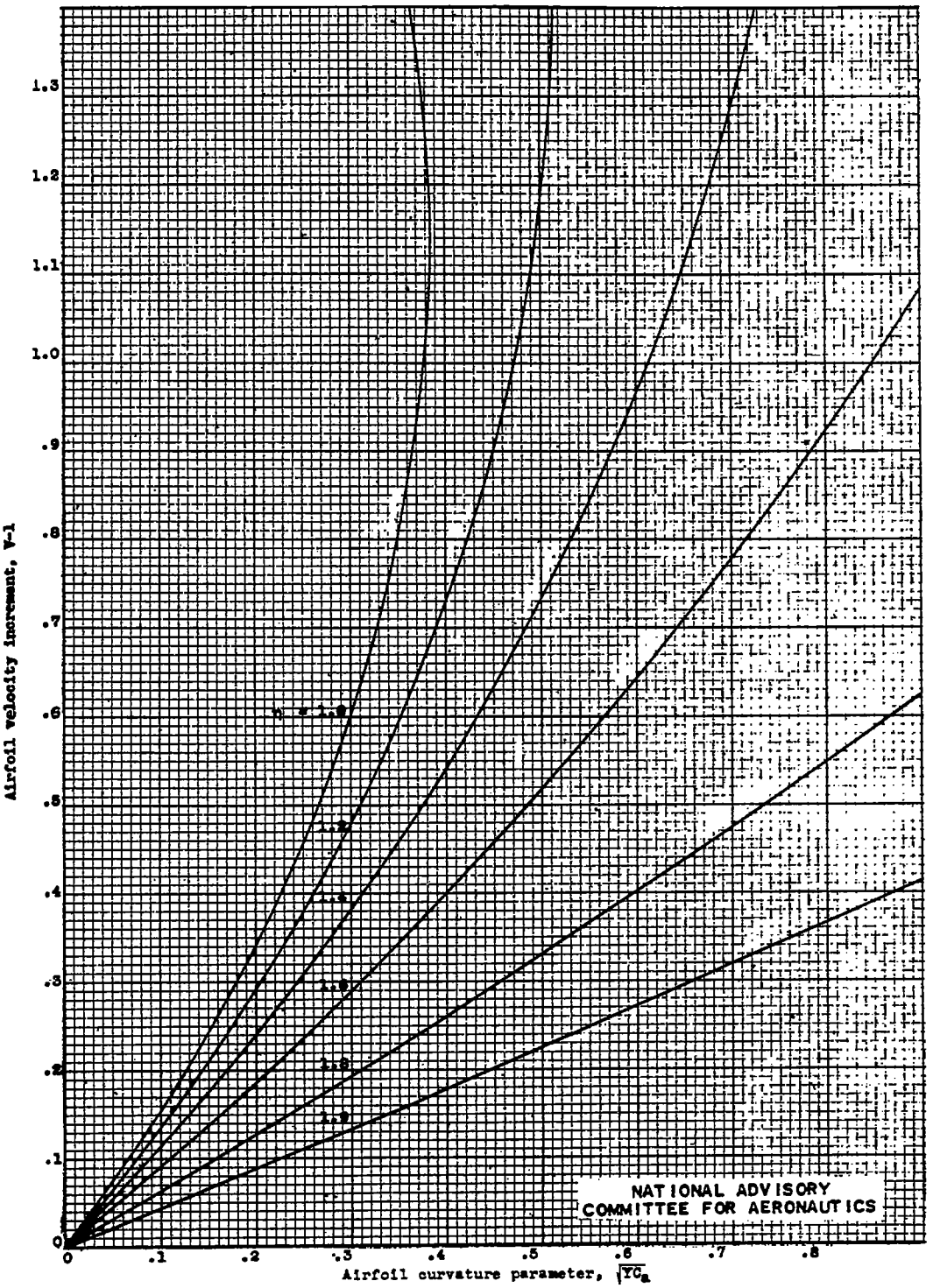

(e) Free-stream Mach number $M_0 = 0.7$.

Figure 3.- Continued. Positive velocity increment on airfoil as a function of airfoil ordinate Y and airfoil curvature C_a for various values of η. Values computed from equation (10) for $V > 1$ and tabulated in table I.

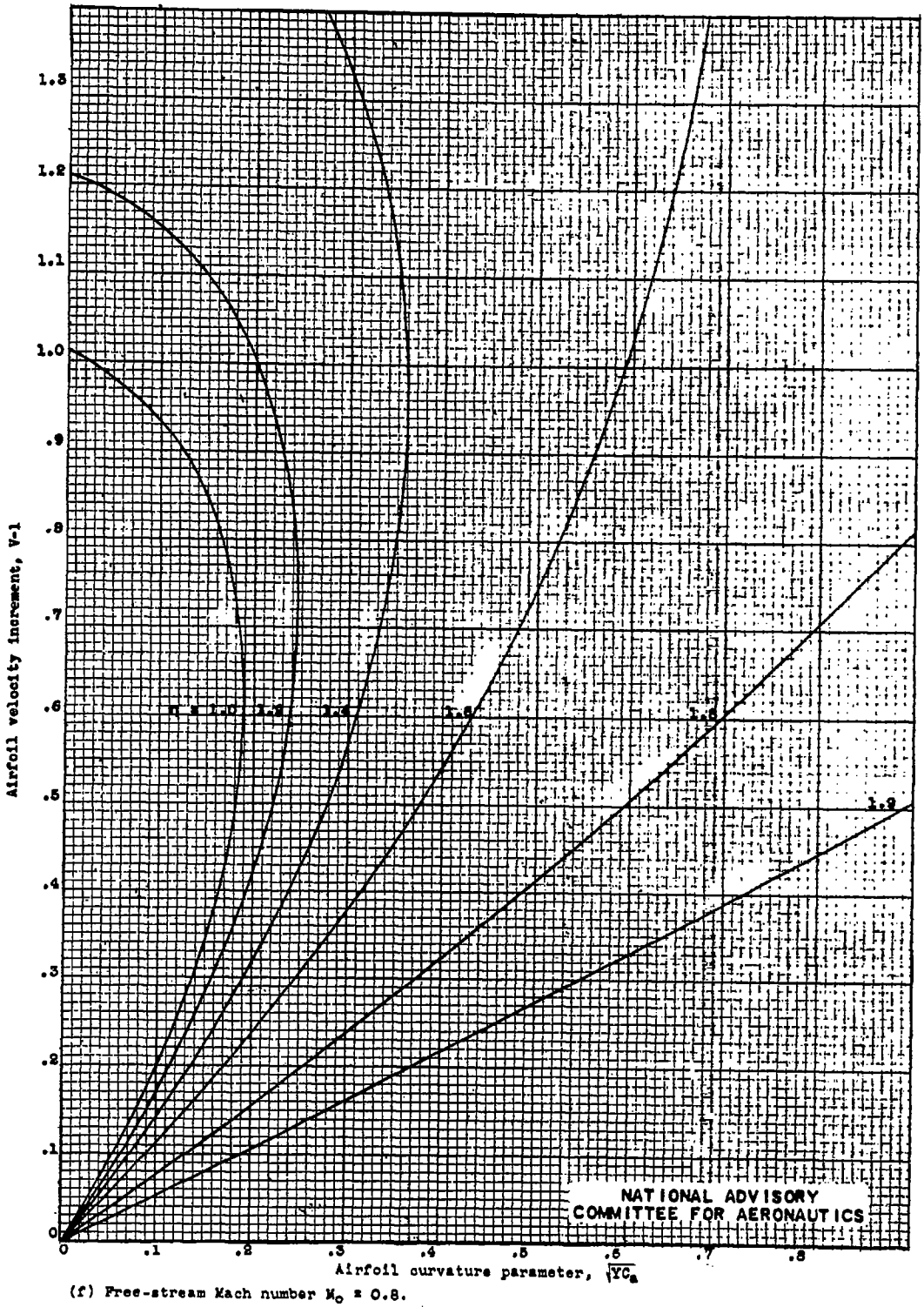

(f) Free-stream Mach number $M_0 = 0.8$.

Figure 3.- Continued. Positive velocity increment on airfoil as a function of airfoil ordinate Y and airfoil curvature C_a for various values of η. Values computed from equation (10) for V >1 and tabulated in table I.

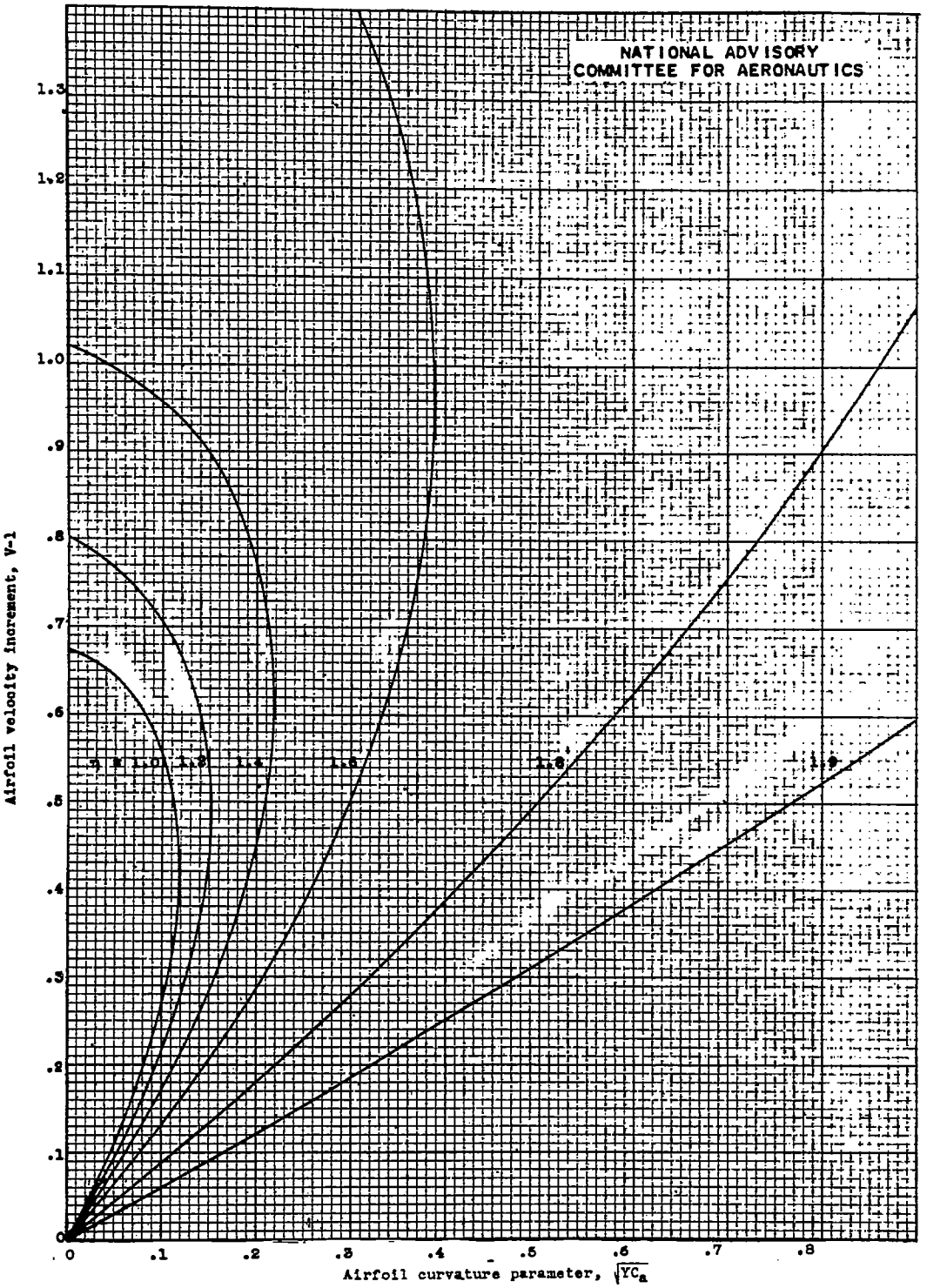

(g) Free-stream Mach number M_o = 0.85.

Figure 3.- Continued. Positive velocity increment on airfoil as a function of airfoil ordinate Y and airfoil curvature C_a for various values of η. Values computed from equation (10) for V >1 and tabulated in table I.

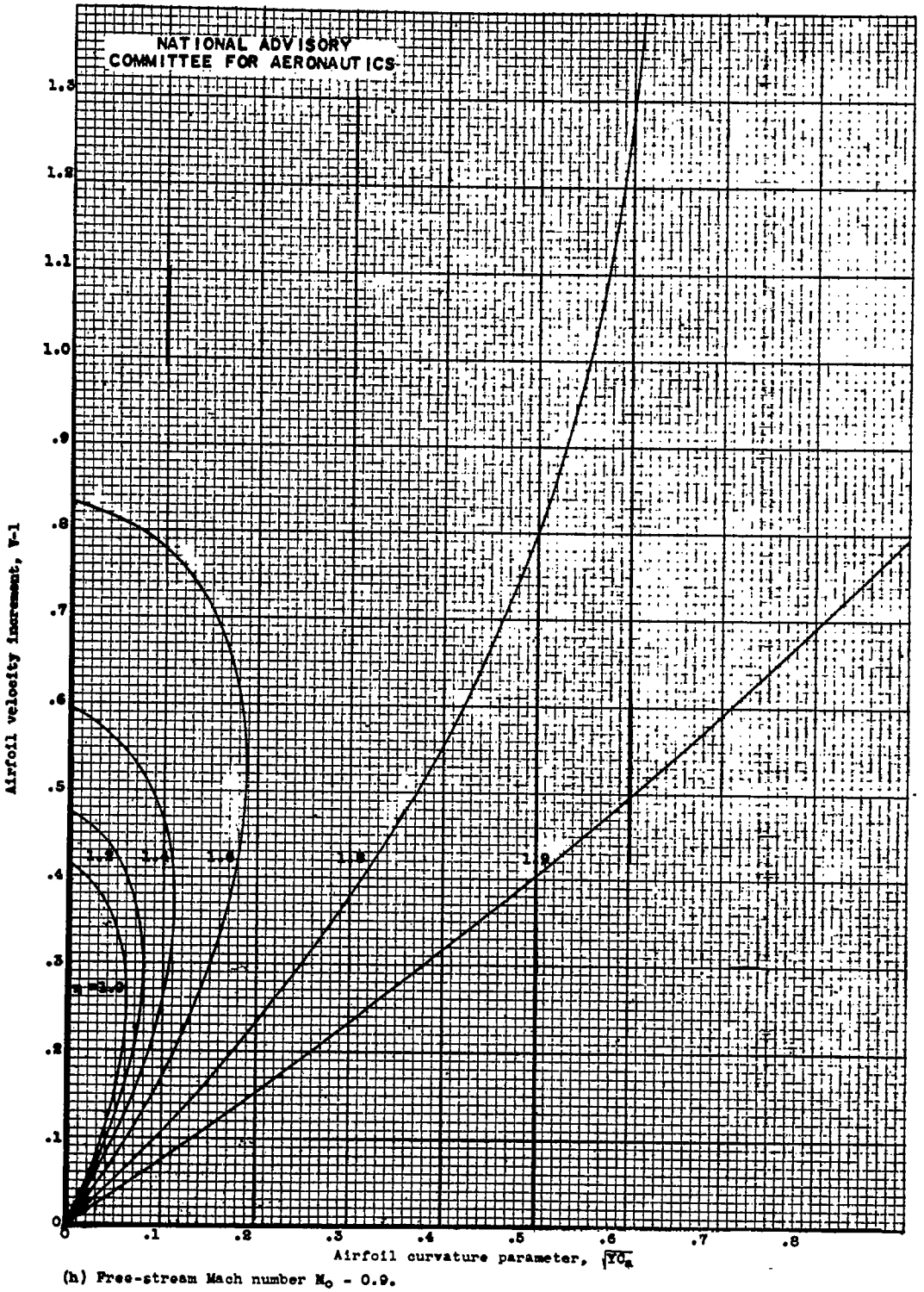

(h) Free-stream Mach number M_o = 0.9.

Figure 3.- Concluded. Positive velocity increment on airfoil as a function of airfoil ordinate Y and airfoil curvature C_a for various values of η. Values computed from equation (10) for V > 1 and tabulated in table I.

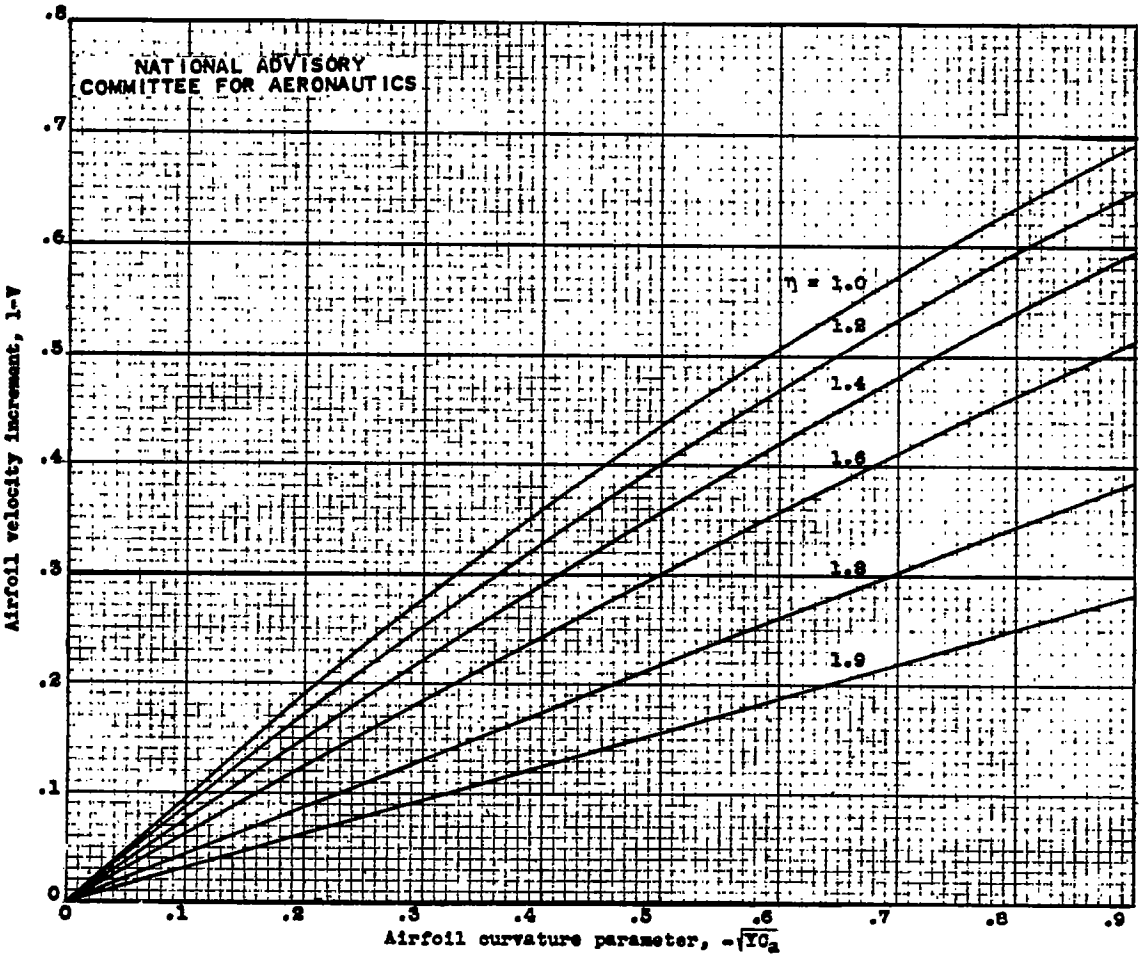

(a) Free-stream Mach number $M_0 = 0$.

Figure 4.- Negative velocity increment on airfoil as a function of airfoil ordinate Y and airfoil curvature C_a for various values of η. Values computed from equation (10) for $V<1$ and tabulated in table II.

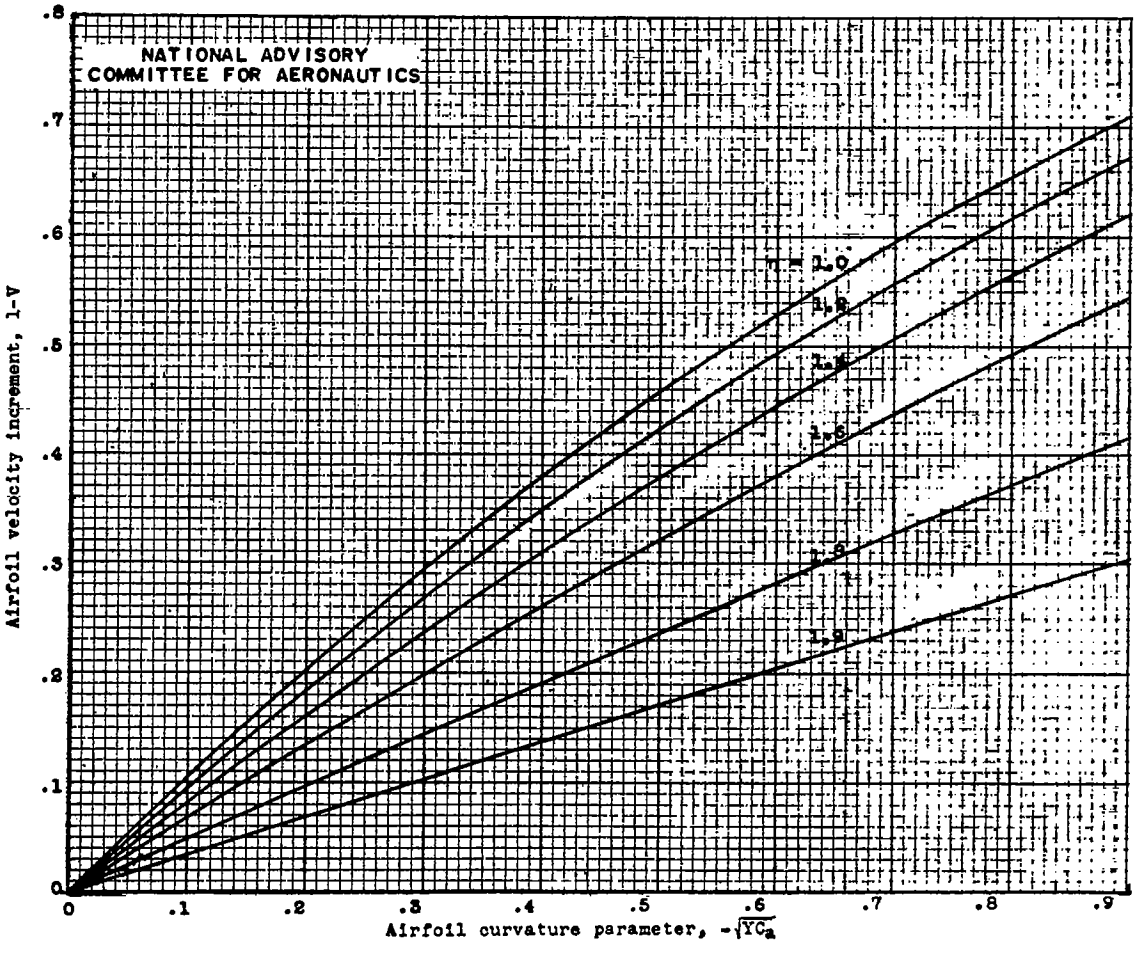

(b) Free-stream Mach number M_0 = 0.4.

Figure 4.- Continued. Negative velocity increment on airfoil as a function of airfoil ordinate Y and airfoil curvature C_a for various values of η. Values computed from equation (10) for $V < 1$ and tabulated in table II.

592

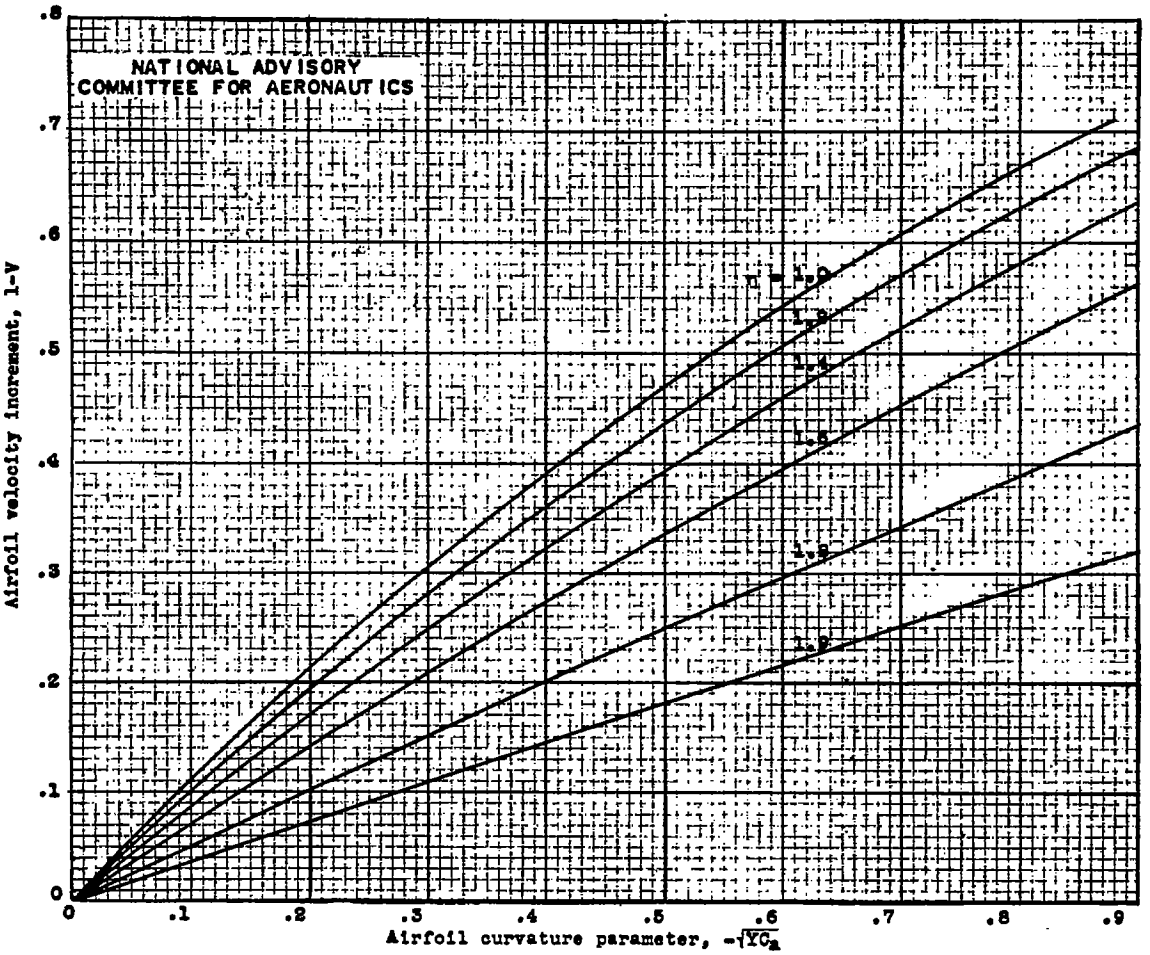

(c) Free-stream Mach number M_o = 0.5.

Figure 4.- Continued. Negative velocity increment on airfoil as a function of airfoil ordinate Y and airfoil curvature C_a for various values of η. Values computed from equation (10) for V < 1 and tabulated in table II.

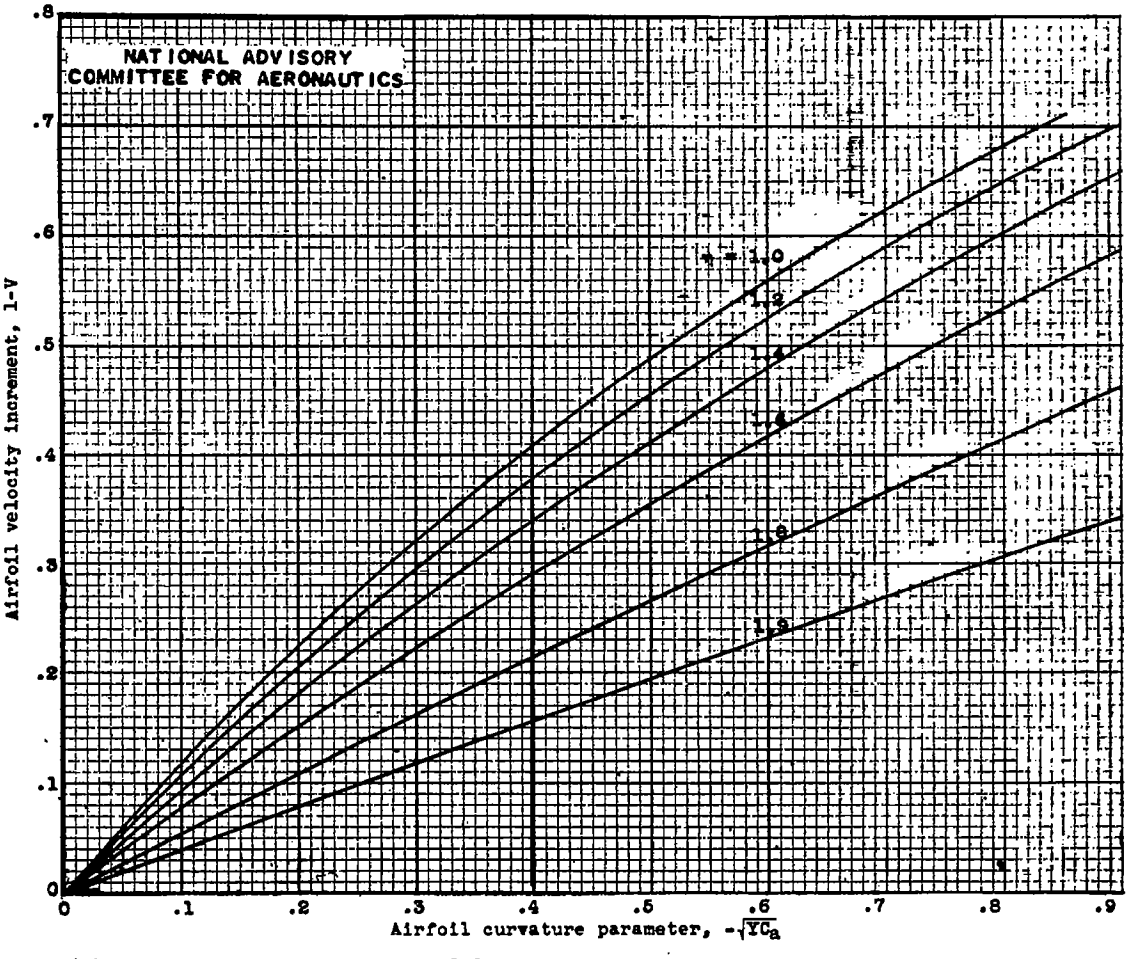

(d) Free-stream Mach number M_o = 0.6.

Figure 4.- Continued. Negative velocity increment on airfoil as a function of airfoil ordinate Y and airfoil curvature C_a for various values of η. Values computed from equation (10) for V < 1 and tabulated in table II.

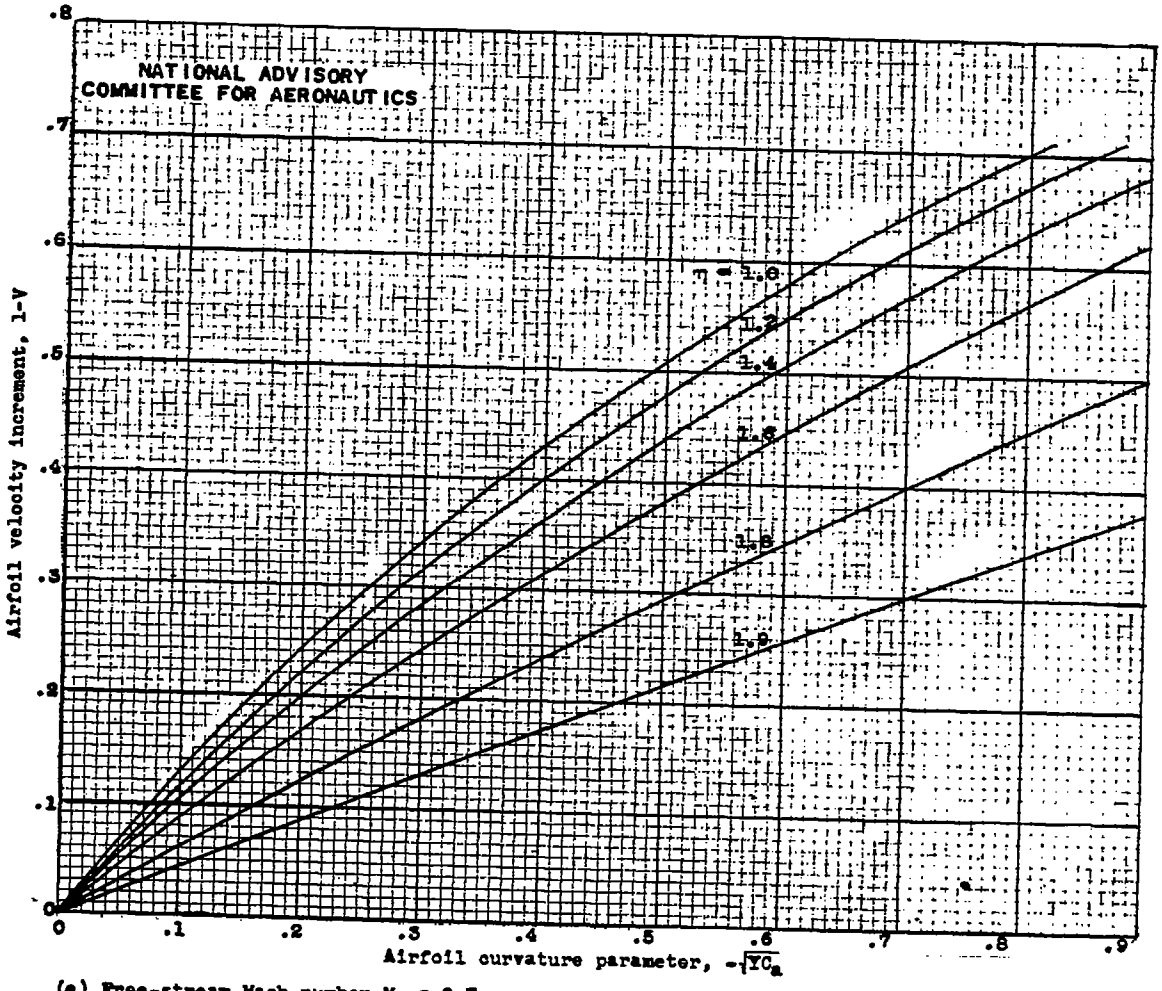

(e) Free-stream Mach number $M_o = 0.7$.

Figure 4.- Continued. Negative velocity increment on airfoil as a function of airfoil ordinate Y and airfoil curvature C_a for various values of η. Values computed from equation (10) for $V < 1$ and tabulated in table II.

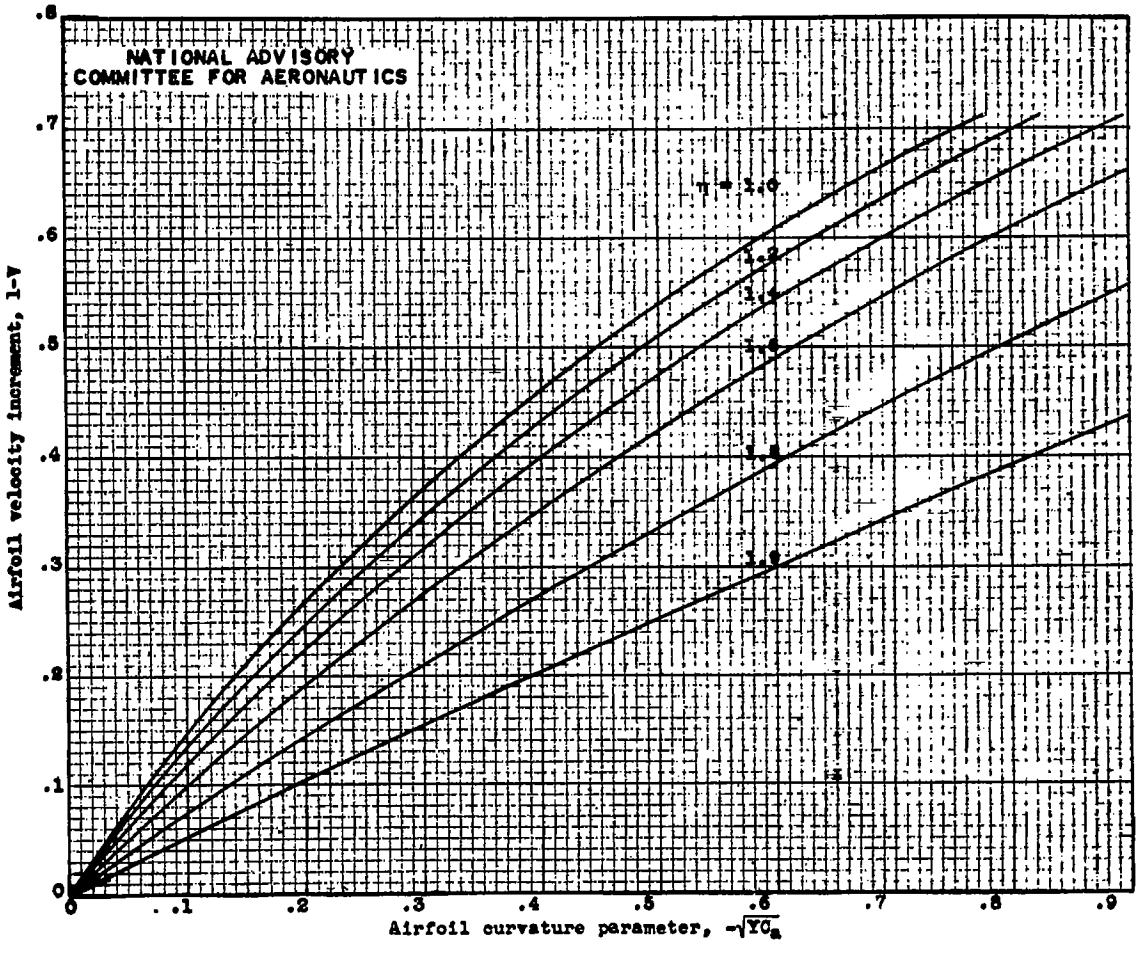

(f) Free-stream Mach number $M_0 = 0.8$.

Figure 4.- Continued. Negative velocity increment on airfoil as a function of airfoil ordinate Y and airfoil curvature C_a for various values of η. Values computed from equation (10) for $V < 1$ and tabulated in table II.

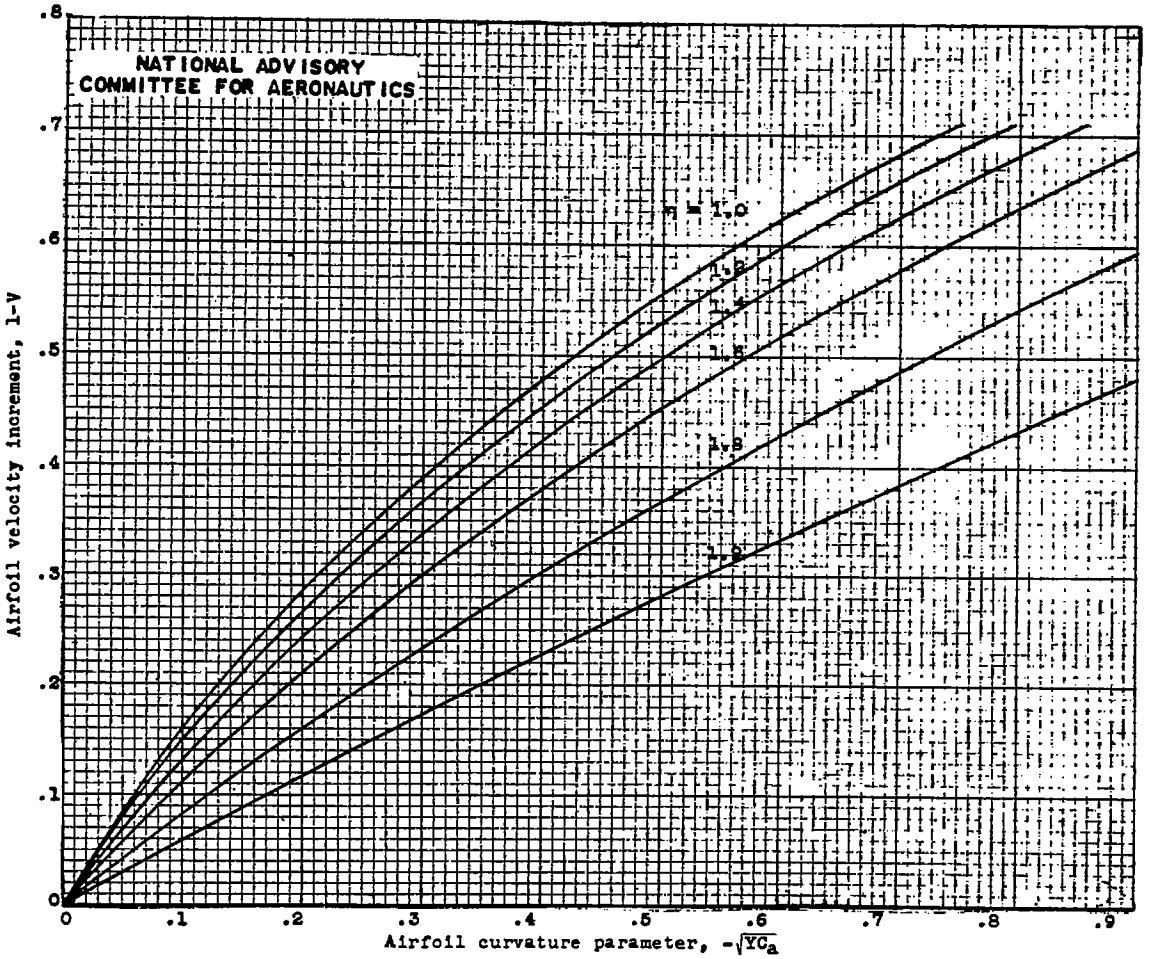

(g) Free-stream Mach number M_o = 0.85.

Figure 4.- Continued. Negative velocity increment on airfoil as a function of airfoil ordinate Y and airfoil curvature C_a for various values of η. Values computed from equation (10) for V < 1 and tabulated in table II.

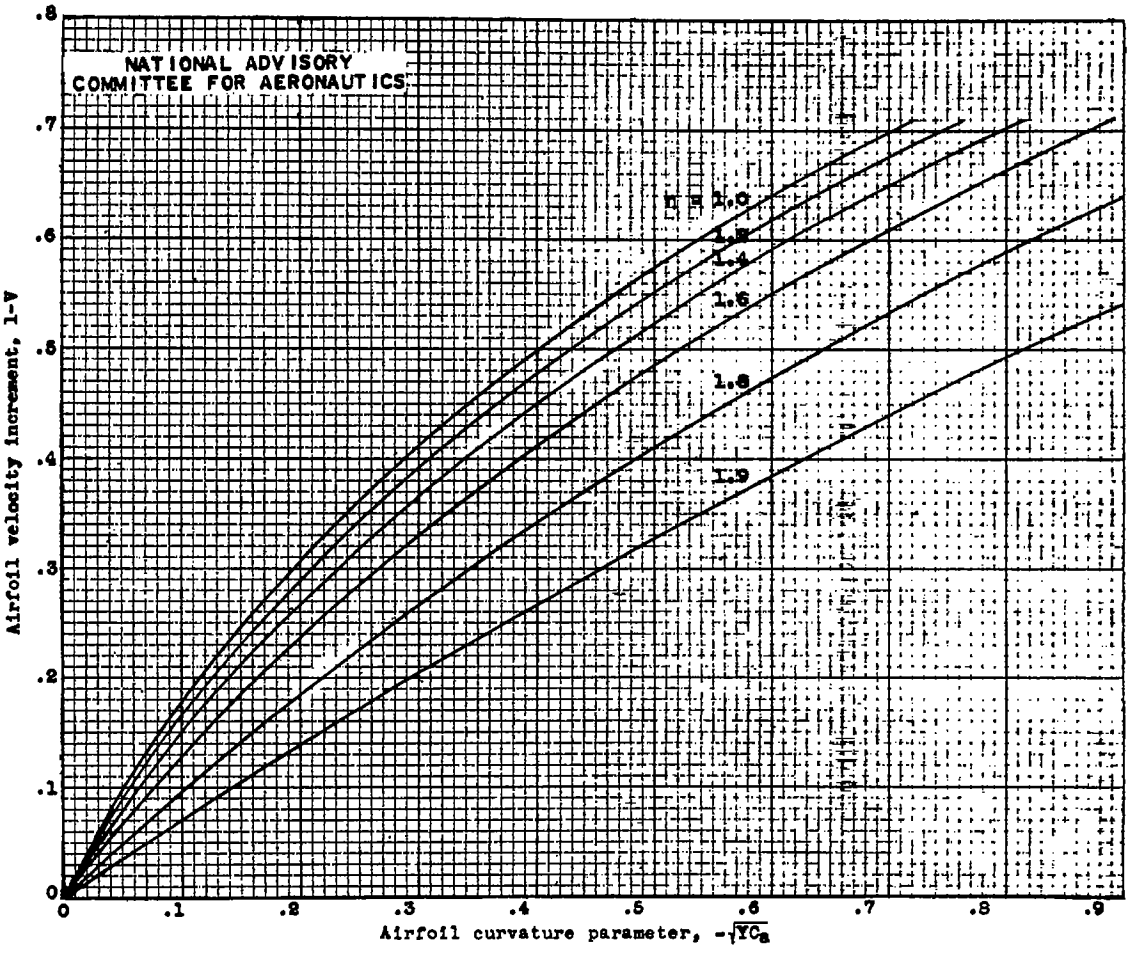

(h) Free-stream Mach number $M_o = 0.9$.

Figure 4.- Concluded. Negative velocity increment on airfoil as a function of airfoil ordinate Y and airfoil curvature C_a for various values of η. Values computed from equation (10) for $V < 1$ and tabulated in table II.

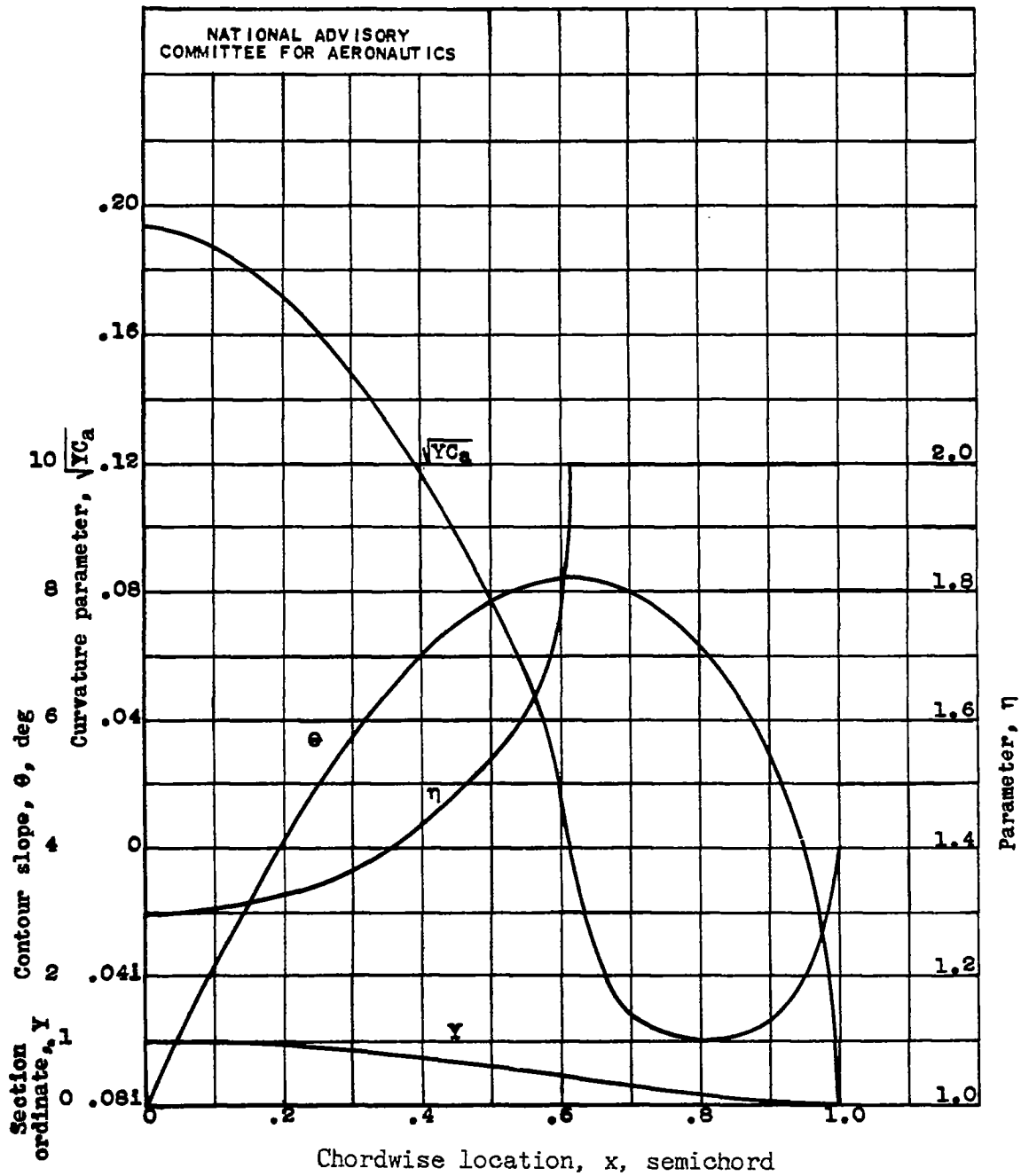

Figure 5.- Basic data for Kaplan symmetrical section of thickness ratio 0.10 (reference 3).

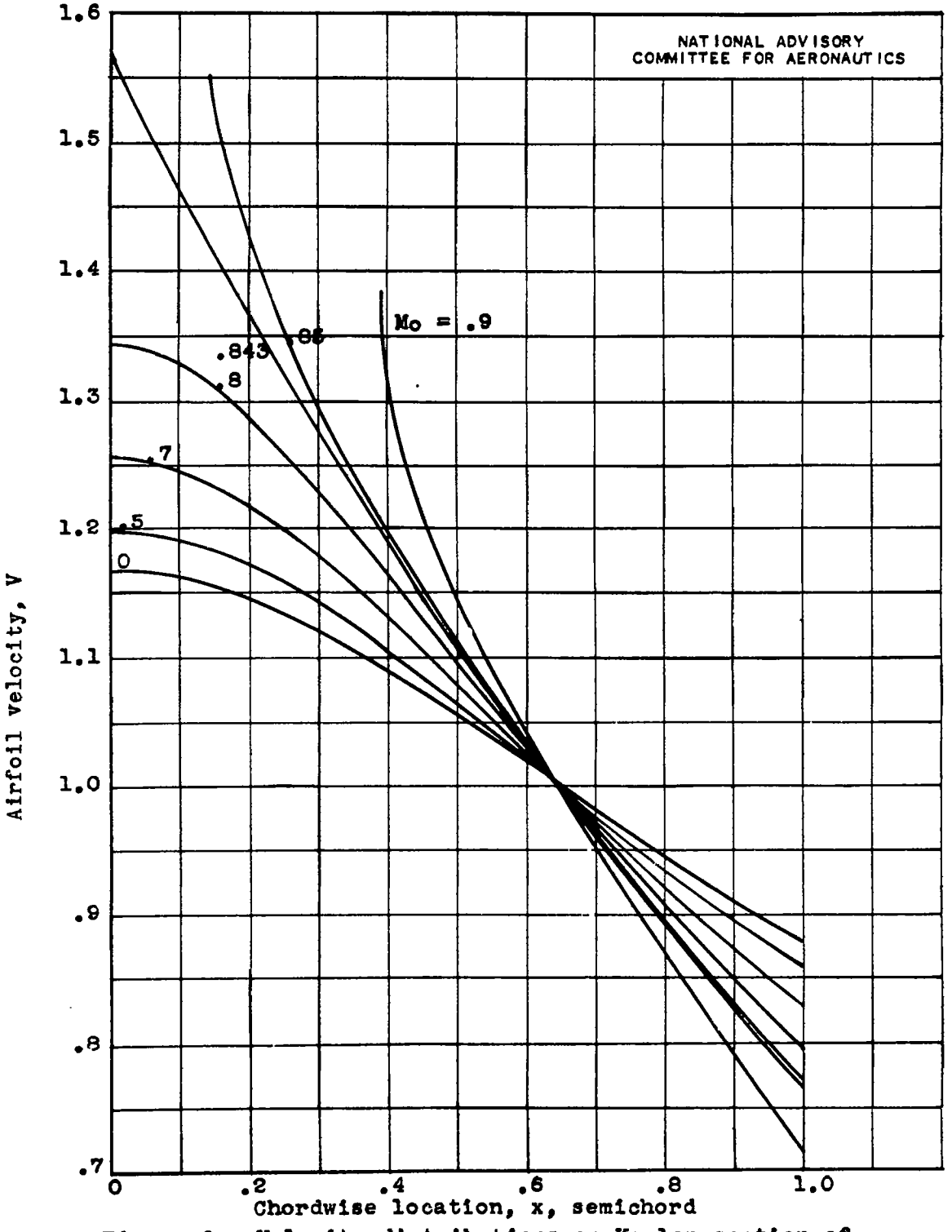

Figure 6.- Velocity distributions on Kaplan section of thickness ratio 0.10 computed by equation (14).

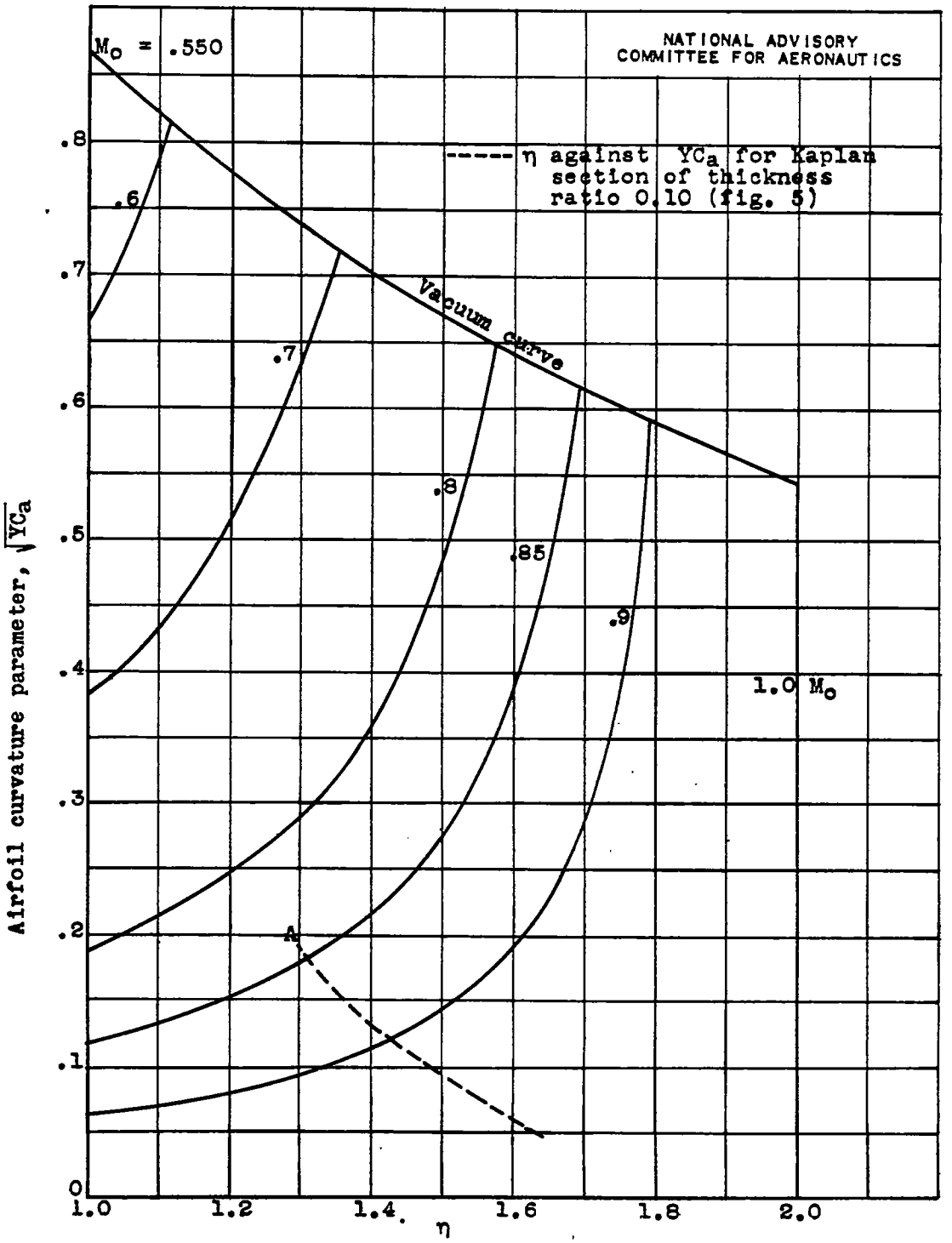

(a) Relation between $\sqrt{YC_a}$ and η.

Figure 7.- Potential limit curves; loci of points of infinite slope in figure 3.

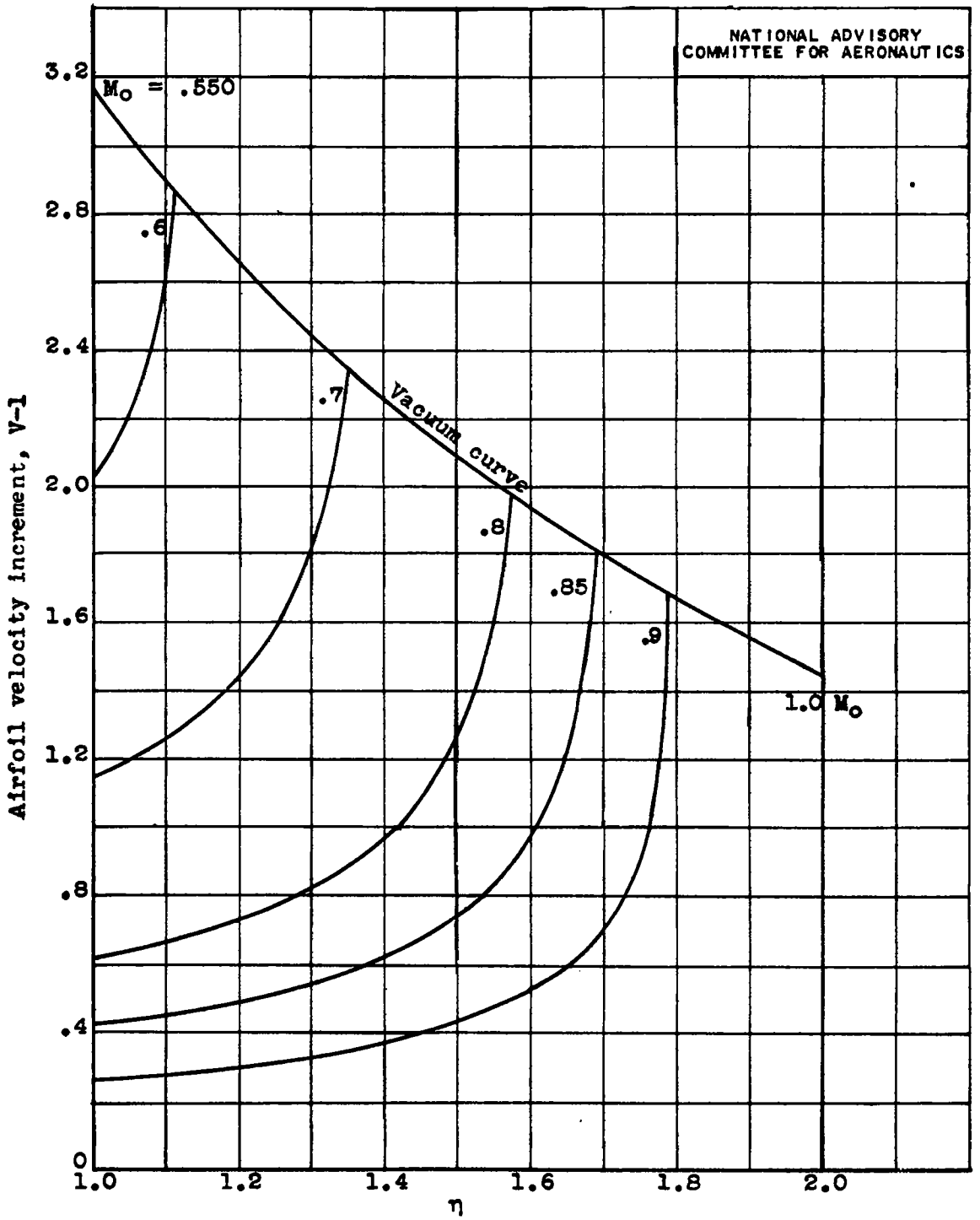

(b) Relation between V-1 and η.

Figure 7.- Continued. Potential limit curves; loci of points of infinite slope in figure 3.

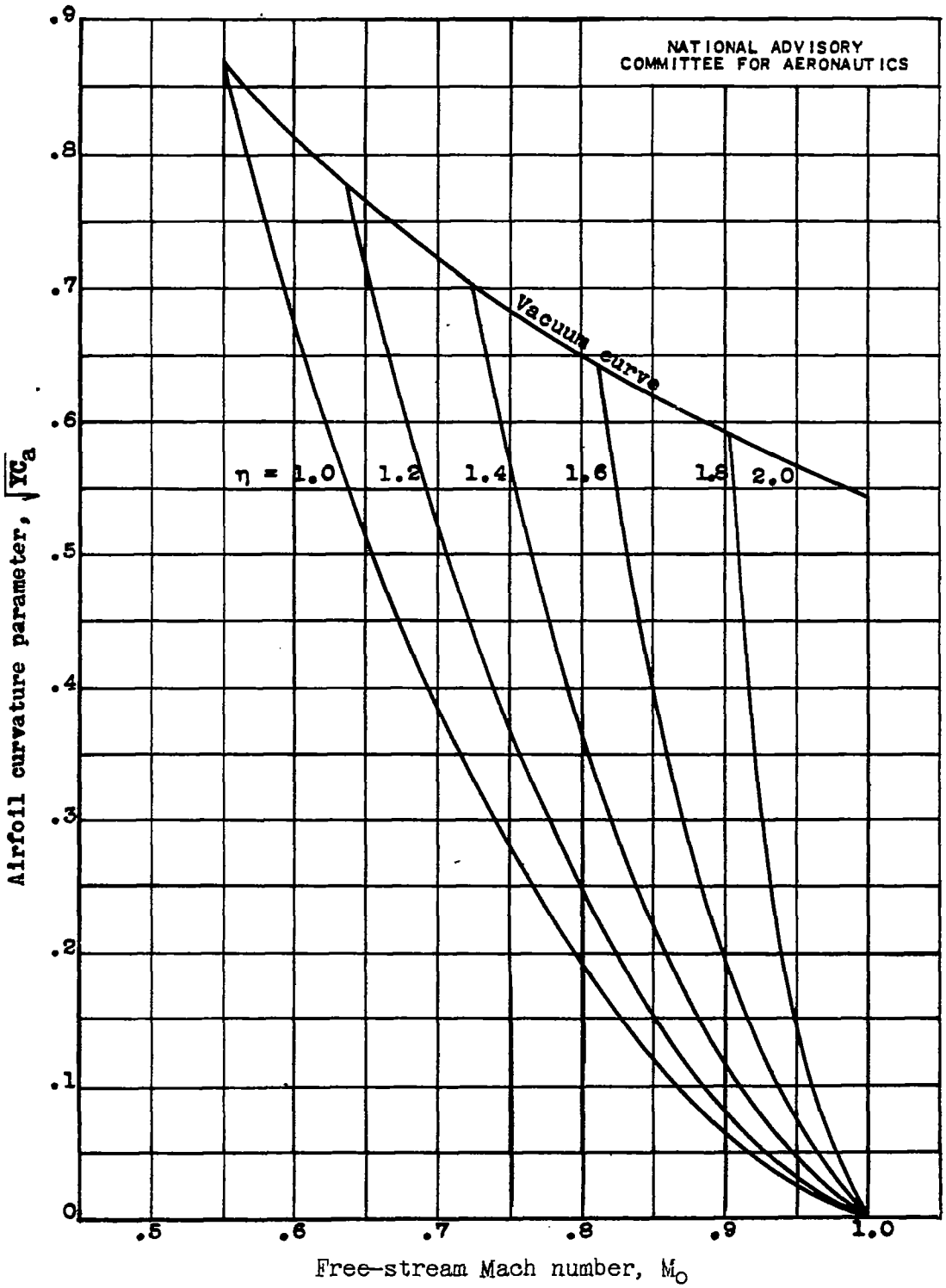

(c) Relation between $\sqrt{YC_a}$ and M_o.

Figure 7.- Continued. Potential limit curves; loci of points of infinite slope in figure 3.

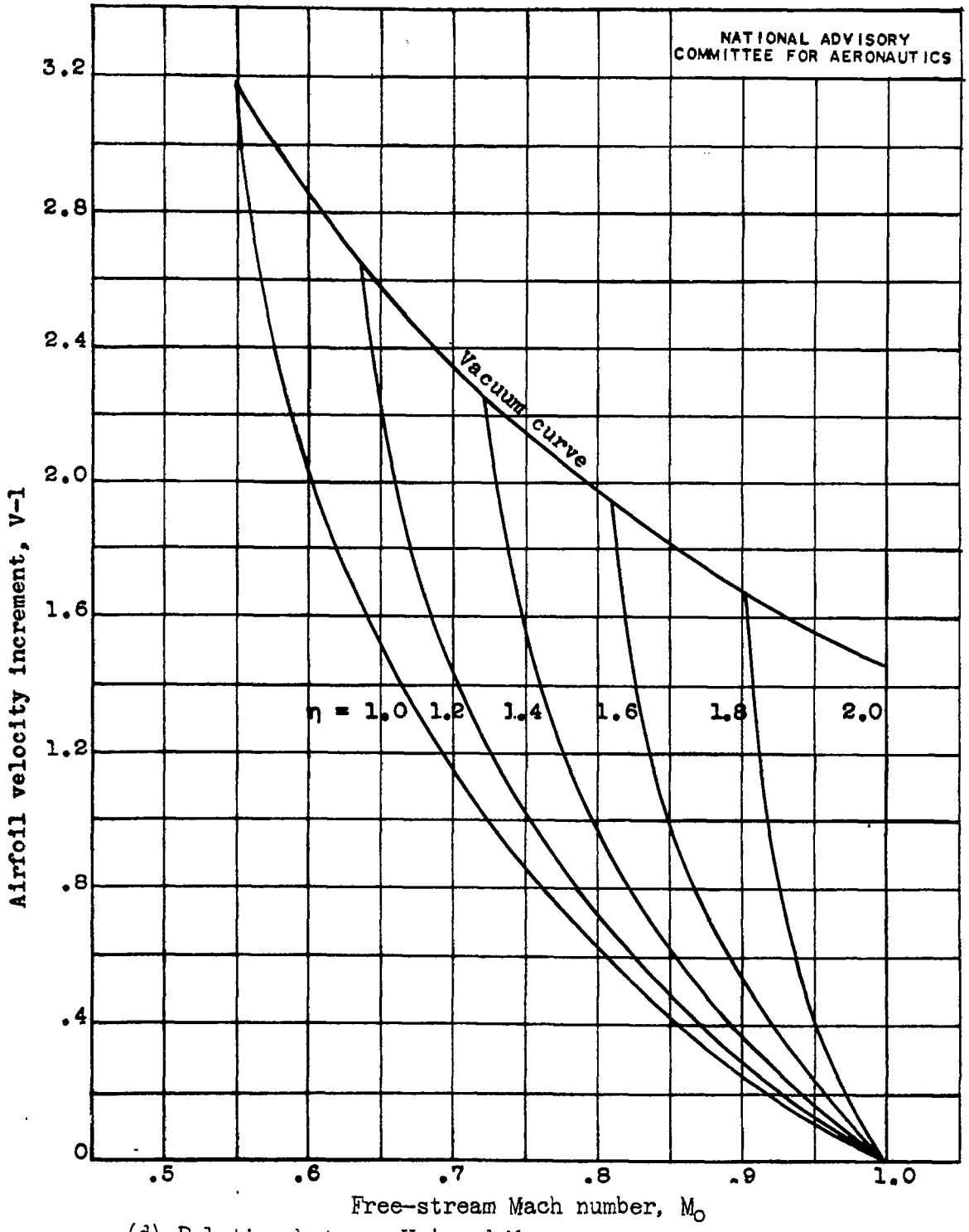

(d) Relation between V-1 and M_o.

Figure 7.- Concluded. Potential limit curves; loci of points of infinite slope in figure 3.

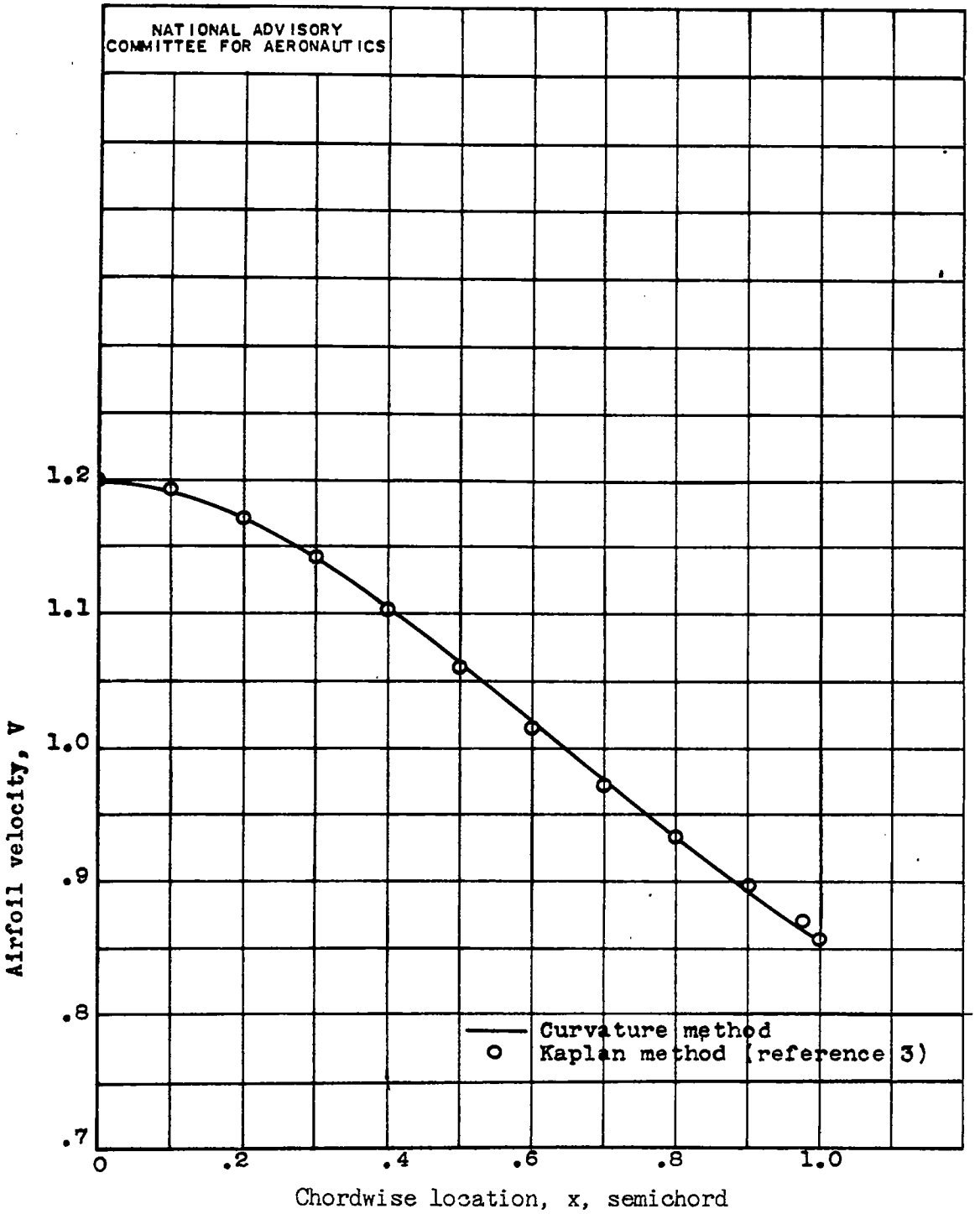

(a) $M_o = 0.5$.

Figure 8.- Comparison of velocity distribution on Kaplan section of thickness ratio 0.10.

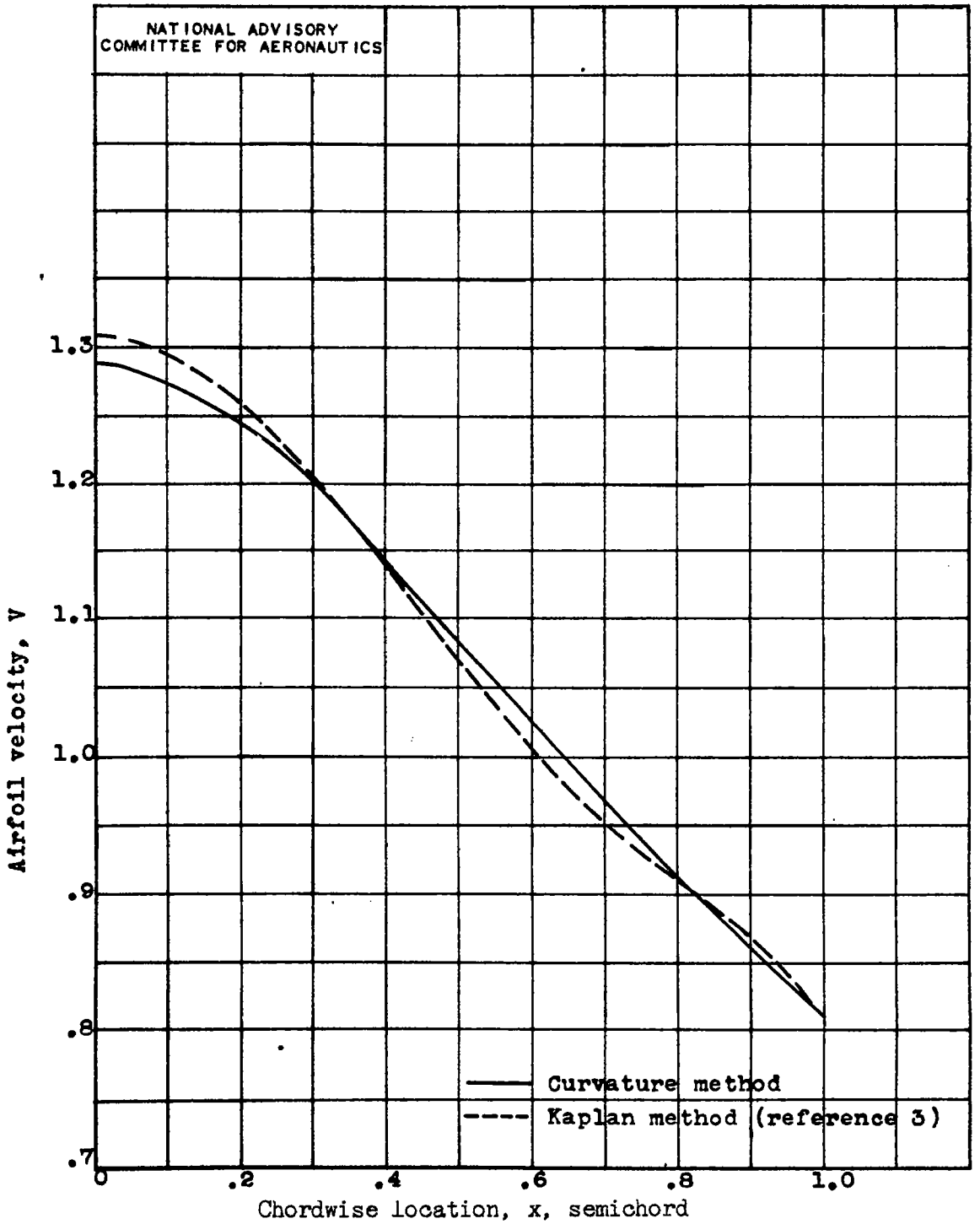

(b) M_o = 0.75.

Figure 8.- Continued. Comparison of velocity distribution on Kaplan section of thickness ratio 0.10.

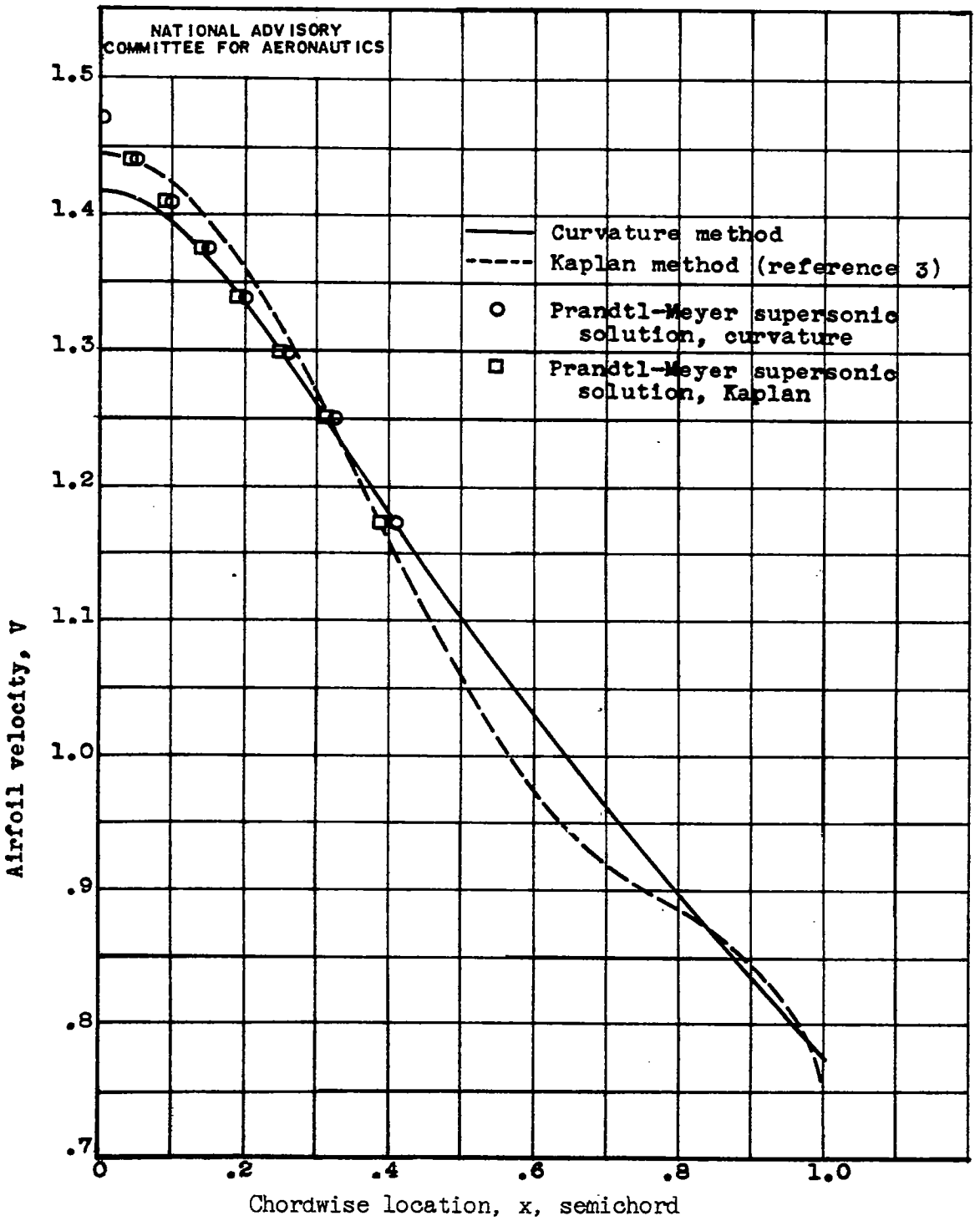

(c) M_o = 0.83.

Figure 8.- Continued. Comparison of velocity distribution on Kaplan section of thickness ratio 0.10.

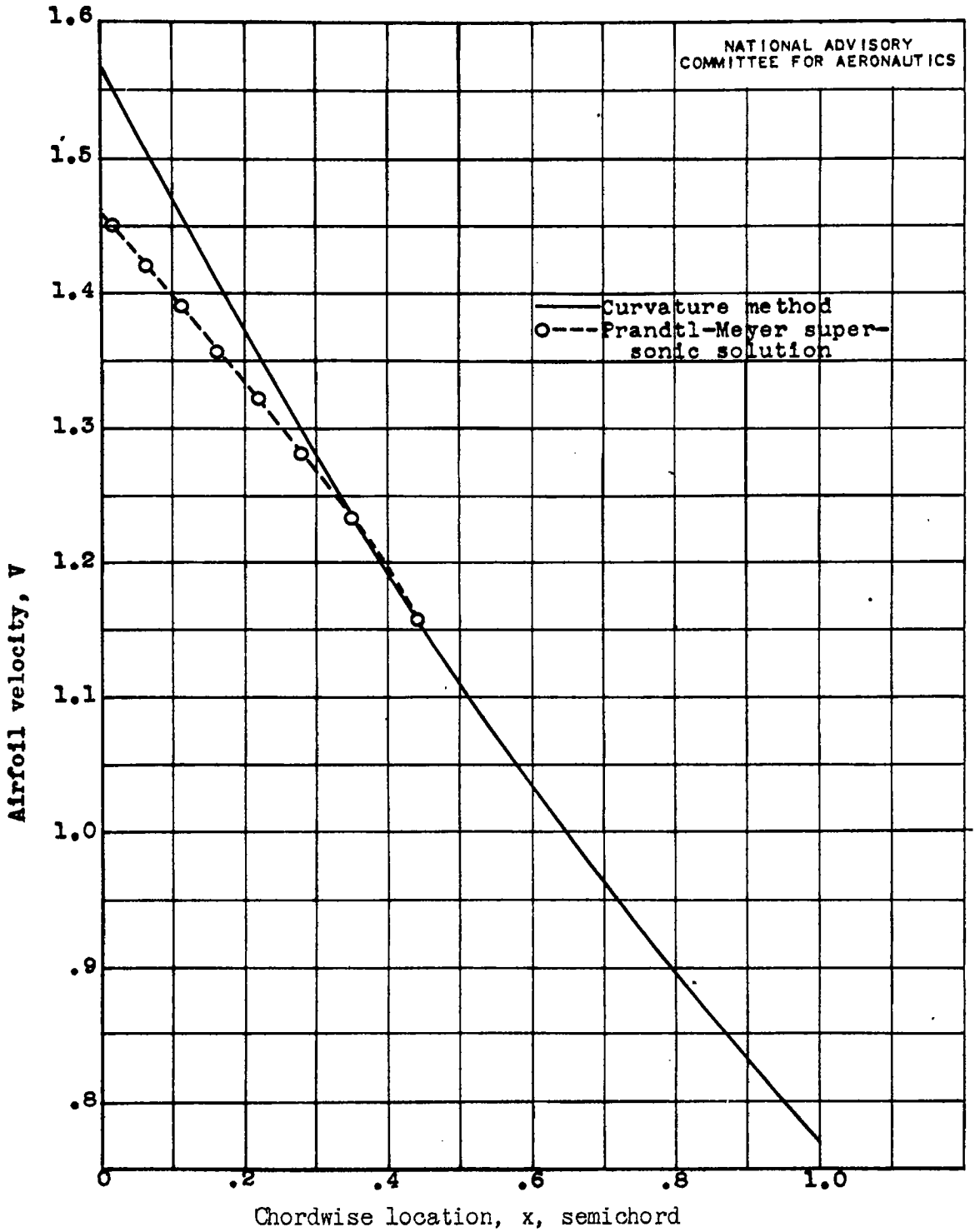

(d) M_o = 0.843.

Figure 8.- Concluded. Comparison of velocity distribution on Kaplan section of thickness ratio 0.10.

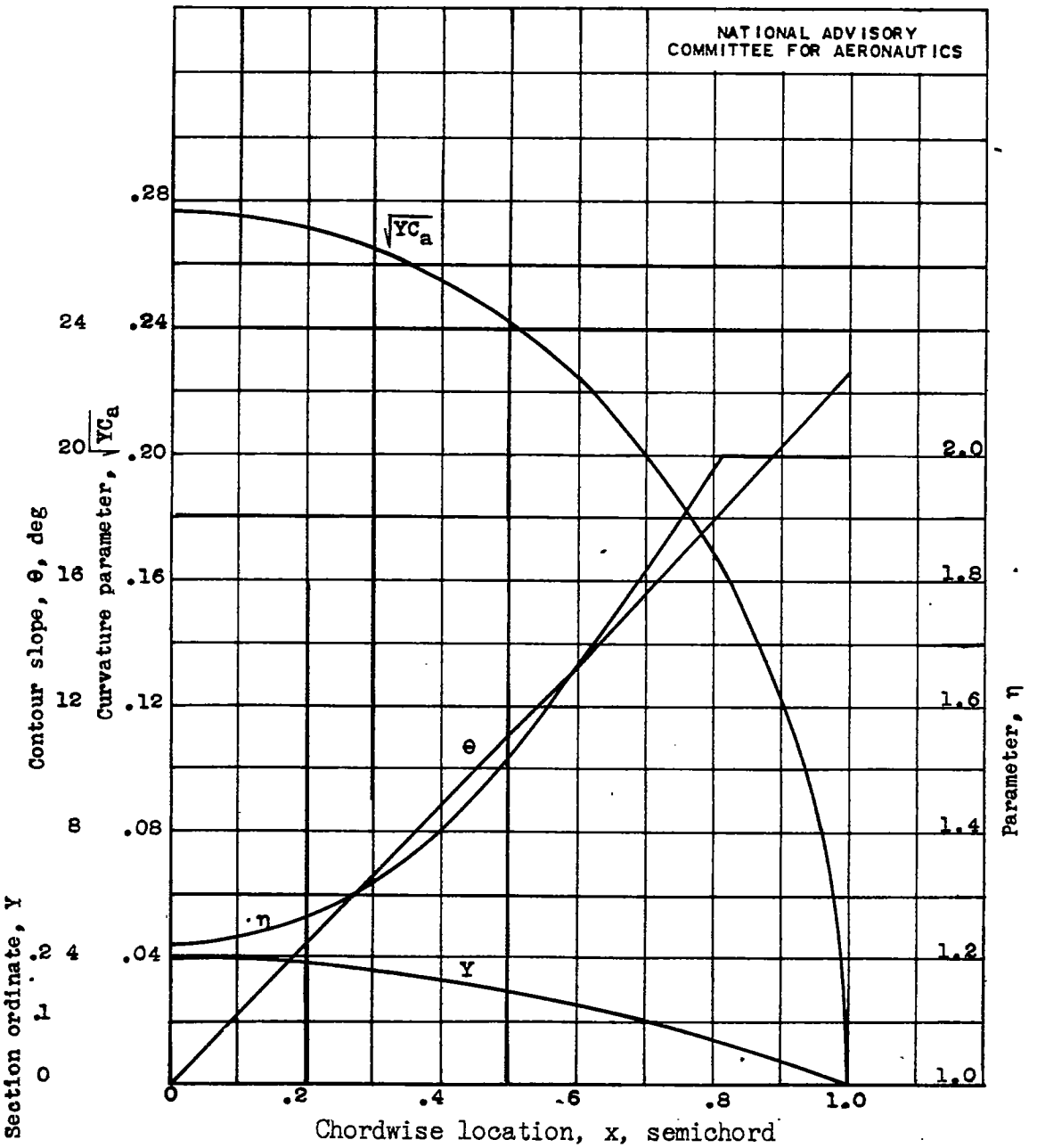

Figure 9.- Basic data for symmetrical biconvex section of thickness ratio 0.20.

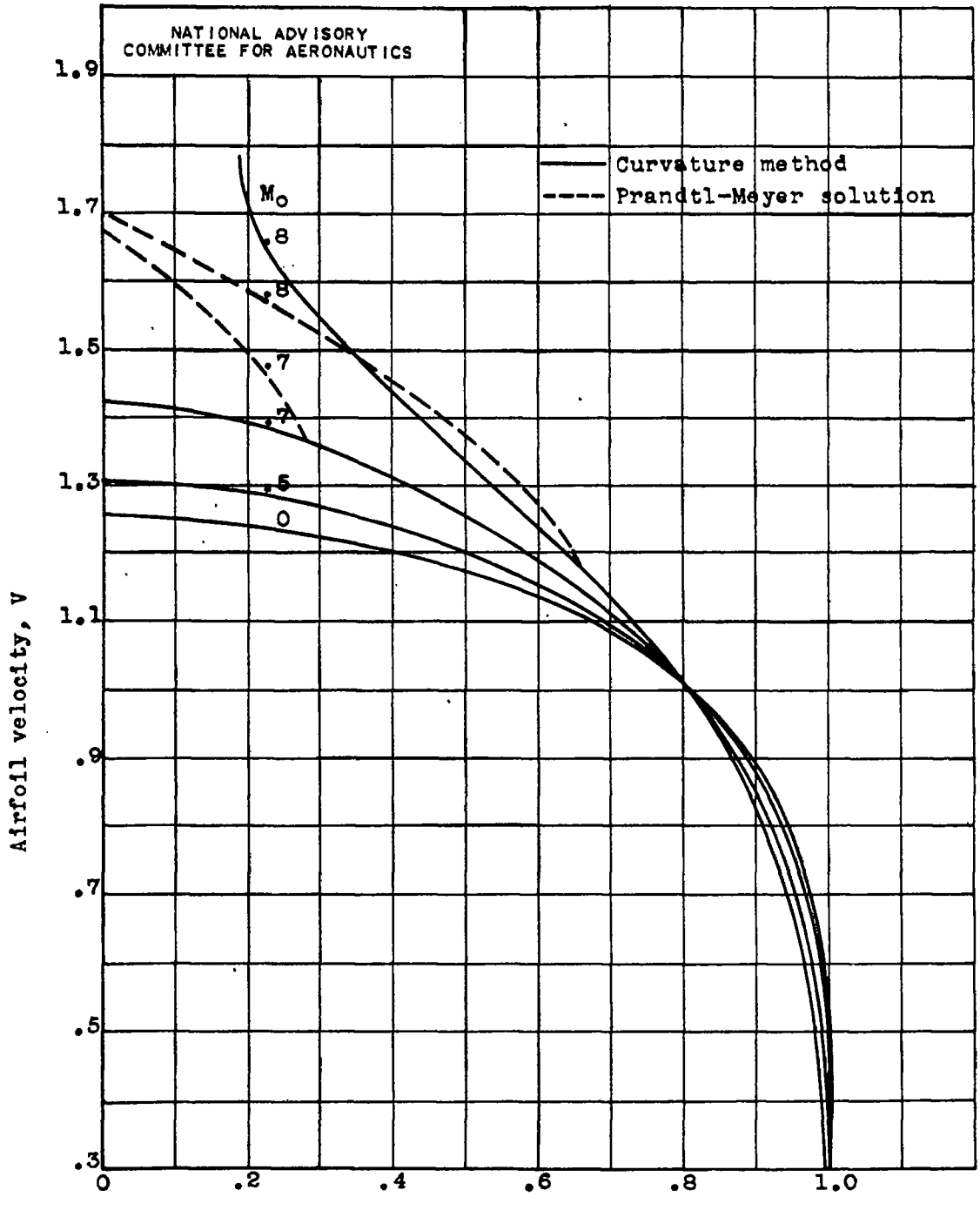

Figure 10.- Velocity distributions biconvex section of thickness ratio 0.20.

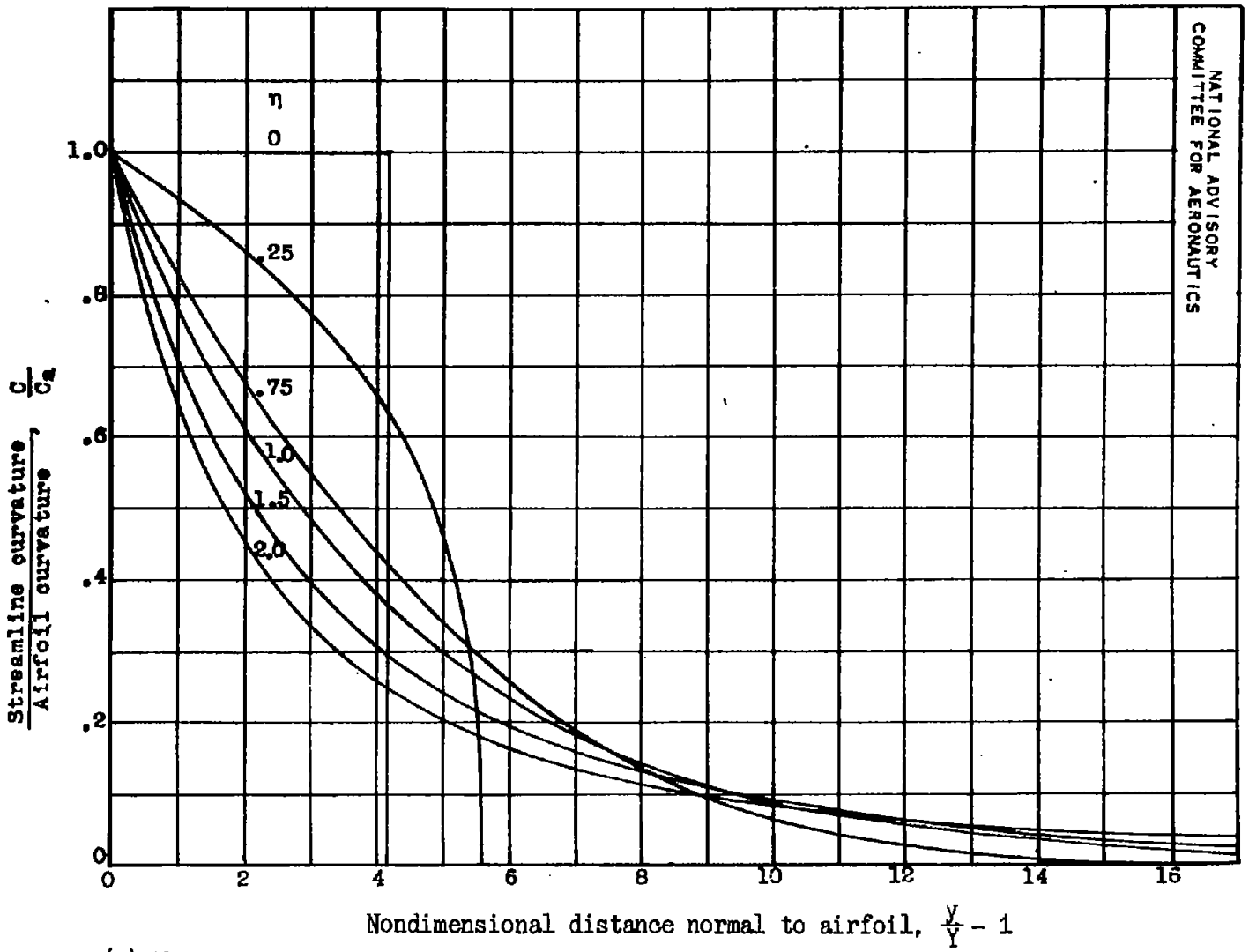

(a) $M_o = 0$.

Figure 11.- Streamline-curvature variation in field of airfoil. Kaplan section of thickness ratio 0.10.

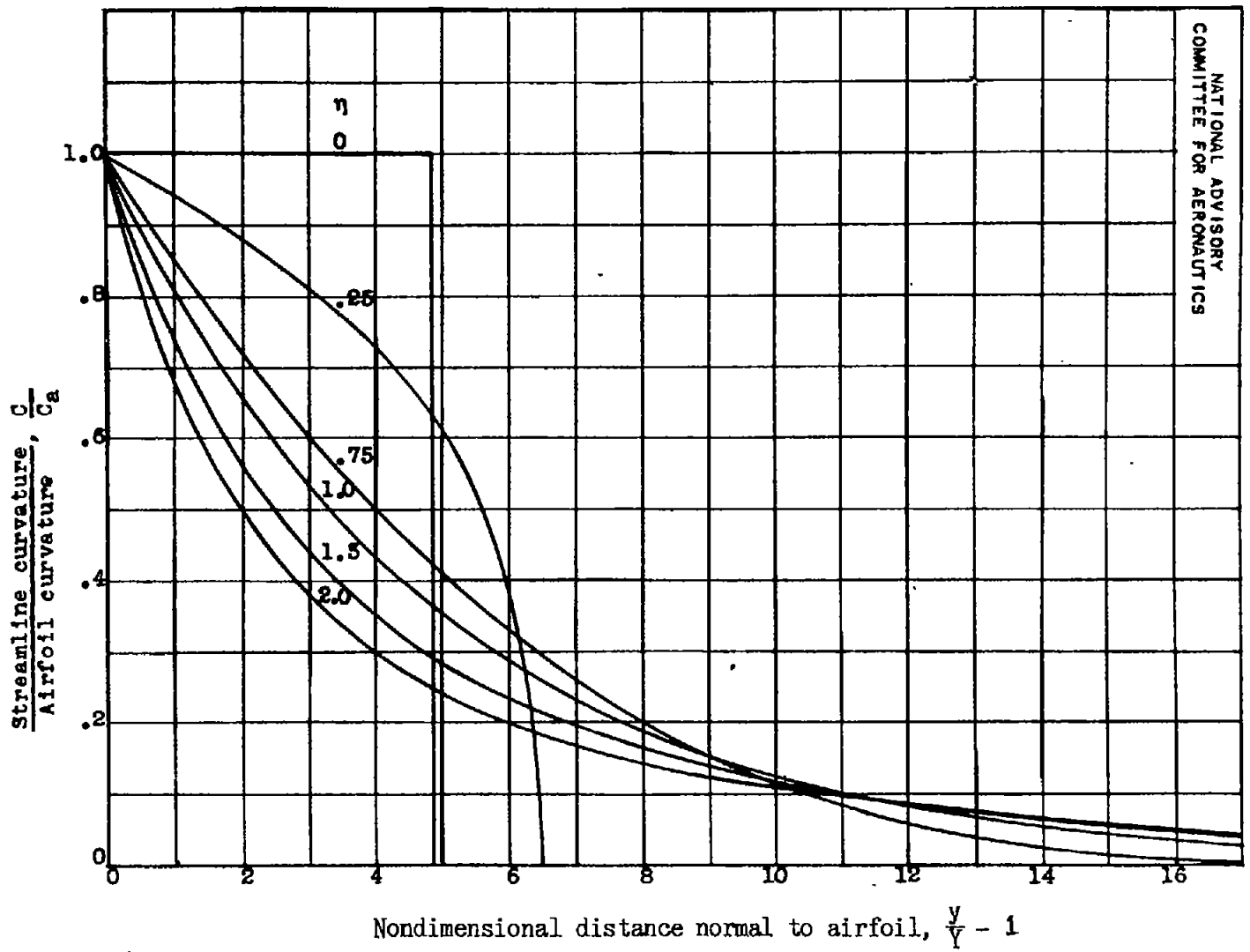

(b) $M_o = 0.5$.

Figure 11.- Continued. Streamline-curvature variation in field of airfoil. Kaplan section of thickness ratio 0.10.

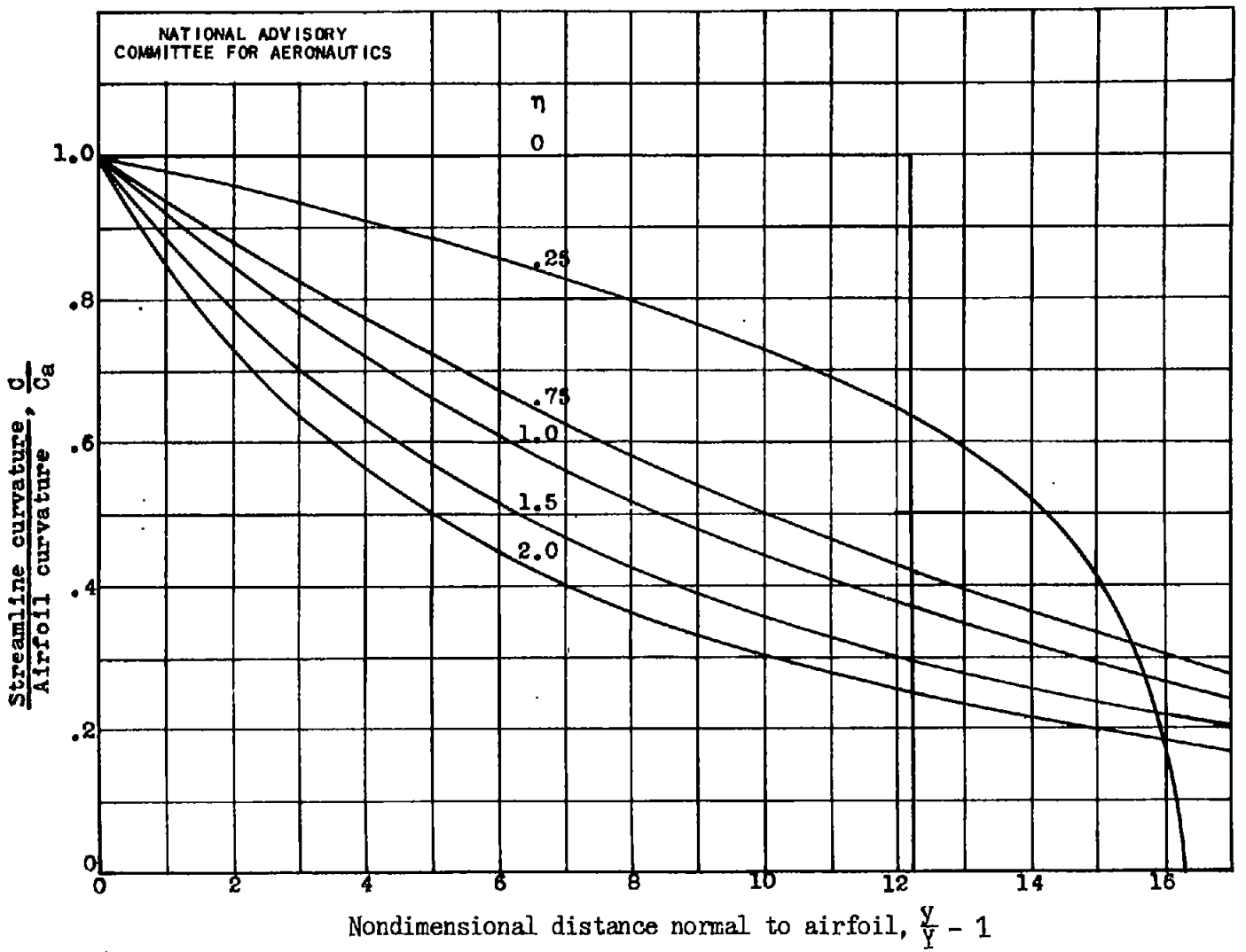

(c) M_o = 0.843.

Figure 11.- Concluded. Streamline-curvature variation in field of airfoil. Kaplan section of thickness ratio 0.10.

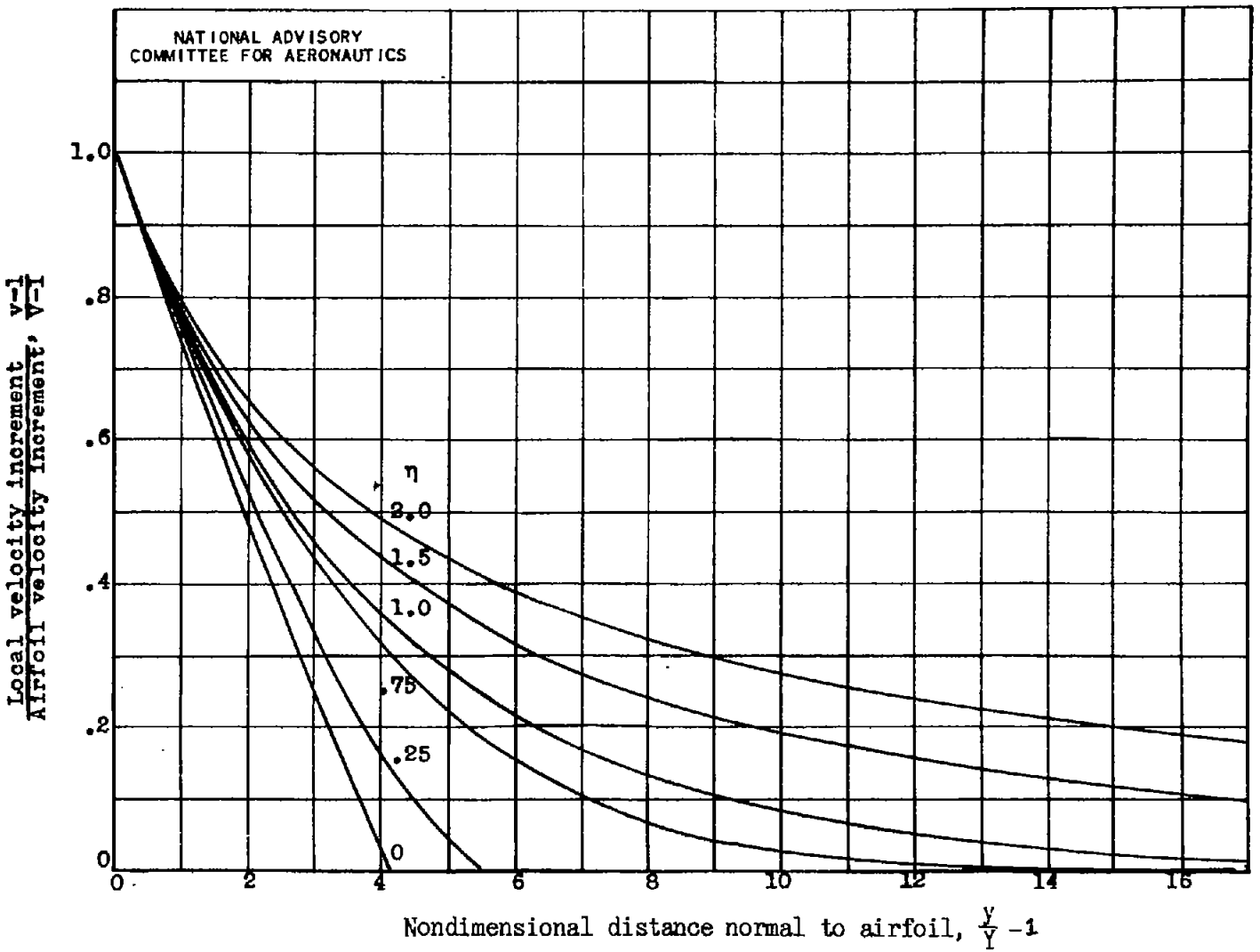

(a) $M_o = 0$.

Figure 12.- Velocity variation in field of airfoil. Kaplan section of thickness ratio 0.10.

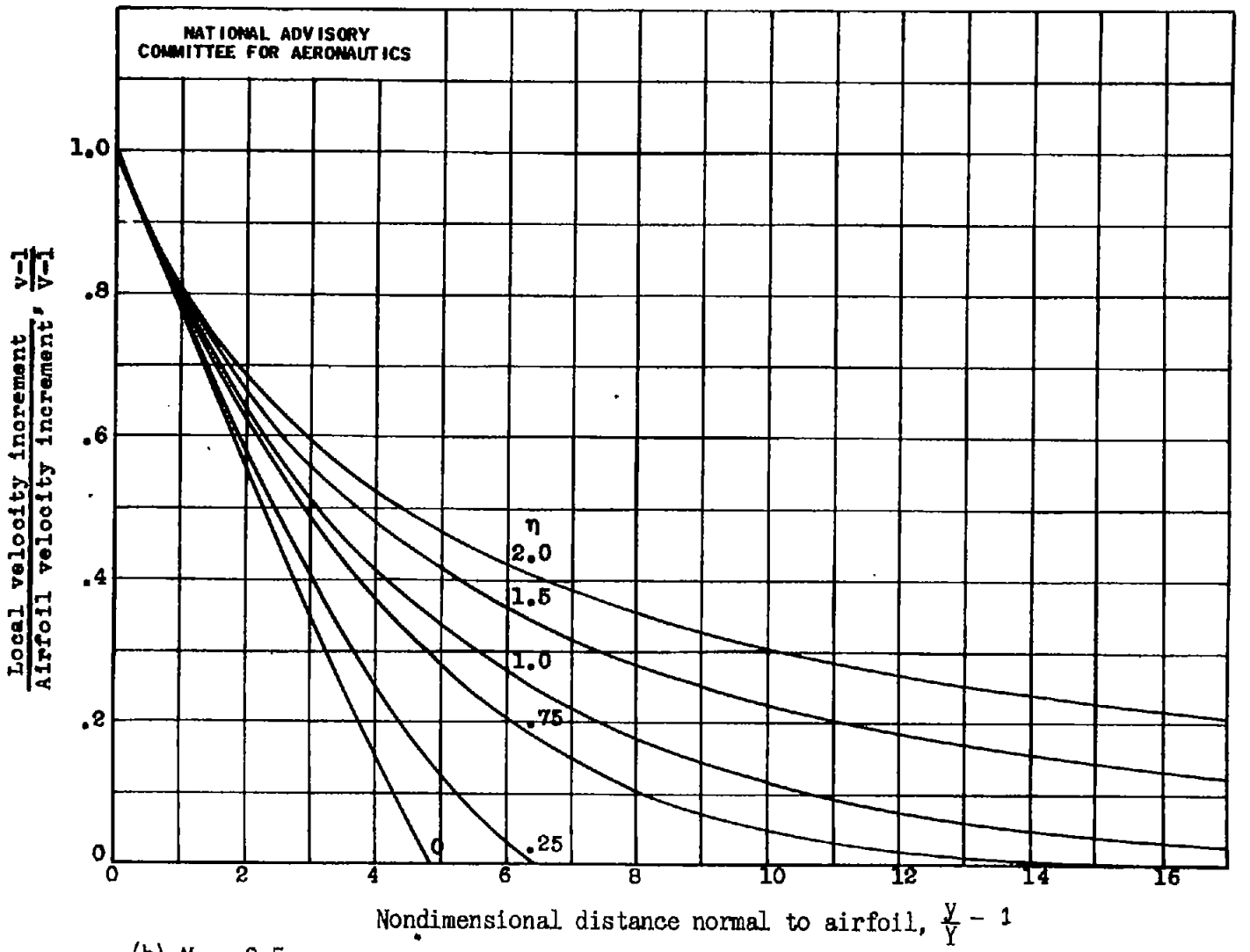

(b) $M_o = 0.5$.

Figure 12.- Continued. Velocity variation in field of airfoil. Kaplan section of thickness ratio 0.10.

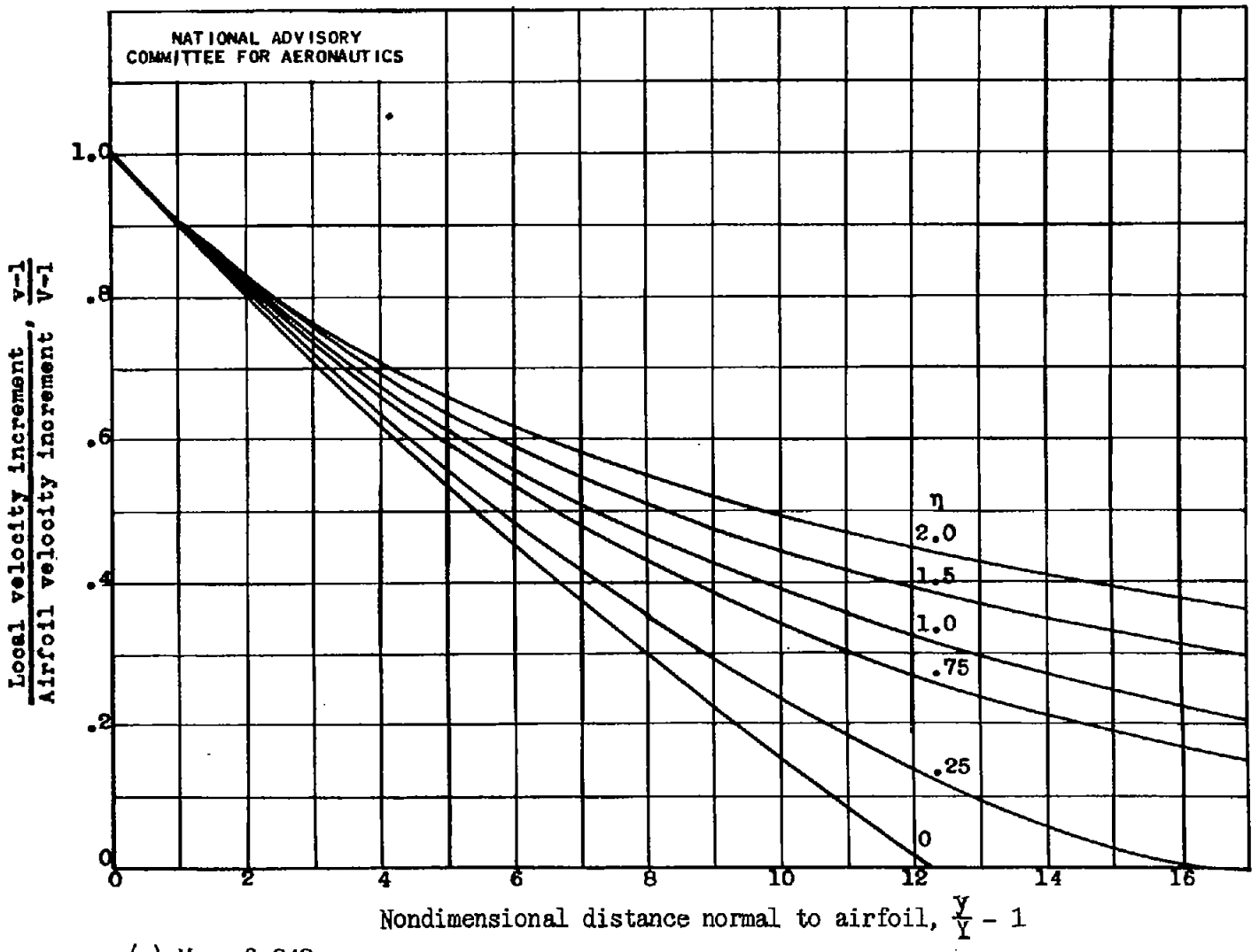

(c) $M_o = 0.843$.

Figure 12.- Concluded. Velocity variation in field of airfoil. Kaplan section of thickness ratio 0.10.

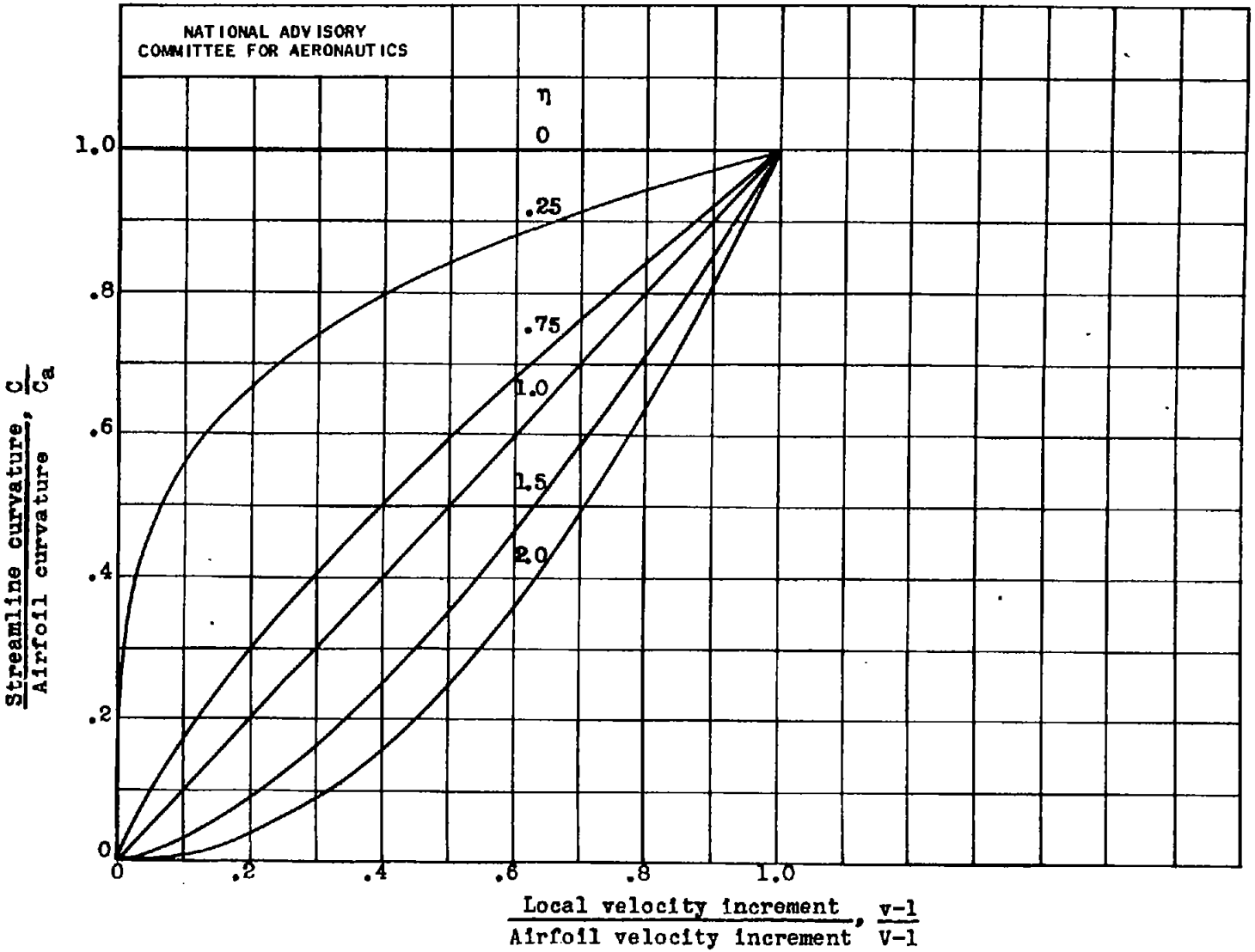

Figure 13.- Plot of curvature function (θ).

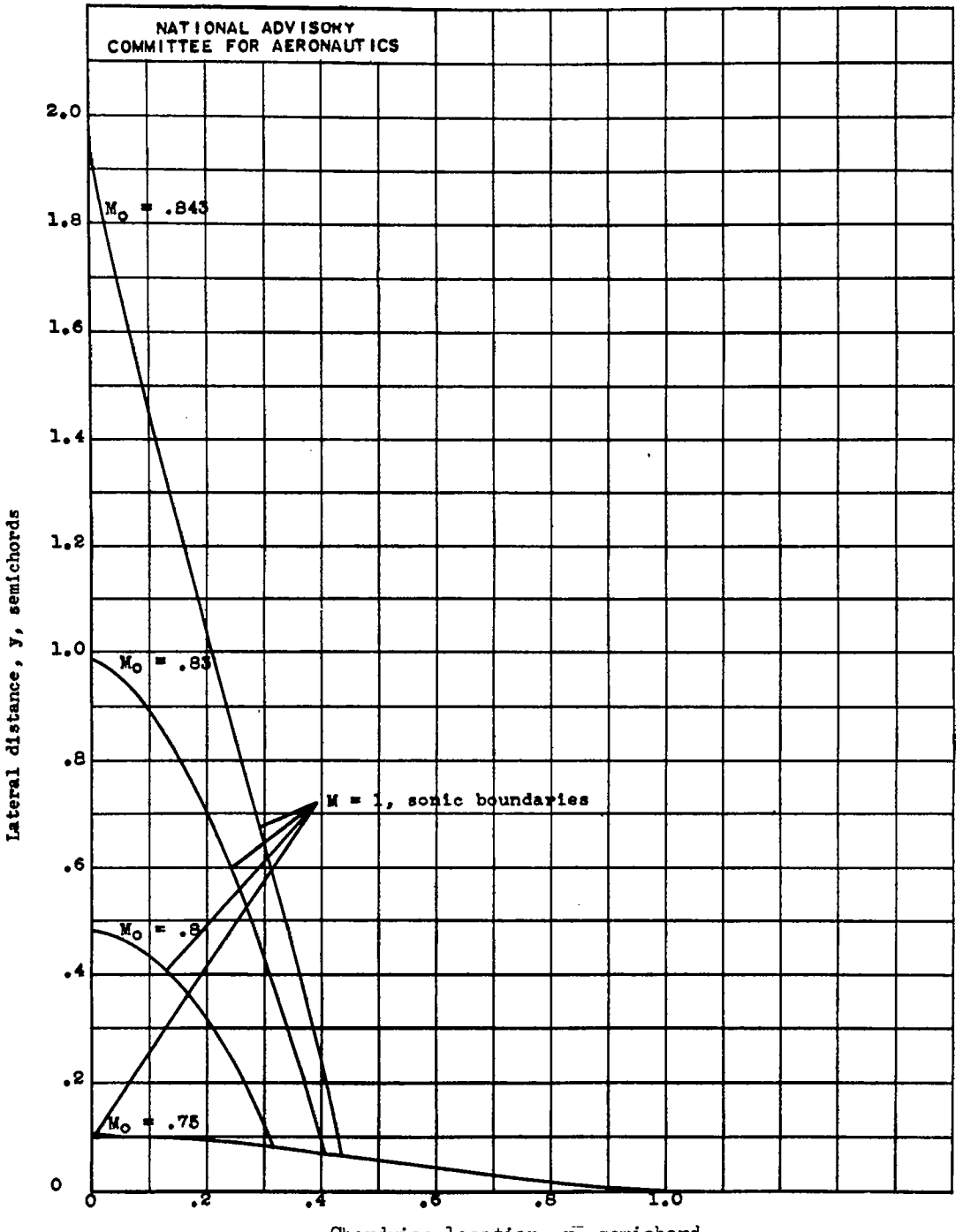

Figure 14.- Local supersonic regions for Kaplan 10-percent section.

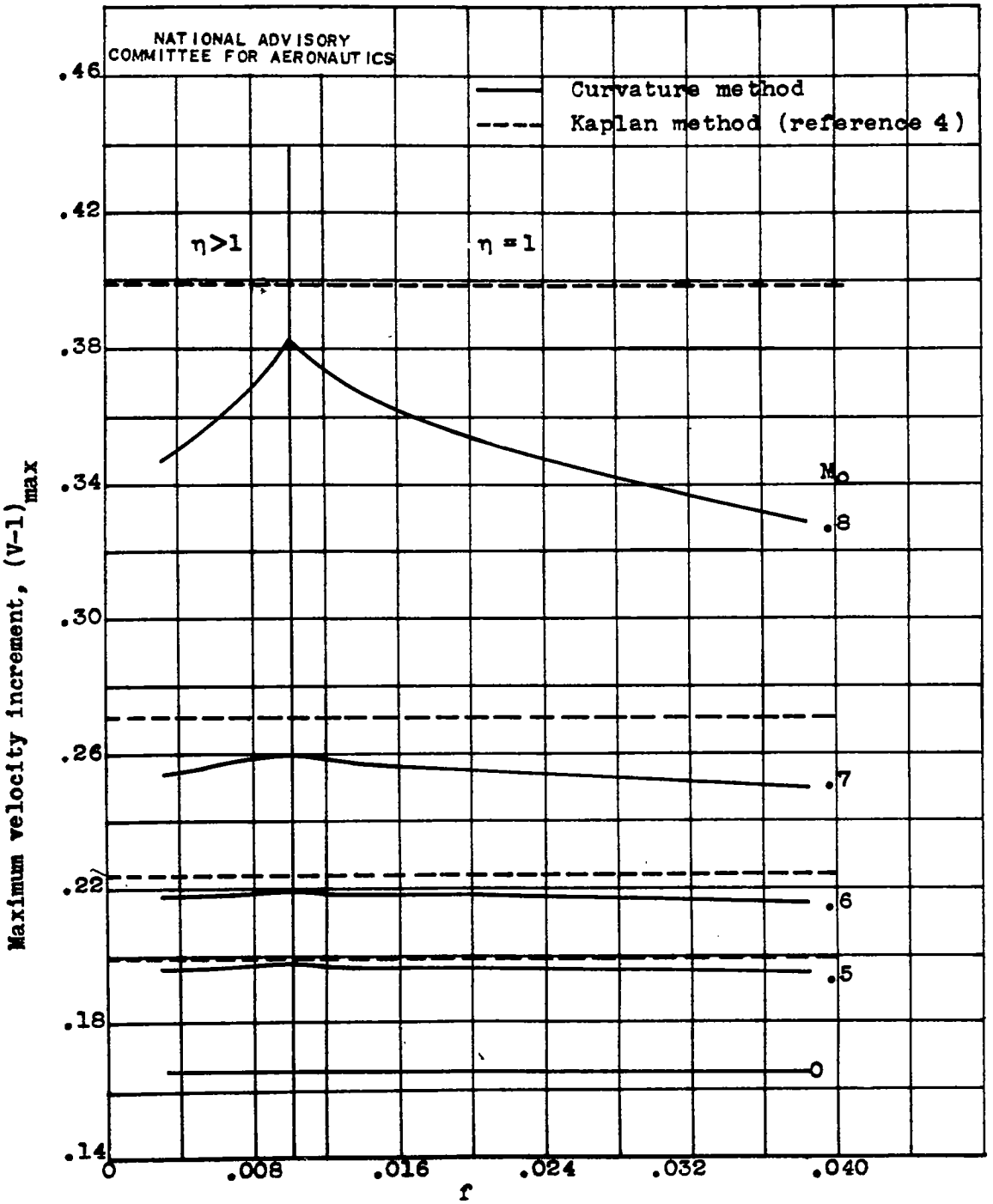

Figure 15.- Dependence of maximum velocity increment on circular arc camber line on position of reference point along airfoil streamline. The quantity f is the ratio in incompressible flow of the velocity decrement at a point on the airfoil streamline to the maximum velocity increment on the circular arc.

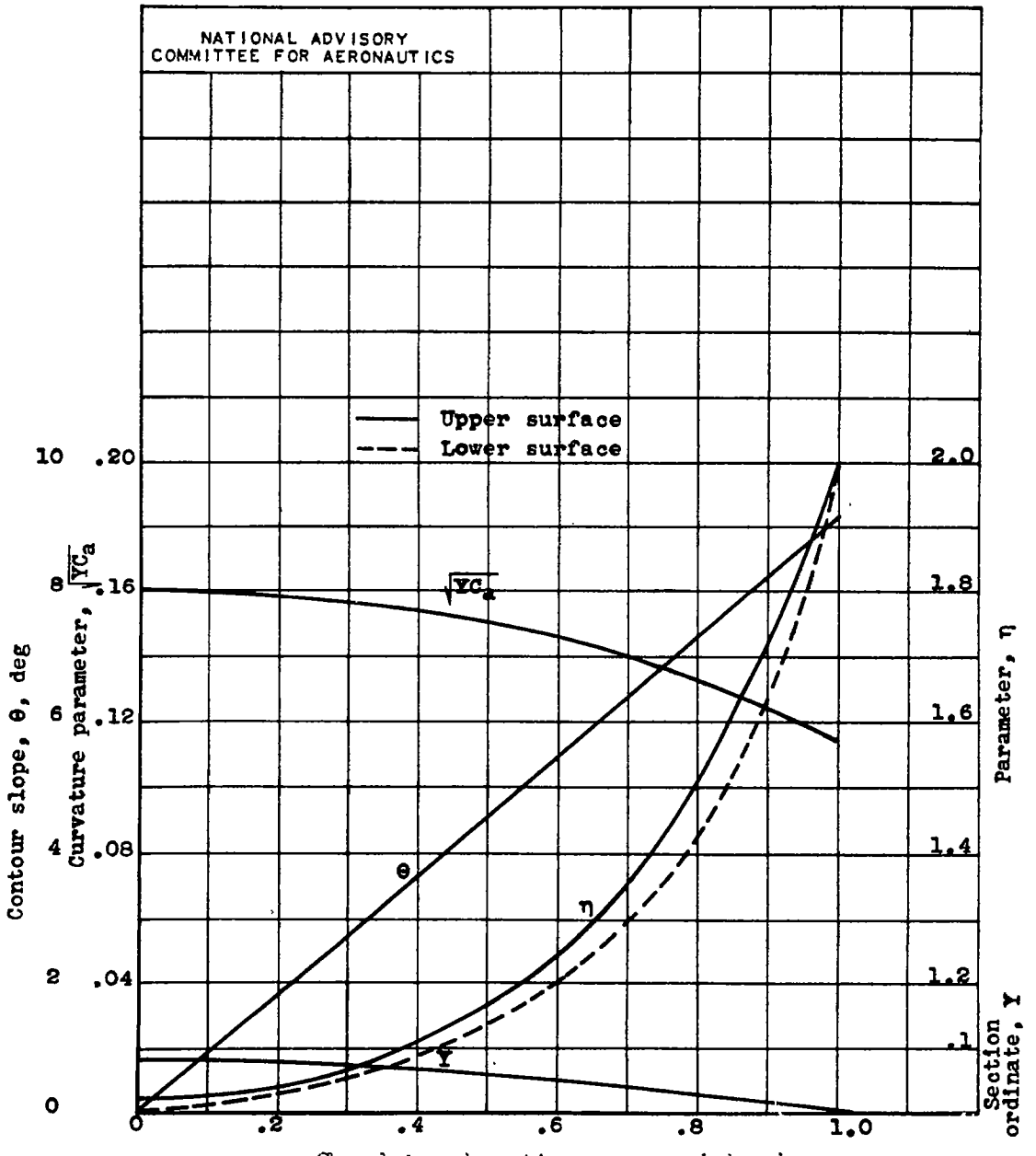

Figure 16.- Basic data circular arc-mean camber line at zero angle of attack camber ratio, 0.04.

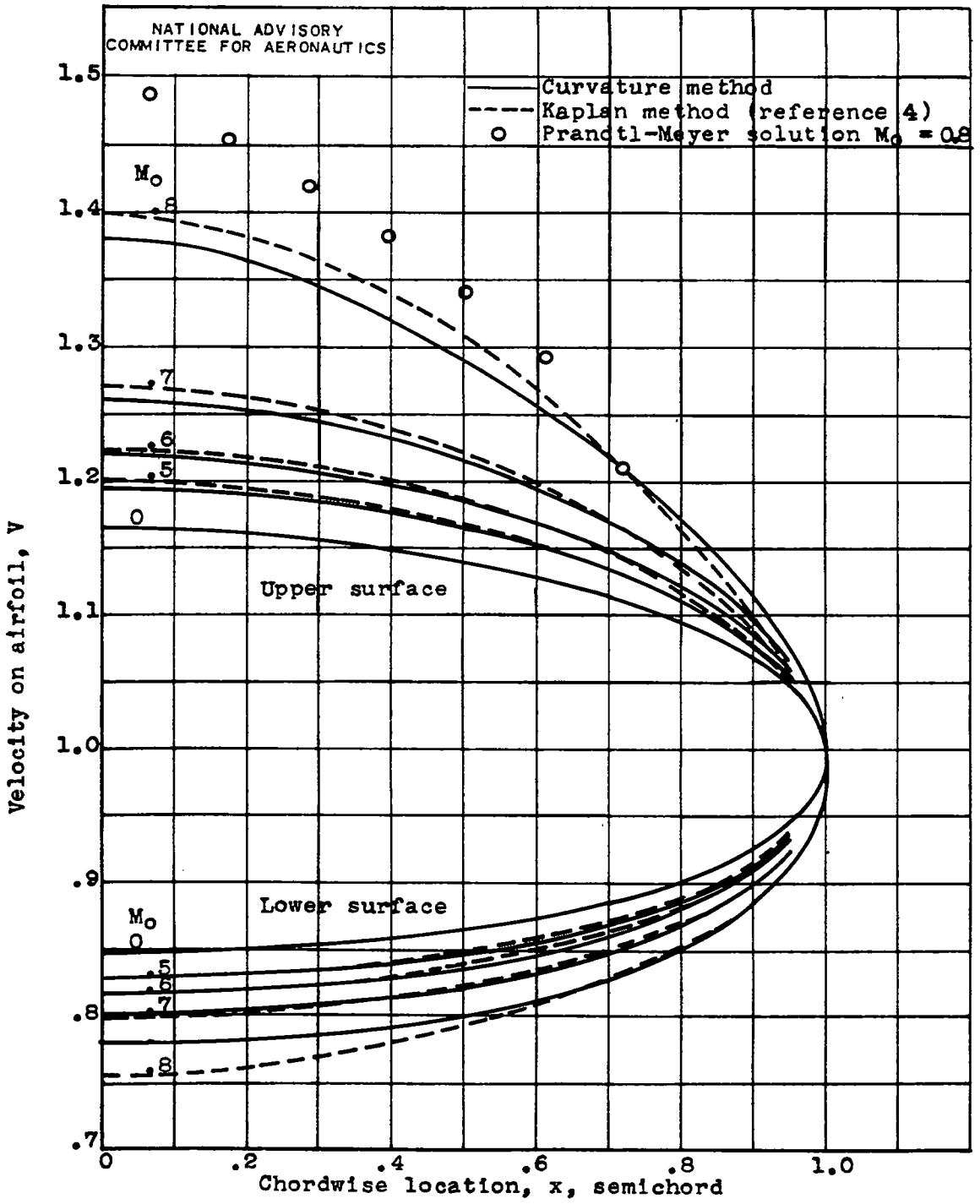

Figure 17.- Comparison of velocity distributions on circular arc mean camber line by different methods. Camber ratio, 0.04.

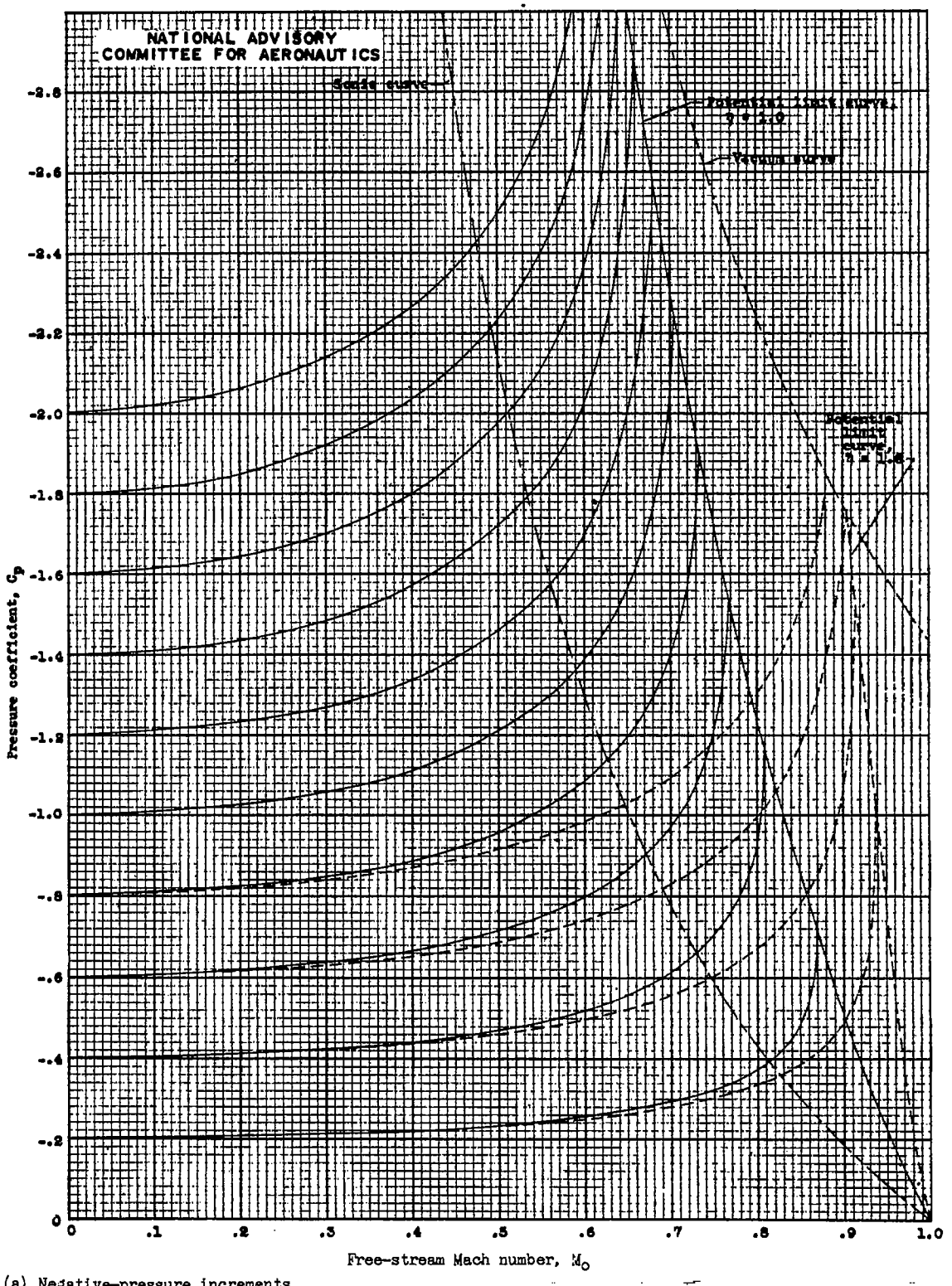

(a) Negative-pressure increments.

Figure 18.- Compressibility-correction rules by curvature method. Potential limit curves from figure 7(d).

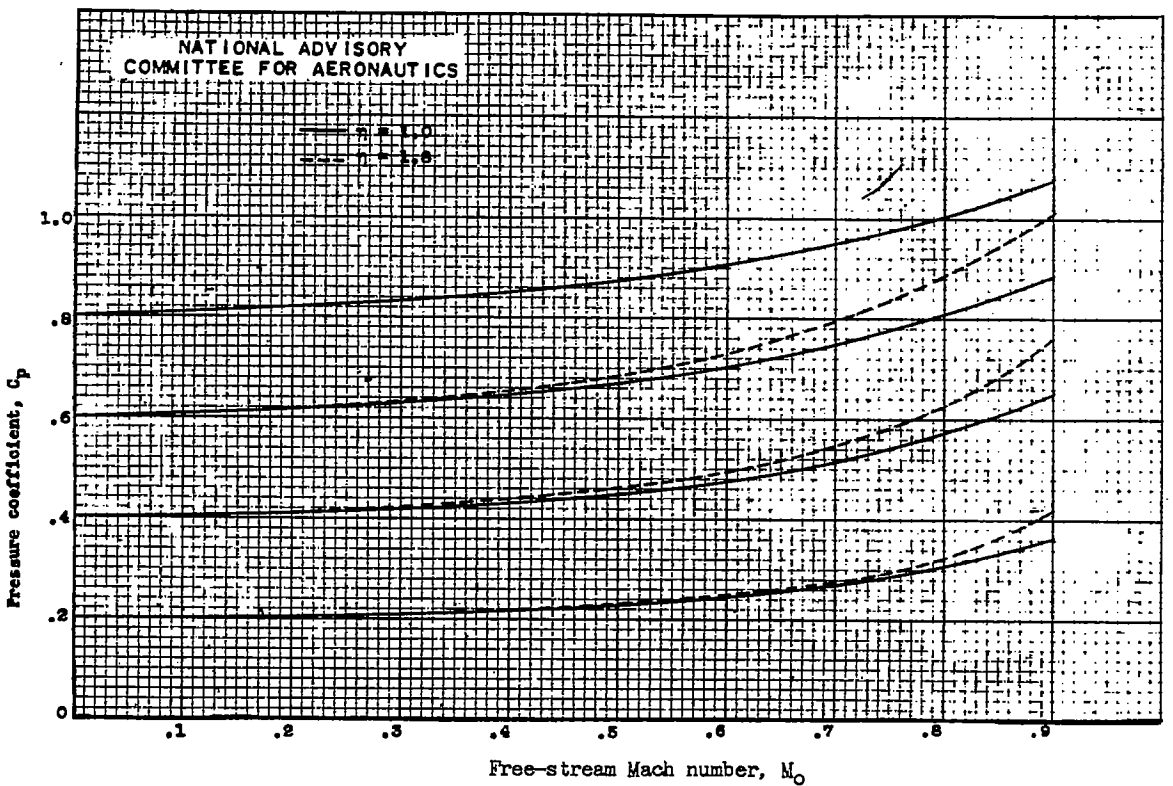

(b) Positive-pressure increments.

Figure 18.- Concluded. Compressibility-correction rules by curvature method. Potential limit curves from figure 7(d).

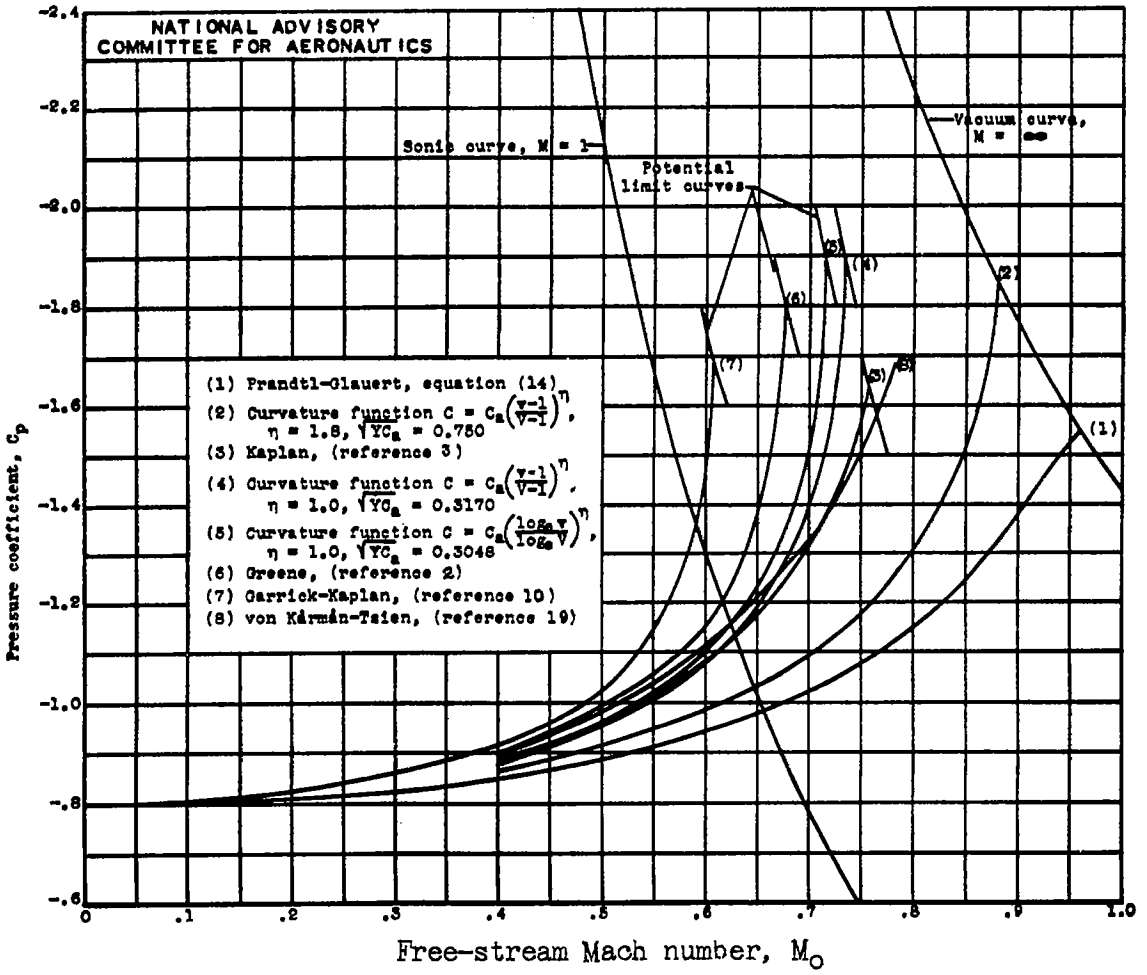

Figure 19.- Comparison of compressibility correction rules.

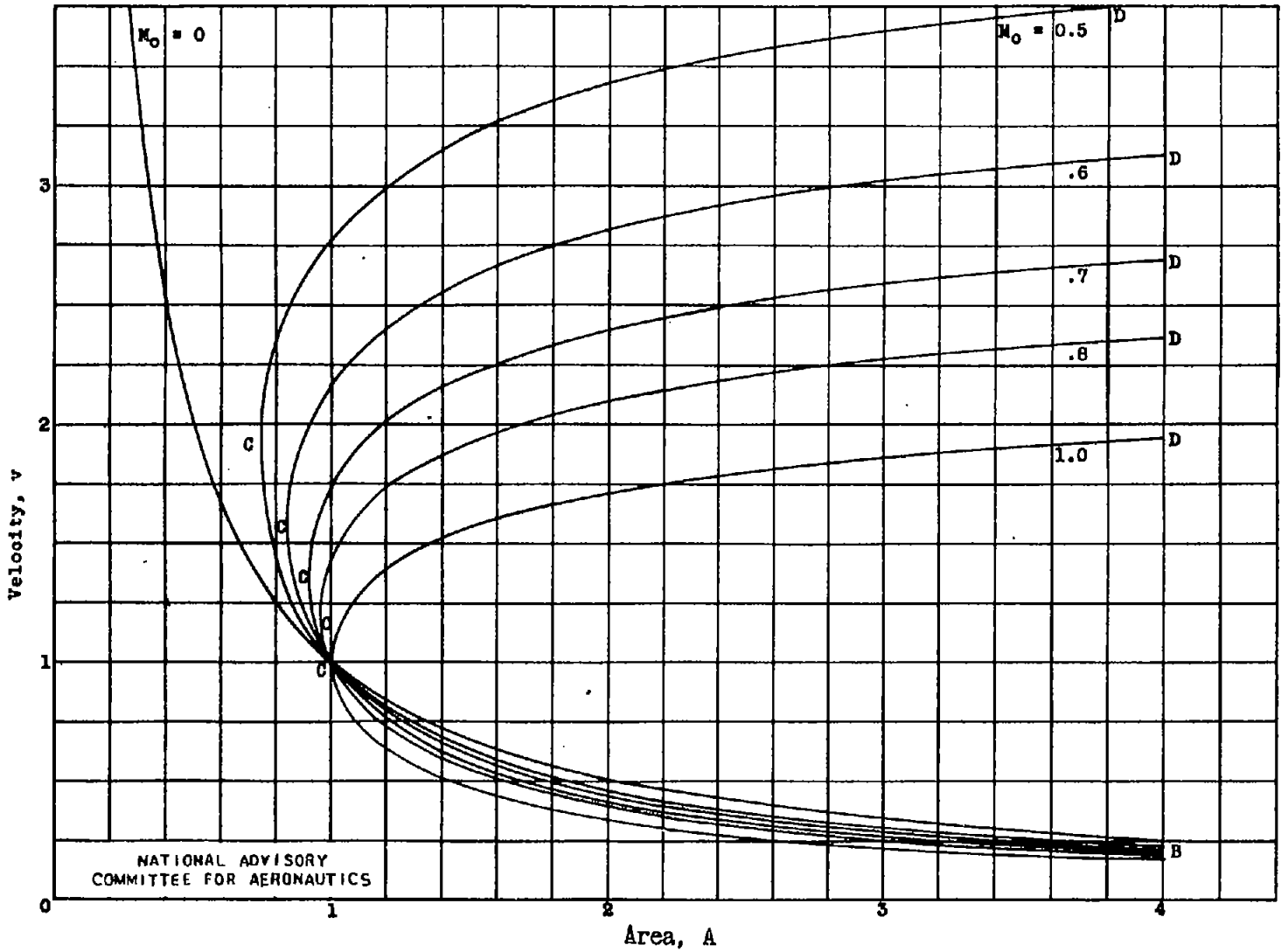

Figure 20.- One-dimensional curves for converging-diverging channel analogous to curves of figure 2. $A = 1/\rho V$.

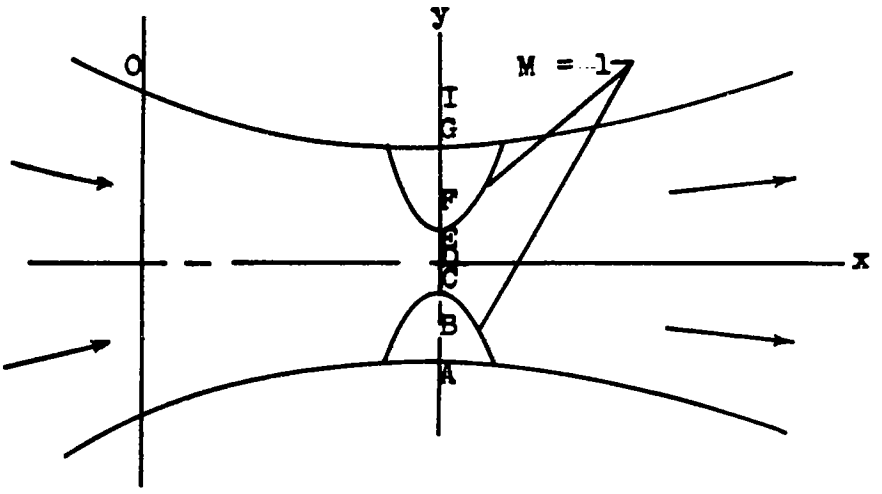

NATIONAL ADVISORY
COMMITTEE FOR AERONAUTICS

Figure 21.- Converging-diverging channel.

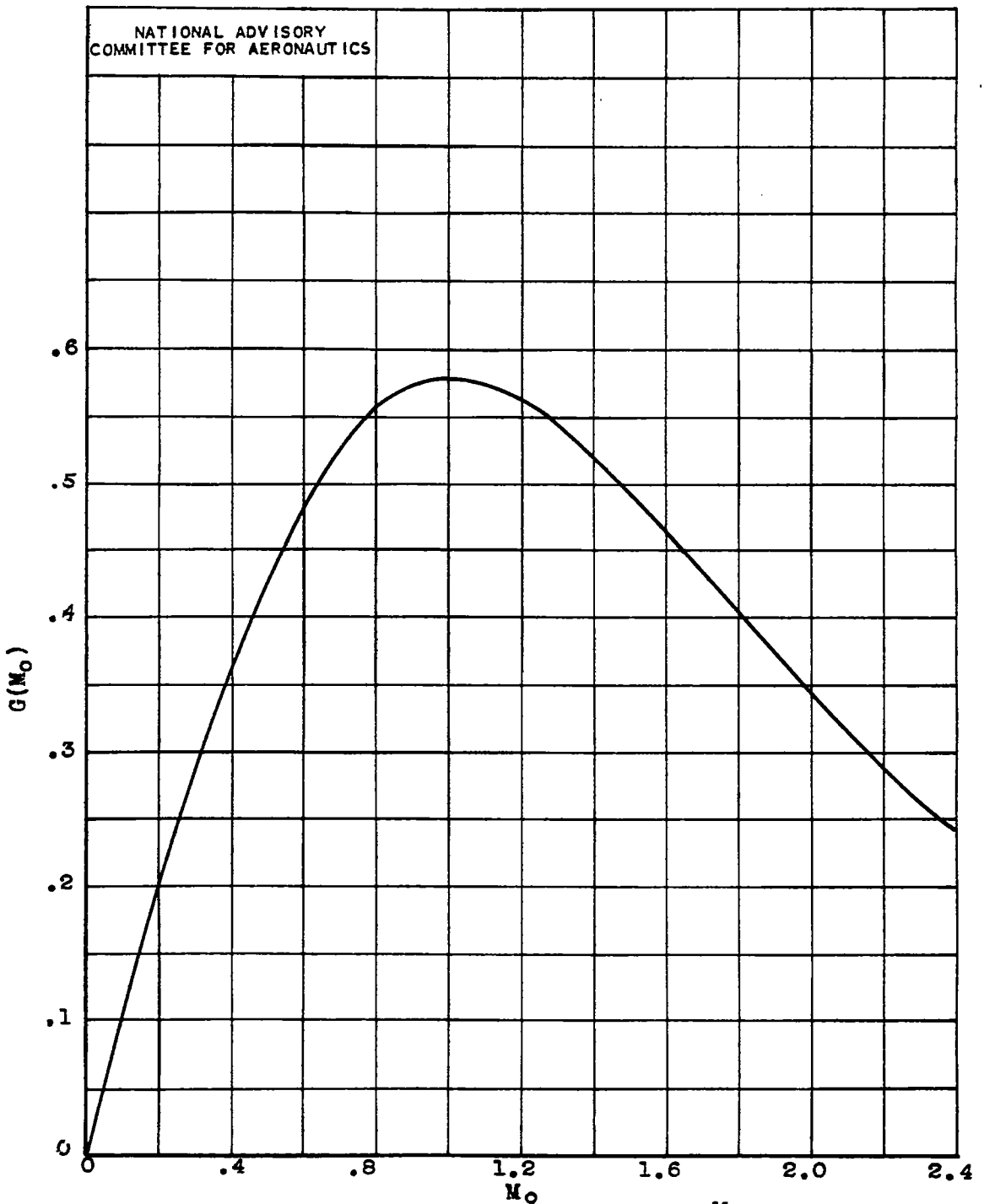

Figure 22.- Plot of function $G(M_o) = \frac{M_o}{(1 + 0.2M_o^2)^3}$.

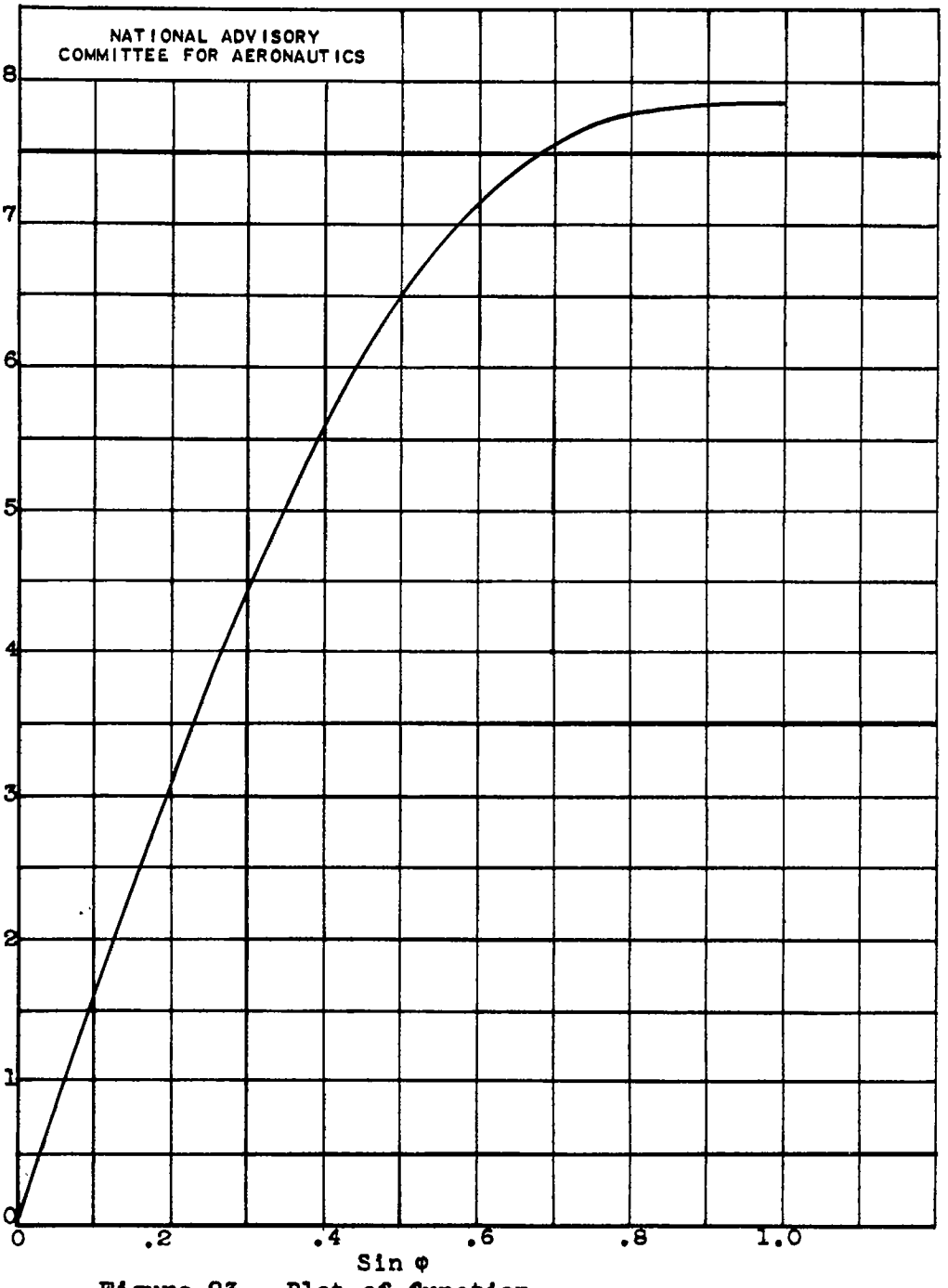

Figure 23.- Plot of function

$$F(\varphi) = \frac{\sin 2\varphi}{6}(\cos 4\varphi + 9\cos 2\varphi + 23) + 5\varphi.$$

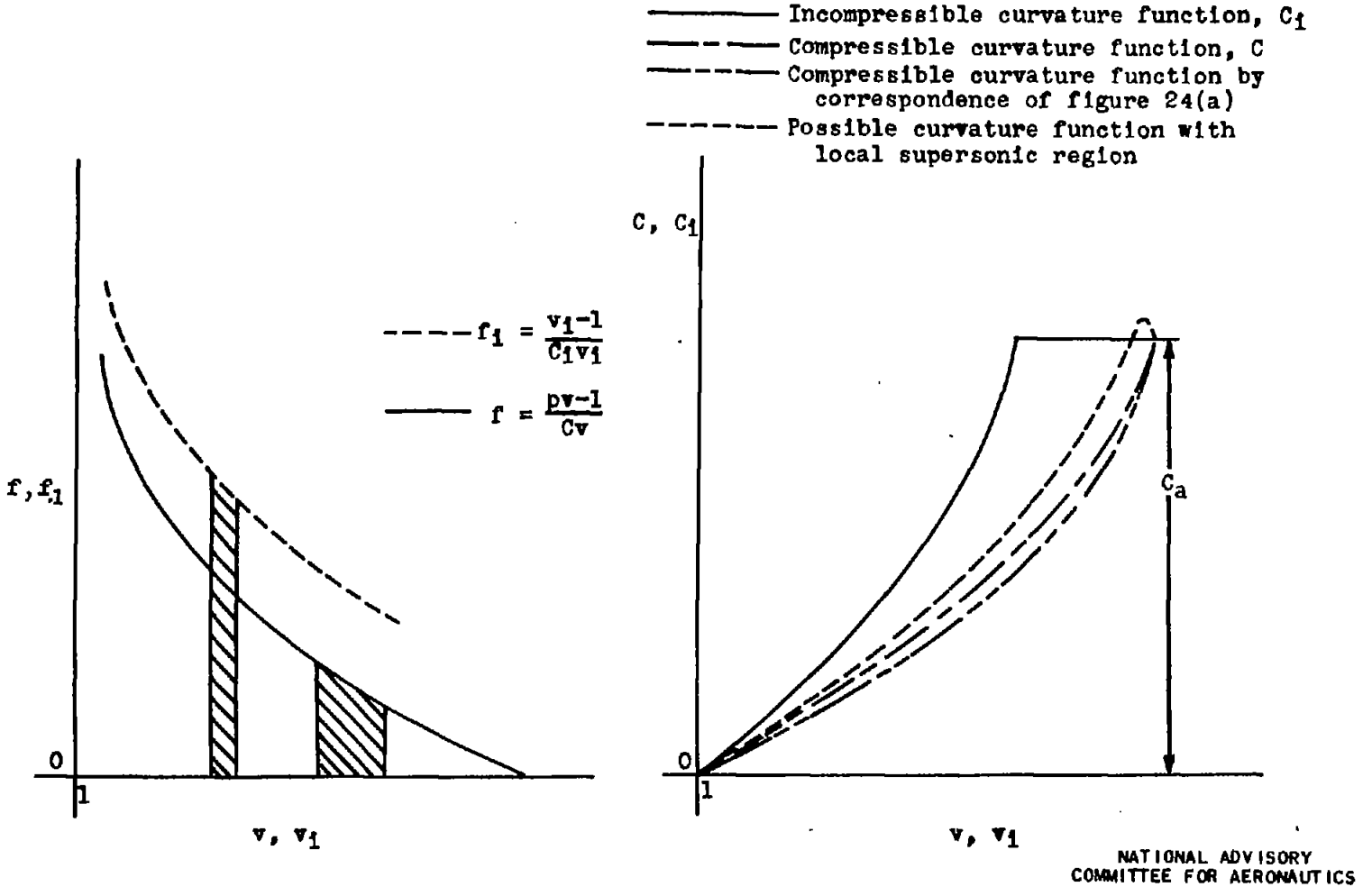

(a) $fdv = f_1 dv_1$.

(b) Curvature functions.

Figure 24.- Correspondence between compressible and incompressible flow for compressibility correction rule of Greene.